Graphene Oxide Enhanced, 3D Printable, Self-Healing, Highly Tough and Elastic Dual-Network Hydrogels for Multifunctional Wearable Biosensors

By

Yitian Wang

A Thesis Submitted to the Faculty of Graduate Studies of

The University of Manitoba

in partial fulfillment of the requirements of the degree of

Master of Science

Department of Biosystems Engineering

University of Manitoba

Winnipeg, Manitoba

Copyright © 2019 by Yitian Wang

Table of Contents

Abstract 1
Acknowledgment 2
List of Figures 3
List of Tables 4
Chapter 1 Introduction 5
1.1 General Overview 5
1.2 Problem Definition 5
1.3 Objectives 6
Chapter 2 Literature Review 8
2.1 Hydrogel 8
2.2 Classifications of Hydrogels 8
2.3 Advanced Functionalizations of Hydrogels for Bioelectronics 10
2.4 Hydrogels with High Toughness 10
2.5 Conductivity 14
2.6 Self-healing 14
2.6.1 Hydrogen Bonding 15
2.6.2 Ionic Interaction 15
2.6.3 Hydrophobic Interaction 16
2.7 Three-Dimensional (3D) Printable Hydrogels 16
2.7.1 Materials for Printable Ink 16
2.7.2 The application of 3D Printing Technique in Different Kinds of Biosensors 18
2.8 Conclusion 19
Chapter 3. Materials and Methods 21
3.1 Introduction 21
3.2 Materials 23
3.3 Preparation of PAA-GO-Ca^{2+} Hydrogel 23
3.4 Material Characterization 23
3.4.1 Fourier-transform Infrared (FTIR) Spectra Characterization 23
3.4.2 Scanning Electron Microscope (SEM) Characterization 24
3.4.3 Swelling Kinetics Performance 24
3.5 Mechanical Properties Testing 24
3.5.1Tensile Test 24
3.5.2 Cyclic Tensile Evaluation 25
3.5.3 Compression Tests and Cyclic Compression Tests 25

3.6 Rheology Evaluation 25
3.7 Evaluation of Self-healing Properties 25
3.8 Mechanism of Self-healing Property 25
3.9 3D printed PAA-GO-Ca^{2+} Hydrogels 26
3.10 Prototype Wearable Biosensors Composed of 3D Printed PAA-rGO-Ca^{2+} Hydrogels 26
3.11 PAA-rGO-Ca^{2+} Hydrogel-based Sensor for Ammonia Vapor Detection 26
Chapter 4. Results and Discussion 28
4.1 Results for Hydrogel Materials Characterization 28
4.2 Results for Tensile Tests 32
4.2.1 Results for Tensile Tests with Different GO Contents 32
4.2.2 Results for Tensile Tests with Different Ca^{2+} Contents 38
4.3 Results of Rheology Tests 40
4.4 Results of Cyclic Tensile Tests 41
4.5 Results for Cyclic Compression Tests 47
4.6 Self-healing Tests 57
4.6.1 Influence of GO Amount on Self-healing Efficiency 58
4.6.2 Influence of Ca^{2+} Amount on Self-healing Efficiency 59
4.6.3 Influence of Healing Time on Self-healing Efficiency 59
4.7 Mechanism of Self-healing Property 60
4.8 3D Printable Hydrogels 62
4.9 PAA-rGO-Ca^{2+} Hydrogels in Wearable Electronic Biosensor 65
4.10 Results for Detecting Ammonia 67
4.11 A Discussion on the Highlights of Our Work as Compared to Peer Research 68
Chapter 5 Conclusion and Future Work 74
Reference 76
Appendix I 88
Biomimicry of oil infused layer on 3D printed poly(dimethylsiloxane): non-fouling, antibacterial and promoting infected wound healing 88

Abstract

Hydrogels have been widely used in the biomedical sector in recent years. However, conventional hydrogels' disadvantages of poor mechanical performance and lack of efficient self-healing ability limit their practical application. A novel versatile hydrogel with excellent mechanical properties and extraordinary self-healing efficiency was developed by integrating graphene oxide (GO) nanoparticles into a polyacrylic acid (PAA) hydrogel network crosslinked by an organic crosslinker N,N' methylenebisacrylamide (MBA) and an inorganic crosslinker Ca^{2+}. The resulting PAA-GO-Ca^{2+} hydrogel, with both covalent and physical dual-crosslinked networks demonstrated remarkable mechanical properties including an ultrahigh strain of 2500% and high toughness (~9.73MJm^{-3}) along with high stiffness (Young's modulus:~753.667KPa). In addition, the hydrogel also shows super effective self-healing ability (~87.47%, 88.02% and 86.93% healing efficiency in tensile strength, tensile strain, and toughness respectively) which is attributed to the reversible hydrogen bondings existing in abundant hydrogen-containing functional groups and ionic interactions between COO^- groups existing in both PAA and GO. To achieve facile fabrication of the developed multifunctional hydrogels for such advanced applications as biosensors, we adjusted the viscosity of the hydrogels by controlling their degree of crosslinking to allow 3D printing. The 3D printed PAA-GO-Ca^{2+} hydrogels were further treated with HI vapor to reduce GO on the surface of the hydrogels and produce conductive PAA-rGO-Ca^{2+} hydrogels for different types of wearable biosensors, including sensors to detect different humans activities such as pulse rate, breathing, finger movement, sensors to monitor sweating levels, and ammonia detectors which detect toxic ammonia gas at low concentrations.

Keywords: PAA, GO, tough hydrogel, self-healing, 3D printing, biosensor

Acknowledgment

I would like to extend my sincere appreciation to supervisor Dr. Wen Zhong and my co-supervisor Dr.Malcolm Xing, thanks for their professional guide and support during my study. They inspired me not only at the academic level but they have encouraged me how to think independently and to be different.

Thank all my lab colleagues especially Dr. Tao Chen for helping me design the biosensor and mobile application, and Dr. Gaoqiang Shi who helped me with animal vivo test.

I would also like to thank Dr. David Levin and Dr.Gregory Bridges for joining as my committee members and giving me suggestions to improve my research.

I am also grateful to my family for their love and support.

Last, thank Natural Sciences and Engineering Research Council of Canada (NSERC) Discovery Grant and NESRC Discovery Accelerator Supplements Awards for their financial support.

List of Figures

Figure 1. Schematic illustration. 23

Figure 2. FTIR results 29

Figure 3. Swelling kinetics behavior of PAA and PAA-GO-Ca^{2+}hydrogels. 30

Figure 4. SEM images 32

Figure 5. Tensile tests results on hydrogels with different GO ratio 34

Figure 6. Tensile tests on hydrogels with different amounts of Ca^{2+} crosslinker 36

Figure 7. Mechanical Performance 37

Figure 8. Rheology tests for hydrogels with different GO and Ca^{2+} contents 40

Figure 9. Cyclic tensile tests on hydrogels 43

Figure 10. Up to 20 times of cyclic tests 45

Figure 11. Compression recovery ability 46

Figure 12. Results for cyclic compression tests 47

Figure 13. Self-healing test on hydrogels 49

Figure 14. Self-healing rheology tests 50

Figure 15.Self-healing mechanical behavior of hydrogels with different GO ratio 52

Figure 16. Self-healing mechanical behavior of hydrogels with different Ca^{2+} ratio 54

Figure 17. Self-healing mechanical behavior of hydrogels with time. 56

Figure 18. Mechanical behavior for self-healed sample 57

Figure 19. Self-healing mechanism 62

Figure 20. 3D printing process 63

Figure 21. Conductive tests 64

Figure 22. Wearable biosensor tests 67

Figure 23. Ammonia detection 68

List of Tables

Table 1 A review on typical multifunctional hydrogels reinforced by introducing GO/rGO.....71

Table 2. A review on recent breakthrough in hydrogels with selfhealing ability.....72

Table 3. 3D printable ink for hydrogels' manufacturing. 73

Chapter 1 Introduction

1.1 General Overview

With a unique structure of three-dimensional (3D) crosslinked polymer networks holding a large amount of water, hydrogels are becoming one of the most promising candidates for such biomedical applications as vehicles for drug delivery, scaffolds for tissue engineering, wound dressings, contact lenses, and wearable electronic devices (*1*-*3*).

Development of novel attachable and wearable electronic devices has been drawing a great deal of attention because these innovations provide easy and conventional approaches for monitoring the real-time health status of human beings. An ideal electronic device is usually expected to be highly sensitive, efficient, reliable, of low cost, and available in different geometries, sizes, and shapes. In addition, an ideal biosensor for healthy monitoring should be capable of deforming freely with the human skin as it is stretching, bending, and twisting (*4*). Traditional metal sensors do not attach to the human body without the assistance of tapes, and they also show toxicity and limited capacity in strain detection (*5*). An alternative approach is to combine stretchable polymers with conductive nanoparticles in a cost-effective electronic device. For example, poly(dimethylsiloxane) (PDMS), a highly stretchable and nontoxic polymer, can be mixed with carbon nanotubes (CNT) for a novel, stretchable, conductive biosensor with high sensitiveness and rapid response (*6*). Conducting polymers such as polypyrrole (PPy), polyaniline (PAni) and polythiophene (PTh) offer excellent conductivity and biocompatibility for developing novel biosensors (*7*-*9*), but display relatively weak mechanical properties. Hydrogels are becoming promising alternative materials for such applications as they can be endowed with such preferable characteristics as high elasticity, self-healing, and conductivity.

1.2 Problem Definition

Remarkable achievements have been accomplished by researchers in developing conductive hydrogels of crosslinked polymers with intrinsic conductivity such as polyaniline (PAni) and

polypyrrole (PPy) (*7, 9*). However, these hydrogels often show weak mechanical properties which hamper their further applications in the biomedical field. Among the modifications to improve the mechanical strength of hydrogels (*10-13*)., hybrid double-network hydrogels, a type of composite hydrogel networks that contain both a covalently crosslinked network and a physically crosslinked network, are becoming an extensively studied strategy to produce hydrogels that may reach similar toughness with that of natural tissues and may sustain substantial internal and external mechanical loads. On the other hand, conductive nanocomponents such as carbon nanotubes (CNT), graphene and nanodiamonds have been incorporated into double-network hydrogels as reinforcements to render further robustness and toughness (*14, 15*). However, it is still a challenge to achieve a desirable distribution of these nanocomponents and effectively prevent their aggregations.

In addition, it is desirable to design and fabricate hydrogel-based electronic devices with specific three-dimensional (3D) architectures in order to meet requirements from different applications. 3D printing, or additive manufacture, provides a promising technology to solve this problem by directly printing hydrogels into complex 3D structures. 3D printing techniques enable facile and quick fabrication of electronic devices for a variety of applications (*16, 17*). However, the development of appropriate bioinks for various applications remains a big challenge. Bioinks are expected to have appropriate viscosity and to gell rapidly to maintain the accurate shapes and sizes as designed.

1.3 Objectives

Despite of their superb hydrophilicity and biocompatibility, traditional hydrogels are usually weak, lack of desirable conductivity and self-adhesiveness. These disadvantages limit the applications of hydrogels in advanced electronic devices that require multiple functionalities. The objective of the current work is therefore to develop 3D printable multifunctional hydrogels that demonstrate super toughness, desirable conductivity, and self-healing. Specifically, hydrogels based on a hybrid double-network polymeric crosslinking system will be fabricated to endow excellent mechanical properties and self-healing ability. Reduced graphene oxide nanoparticle will be incorporated into the hydrogels to enhance both their conductivity and toughness. The formulation of the hydrogels

will be optimized to allow 3D printing fabrications into hydrogel-based electric devices that may be potentially useful for a variety of advanced sensing applications.

Chapter 2 Literature Review

This chapter starts with a brief introduction to the basics of hydrogels, then focuses on the advanced functions of hydrogels that are essential for their applications in biosensors, including high mechanical performances, self-adhesiveness, self-healing capacity, and conductivity. This chapter also discusses the application of 3D printing in the preparation of hydrogels, which is a versatile approach to building hydrogels into complex 3D architectures.

2.1 Hydrogel

Hydrogels are three-dimensional, chemically or physically crosslinked networks of polymeric materials (*18-20*). Hydrogel networks contain numerous hydrophilic functional groups, rendering them capable of holding large amounts of water (*20, 21*). Owing to their unique properties, hydrogels have been received considerable attention over the past decades (*22, 23*). Hydrogels have also been widely explored and used in a variety of applications, including wound dressing (*1, 24, 25*), contact lenses (*26-28*), cosmetic materials (*28, 29*), water filtration (*30-32*), scaffolds for tissue engineering (*33-35*), drug delivery systems (*36-38*), biosensors and electronic devices(*34, 39, 40*). Among these applications, the development of novel, scalable, wearable, low-cost and multifunctional hydrogel-based biosensors for the rapid and sensitive detection of human health signals has been of great interest recently (*41-43*). Extensive research and remarkable progress in biosensors have been reported to detect human heart rate, breathing, and metabolites (*39, 44*). However, it is still a challenge to develop biosensing platforms that can detect multiple health signals simultaneously with high sensitivity and quick response (*42, 45*).

2.2 Classifications of Hydrogels

Hydrogels can be classified based on sources of polymers, crosslinking methods, network electrical charges, and physical formats. The details are discussed below.

Hydrogels can be grouped according to their original sources. **Natural polymer hydrogels** are produced by chemical or physical crosslinking of natural polymeric materials including natural

proteins such as collagen (*46, 47*) and gelatin (*48, 49*), or natural polysaccharides such as chitosan (*50, 51*) and alginate (*52, 53*). **Synthetic polymer hydrogels** are produced by chemical or physical crosslinking of synthetic polymeric materials, for example, Polyacrylamide (Pam) (*54, 55*), and poly(vinyl alcohol) hydrogels (*56, 57*). **Combined polymer hydrogels** are produced by mixing and crosslinking both natural polymers and synthetic polymers. For example, collagen-based polyacrylamide hydrogels were developed for drug delivery (*58*). Alginate and poly (ethylene glycol) (PEG) were combined in hydrogels for fabrication of extracellular matrix (ECM) (*59*). Both chitosan and alginate have shown favorable biocompatibility concerning their utilization on hydrogel scaffolds for tissue engineering (*60, 61*). However, natural polymer hydrogels often fail to show as excellent mechanical properties as synthetic polymer hydrogels. In order to enhance both the mechanical properties and the biocompatibility of hydrogels for biomedical applications, some non-toxic synthetic polymers such as poly(ethylene oxide) (PEO), poly(vinyl alcohol) (PVA) and poly(ethylene glycol) (PEG) have been selected to form hydrogels with natural polymers together. The resultant hydrogels usually show good mechanical properties along with admirable biocompatibility (*62-64*).

Based on the nature of the crosslink junctions, hydrogels can be divided into chemically crosslinked networks and physically crosslinked networks. In chemically crosslinked networks, the polymer chains are covalently linked by crosslinker agents, which results in permanent junctions (*65-67*). However, in physically crosslinked networks, the junctions occur due to either polymer chains entangled with each other or physical interactions, such as hydrogen bonds (*68-70*), ionic interactions (*71-73*) or hydrophobic interactions (*74, 75*). Intermediate crosslinking density usually allows polymer solution or melts to be transformed into solid or gel state materials with elastomeric property and potentially higher strength. However, a very high crosslinking density may lead to rigid or glassy materials (*76, 77*).

Chemical or covalent crosslinks in hydrogels result in stable mechanical and thermal properties. Once formed, it is difficult to break these kinds of interactions (*78, 79*). On the other hand, physical

crosslinking forms in the presence of intermolecular forces, such as hydrogen bonds (*80, 81*), Van Der Walls forces (*82, 83*), hydrophobic interactions (*84, 85*) or ionic interactions (*86, 87*). Compared to chemical crosslinking, physical crosslinking is relatively weak and reversible (*24, 36*).

2.3 Advanced Functionalizations of Hydrogels for Bioelectronics

Hydrogels for different applications are expected to have different properties. For example, hydrogel-based contact lenses require hydrogels to maintain an integrated physical shape over a long period (*28, 88*); Hydrogel-based scaffolds require hydrogels to have an excellent mechanical property to accommodate substantial deformation and loads (*34, 89*); Hydrogel wound dressings require the hydrogels to have the ability to absorb blood and tissue fluid (*1, 25, 90*). Recently, extensive attention has been directed to the development of hydrogels for electronic biosensors (*39, 91*). Ideal hydrogel-based electronic biosensors are expected to have continuous 3D microstructures (*43, 92*), excellent mechanical properties (*93, 94*), superb hydrophilicity (*95, 96*), good biocompatibility (*97, 98*) and large surface area (*99, 100*).

Moreover, certain biosensors are expected to have reversible swelling behavior in response to both internal and external stimuli, such as temperature (*101, 102*), pH (*103, 104*), the electric field (*95, 105*), and specific analyte concentrations. Therefore, it is of great significance to design and engineer hydrogels with versatile functions, such as high toughness (*106, 107*), superelasticity(*108, 109*), conductivity (*110, 111*) and self-healing capacity (*75, 112*).

2.4 Hydrogels with High Toughness

Swelling of hydrogels in water often makes the polymer networks weak and brittle, leading to a decrease in mechanical properties (*68, 113, 114*). However, many applications require hydrogels to have similar mechanical properties with those of natural hydrogels in plant or animals, which have high toughness in order to bear substantial internal and external mechanical loads and deformations (*115, 116*). Many modifications have been done to improve the toughness of hydrogels, and they have shown significant enhancements. Different strategies and methods have been developed to

make tough hydrogels capable of resisting deformation, including double-network hydrogels (*117-119*) and nanocomposite integrated hydrogels (*120-122*).

Double network (DN) hydrogels comprise of two different covalently crosslinked polymeric networks. Gong et al. first synthesized this type of hydrogels, which displayed improved toughness and excellent mechanical strength (123). The double-network hydrogels are usually produced by immersing a densely crosslinked polymer network into a second monomer solution and then polymerizing the second monomer to form a relatively loose network. In the resulting hydrogel, the first network provides support and strength while the second network provides high energy dissipation upon large strains. Such double-network hydrogels made from poly(2-acrylamido2-methylpropane sulfonic acid) (PAMPS) polyelectrolyte and linear polyacrylamide (PAAm) were found to have a fracture energy of 400 J/m^2 (118). Chen et al.(39) fabricated a DN hydrogel, in which physically crosslinked Agar was introduced to hydrophobically associate polyacrylamide (HPAAm). The resulting Agar/HPAAm DN gels exhibited excellent mechanical strength, high toughness and notable self-healing property. Xing et al. (124) recently designed a DN hydrogel by introducing ferric ions to the poly(acrylic acid) network to enhance mechanical behavior as well as achieve rapid self-healing efficiency. Double-network hydrogels are tough owing to their special yielding, and hardening mechanisms during deformation. Upon deformation, the first network of the double-network hydrogels breaks up and forms lots of fractures which act as clusters and the second network dissipates energy and causes shielding. However, a disadvantage of this type of hydrogels is that once covalent bonds are broken, the destruction is permanent (*125*).

Instead of integrating two chemically crosslinked networks into one hydrogel system, **hybrid double-network (hDN) hydrogels** are produced by integrating a chemically crosslinked network and a physically crosslinked network into one hydrogel system. Physical crosslinking, such as ionic crosslinking (*118, 126*) or hydrogen bonds (*68, 95*), are generally weaker than chemical crosslinking based on covalent bonds. As a result, it is easier for polymer chains to get detached from physical crosslinking under mechanical loads, or changes in environmental conditions such as

pH values and temperatures. The detachment takes place and therefore dissipates energy in the polymeric networks. Furthermore, unlike DN hydrogels, the physical crosslinking in hDN hydrogels are reversible, which means that the crosslinking can be re-established (*127, 128*). Zhao and his co-workers fabricated hDN hydrogels using sodium alginate and poly (ethylene glycol) (PEG) which are both biocompatible (*129*). The resultant hDN hydrogels were composed of covalently crosslinked PEG and ionically crosslinked alginate. They found that by introducing reversible crosslinking, the toughness of the hydrogel system was dramatically increased (*129*).

Nanocomposite integrated hydrogels are hydrogel networks incorporated with various nanosize reinforcements such as carbon nanotubes (CNTs) (*14*), graphene (*15*) and nanodiamond (*130*) to enhance their mechanical properties. The mechanism is that these nanosize fillers enable the transfer of mechanical forces within polymer chains and result in the enhancement of mechanical strength and toughness.

In recent studies, GO, and rGO are the most popular nanoparticles that can not only mechanically reinforce hydrogel's physical properties but can endow self-healing efficiency However, electrically enhancing hydrogels' properties which are fabricated by covalently conjugating nanosize reinforcements with the polymers is still remained a challenge. Liu's group integrated graphene oxide (GO) with polyacrylamide. In this study, GO sheets first experienced peroxide process to be turned into graphene peroxid (GPO), which was then covalently crosslinked with the polymer chains to obtain the nanocomposite hydrogels (*131*). The resultant hydrogels displayed very high tensile strength (0.2–1.2 MPa), extremely high elongations (2000–5300%), and excellent resilience. Yu *et al.* (*132*) intertwined GO and poly(acryloyl-6-aminocaproic acid) (PAACA) to fabricate GO/PAACA composite hydrogels using calcium ionic crosslinkers. Yan *et al.* (*133*) introduced rGO nanoparticles into cellulose ester based hydrogels to prepare rGO/cellulose conductive hydrogel films which have a potential application in electrodes for supercapacitors due to its excellent capacitance even at a high current density.

Another carbon-based nanoparticle often investigated for improving hydrogels' properties is CNT, which can be classified as either muti-wall or single wall CNTs. Either of them can be utilized in hydrogel engineering to enhance both mechanical behaviors and conductivity, which makes CNT nanoparticle enhanced hydrogels better for biomedical applications (*134-136*). However, due to the intrinsic hydrophobic nature of CNTs which is mainly attributed to large and strong π-π stacking which leading to massive aggregation (*137, 138*), it is of great difficulty to integrate CNTs with other hydrophilic polymers, such as PEG, PLA, and PAA (*139*). Some efforts have been dedicated to improve the dispersion of CNTs such as modified CNTs surfaces with various polar groups like hydroxyls (OH) (*140*), amines (NH2) (*141*) (*142*) and carboxyl (COOH) (*143*) groups which are hydrophilic groups and can facilitie CNTs better integration of CNTs with other polymers. Not only owing to that the CNTs have intrinsic high electrical conductivity. CNTs based hydrogels are utilized for detecting and converting biological signals to electrical signals. For example, CNTs-based nano hydrogels can be employed to immobilize enzymes due to their efficient and fast response time and high stability (*144-146*).

Nanodiamonds (NDs) are an emerging carbon-based nanoparticle which have various physical and chemical advantages that can be used to carry numerals biomedical application. In contrast with GO and CNTs, NDs have better biocompatibility in respect to biomedical applications (*147*). In addition, NDs possess an extremely high surface area-to-volume ratio which endows them with an impressive advantage for drug delivery application (*148, 149*). On the other hand, relatively high cost hinders the practical application of corporating NDs in hydrogel networks.

Overall, carbon nanoparticles-based hydrogels have been a hot topic over the past decades. Among them, GO and CNTs nanoparticles enhanced hydrogels are most popular. Due to massive oxygen-containing functional groups in GO, it is easy to integrate GO nanoparticles with other hydrophilic polymers, but the relatively low conductivity limits their application in the electrical field. In contrast, CNTs have much better electrical conductivity, but their hydrophobic nature makes it hard to embed CNTs into other polymers. Fortunately, strategies have been developed to address these

concerns. GO can be reduced to rGO to improve the conductivity and CNTs can be modified for better dispersion. Nanodiamonds (NDs) are a new class carbon-based nanofiller, which can be employed especially in biomedical fields due to its non-cytotoxicity and large surface area.

2.5 Conductivity

Flexible and soft conductors are promising materials for bioelectronics which have wide applications in biomedical sectors, such as implantable and wearable electronic biosensor for health monitoring (*44*), cardiovascular tissue engineering (*150*), and electronic skin (*151*). Significant progress in developments of conductive hydrogels have been achieved in the past several decades. Conductive hydrogels can be produced by incorporation of conductive polymers, such as polyaniline (PANI) (*7*, *8*) and polypyrrole (PPy) (*9*, *152*), which have intrinsic electrical conductivity. Unfortunately, both PANI and PPy hydrogels show weak mechanical strength which limits their biomedical applications. An alternative way to produce hydrogels with both excellent mechanical strength and desirable conductivity is to incorporate conductive nano-reinforcements such as carbon nanotubes (*14*), graphene sheets (*15*, *153*), and metallic nanoparticles (*7*) into hydrogels via either covalently crosslinking or physically incorporation. These practices not only render hydrogels with desirable conductivity, but also improve their mechanical strength and toughness. However, these conductive nanoparticles are easy to aggregate in the polymeric networks and affect the conductivity of the composite hydrogels (*154*, *155*).

2.6 Self-healing

An intrinsic property of some natural tissues, self-healing is very desirable for manufactured hydrogels, especially for those applied in electronic skins (*7*), ligaments (*156*) and tendons (*157*). Self-healable hydrogels are capable of repairing themselves upon breakage caused by mechanical loads to restore their original structures and mechanical properties. Progress has been achieved for nanocomposite hydrogels with high mechanical strength as well as self-healing capacities, but the tensile strength for most recoverable hydrogels after healing is below 300 KPa, and the self-healing

efficiency is below 80%. Therefore, development of novel hydrogels with excellent self-healing efficiency without sacrificing their machinal strength is still a great challenge.

Self-healable hydrogels have usually been engineered by introducing reversible bonds, including hydrogen bonds (*158*), ionic interaction (*158*), and hydrophobic interaction (*75*). These interactions can break up when hydrogels are undergoing mechanical loads or deformation, making polymer chains detached. However, these interactions can be re-established to restore the materials if the broken surfaces are allowed to get into contact again. Self-healable hydrogels display loads of advantages especially when it comes to biomedical applications.

2.6.1 Hydrogen Bonding

Hydrogen bonds which are formed when a hydrogen atom interacts with other atoms that are highly electronegative such as O, N or F have a relatively weaker physical interactions compared to covalent bonds and ionic interactions. Reversible physical crosslinking occurs between the electronegative atoms (hydrogen bonding acceptors) and different polymer chains with hydrogen atoms (hydrogen bonding provider). Reversible Hydrogen bonds enable hydrogels with self-healing ability, for example, hydrogen bonding develops between adjacent polymer chains in poly(vinyl alcohol)(PVA) hydrogels shows great self-healing property, which can recover 72% tensile stress after 48 hours (*159*). Xing et al. reported to use tannic acid (TA) as an effective hydrogen provider which can create sufficient hydrogen bonds to gelatin-MA polymer chains (*160*), the resultant hydrogel not only recovered 80% tensile strength after 6 hours but recorved electrical conductivity.

2.6.2 Ionic Interaction

Ionic interactions are a stronger than hydrogen bonds occur and between oppositely charged ions, they often involves a charged polymer chains with an oppositely charged ions or with another oppositely charged polymer chains. For example, a facile strategy was engineered by integrating Poly(acrylic acid) with ferric ions, which leads to an autonomous self-healing hydrogel due to the migration of ferric ions (*161*). Another example was prepared by crosslinked graphene oxide (GO)

with poly(acryloyl-6-aminocaproic acid) (PAACA) by calcium ions which possess enhanced mechanical properties and efficient self-healing ability (*132*).

2.6.3 Hydrophobic Interaction

Hydrophobic interactions are generated in polymer hydrogels by micellar incorporation of a small number of hydrophobic sequences with hydrophilic polymers where the hydrogels have a balance of hydrophobic and hydrophilic interactions. The dynamic hydrophobic interaction between hydrophobic domains of polymer chains as well as micelles surface can greatly the self-healing abilities of hydrogels (*162-164*). For example, the hydrophilic monomer acrylamide (AAm) was modified by micellar copolymerization with a small amount of hydrophobic comonomer, in this design due to a high local concentration of the blocks of large amount hydrophobe within the PAAm polymer network, the polymer chains developed strong hydrophobic interactions that maked self-healing efficient (*162*).

Overall, the basic idea for enabling hydrogel self-healing ability would be creating dynamic interaction in the polymer networks. These interactions can break temporarily and recover after rupture. Among prevalent strategies, introducing hydrogen bonding, ionic interaction and hydrophobic association are the most popular ideas. Ionic bonding is the strongest interaction in contrast to the other two, and it often provides the hydrogels with improved mechanical behaviors and better self-healing efficiency. Hydrogen bonding is relatively weak but is also enough for improving hydrogels' properties when there would exist sufficient hydrogen bonds. Hydrophobic interaction can enhance hydrogels with effective self-healing ability but has a limited ability to improve mechanical properties, and hydrophobic interaction often requires a complex chemical reaction to form, makes it less attractive than the other two strategies.

2.7 Three-Dimensional (3D) Printable Hydrogels

2.7.1 Materials for Printable Ink

3D printing, a form of additive manufacturing, which allows polymer solution or mixture to directly and precisely generate various structures and patterns through computer-assisted software from a variety of polymers has become a popular and advanced technique that applied in biomedical sector (*165, 166*). It is promising to utilize 3D printing technology in hydrogel manufacturing because hydrogels can be generated with more freedom in design to meet different requirements without the need of any molds, especially in tissue engineering, wearable biosensor, drug delivery and wound dressings. However, about injectable and printable hydrogel formulation, it is necessary to take the preparation of hydrogel precursor into consideration. There has been an intensive investigation concerning this field. Hydrogel precursor that can be considered as printable ink should have certain rheological property to guarantee the easy and success printing progress, and also the precursor should also be crosslinked quickly enough to maintain the desired shape. Alginate and chitosan which are both natural materials are often integrated with other polymer solutions such as PLA, PEGDA, PCL, PAA, PAM for endowing them with better viscosity when printing out. Besides, alginate and chitosan assisted hydrogel can be crosslinked by ionic ions such as calcium, ferric and copper ions. Therefore, the pattern can be maintained. Another natural material that is suitable for 3D printing hydrogel is gelatin, which can be achieved by adjusting the concentration of the gelatin solution. Also, gelation can be addictive into other polymer precursors for mixing printing, such as PEG, PAA, and PAM. Adding another material with a high viscosity not only help print out hydrogel with designed structure but can also render hydrogel with other property, such as improvement in mechanical properties, efficiency in self-healing ability and enhancement in conductivity. However, this procedure sometimes can be complex; other strategies include thermal sensitive printing which means integrating thermal sensitive materials or grafting thermal sensitive sequence into the polymer, this kind of polymer precursor can be crosslinked at a certain temperature, makes it possible for quick crosslinking and maintaining and locking the desired shapes.

In this project, we use a novel strategy which does not involve complex chemical reaction or mixing with other supporting materials for 3D printing. The crosslinking density of the polymer is tuned by choosing an optimum pre-curing time to obtain printable ink with appropriate rheological properties. The printed hydrogel is allowed additional time for a complete curing with permanent shape and structure.

2.7.2 The application of 3D Printing Technique in Different Kinds of Biosensors

Strain sensors (mechanically stimulated biosensors): Wearable strain biosensors connected to the human body that provides real-time information about the wearer's health and fitness (*167*) are of great interest both academically and commercially. Developments of such platforms have mainly focused on sensors that measure physical, vital signs (e.g., pulse rate, movements). Biosensors targeting physiologically relevant analytes are more challenging but can provide important information about health and fitness (*168, 169*). There have been extensive interests in employing 3D printing technic to design and fabricate sensing electronics due to its capacity to produce custom-designed shapes and structures. Xing et al. developed a 3D printed conductive self-healing hydrogel composed of PAA, chitosan and PPy which has ultrastrechability (1500%), which can be potentially used for strain sensors. The 3D printed sensor with excellent conductivity can detect a large strain change and be utilized to detect different body movements such as finger bendings and muscle movements (170). Lewis et al. extruded carbon conductive grease (MG Chemicals) which is a kind of conductive viscoelastic ink into EcoFlex, an elastomeric polymer, to fabricate strain sensor with high conformal and highly programmable manner. The resulted strain sensor exhibits an extensibility up to 900%, making it promising for soft sensing devices (*171*). Li et al. programmed and printed a conductive CNTs into polydimethylsiloxane(PDMS) or Ecoflex TM to produce a low cost, stretchable and highly sensitive electrode sensors (*172*).

Biochemical sensor Another promising application of 3D printed biosensors is electronic skin, which usually composed of flexible, non-toxic and highly stretchable sensors that can perform a

variety of health monitoring functions such as blood glucose (*173*). These sensors are often composed of functional polymer networks like hydrogels and conductive materials. Michelini et al. developed 3D printed acrylonitrile-butadiene-styrene (ABS) polymer-based biosensors to detect oral fluid and sweat. Lactate oxidase was mixed with horseradish peroxidase for lactate determination in oral fluid and sweat (*174*). Martyn et al. presented a robust 3D printed microfluidic analysis system that can monitor human tissue metabolite levels. This system was an 3D printed electrode holder composed of a compressible elastomer and incorporated with a removable needle type integrated biosensor that detects glucose and lactate in the human tissues (*17*). Chris.R et al. fabricated, characterized and evaluated a 3D printed hydrogel thin film that can be used to measure protein bonding and antibody functionality in a microarray format. The protein toxin, staphylococcal enterotoxin B(SEB) was integrated with polyacrylamide and printed out on a 2D glass surface. The resulted hydrogel film was of great sensitivity to various protein and with immobilization efficiencies (*175*).

2.8 Conclusion

In conclusion, owing to unique properties like biocompatible, non-toxic, and low-cost, hydrogels become a suitable candidate in biomedical applications. However, the disadvantages including weak, lack of conductivity and self-healing ability also hinder the progress. We are dedicated to design a novel tough hydrogel with remarkable toughness and excellent self-healing efficiency; meanwhile, for better application in the wearable biosensor, we also improve hydrogel's conductivity to meet the requirement.

Moreover, 3D printing technology has been utilized in many fields in the medical sector, especially in wearable electronic biosensors. However, it is still a challenge to develop a novel 3D printed biosensor with high sensitivity and fast response, long-serving time and low maintenance cost.

In this project, we proposed and successfully 3D printed out a novel kind wearable biosensor with ultrastrechability(~ 2500% means high sensitivity), high toughness (~9.73MJm^{-3} which can long

serve time), improved conductivity (fast response), and self-healing efficiency(88.02% in tensile strain which can lower maintenance cost). This thesis provides a novel idea for 3D printed hydrogel-based wearable biosensor and also elaborates on the rational principles behind it.

Chapter 3. Materials and Methods

3.1 Introduction

In this work, we developed a multifunctional hydrogel that combines the two features of double-network and nanocomposite reinforcement as an easy and simple way to fabricate a novel hydrogel with greatly improved mechanical behavior and excellent self-healing efficiency. As shown in Schematic illustration, GO firstly experienced a thorough dispersion; then acrylic acid (AA) solution mixed with photoinitiator APS and crosslinker MBA was introduced to the GO dispersion for *in situ* polymerizations, followed by an introduction of calcium ions (Ca^{2+}) into the mixture as the dynamic and reversible crosslinkers for adjacent GO nanoparticles and a bridge between the COO^- groups in both PAA and GO. The resulted PAA-GO-Ca^{2+} hydrogels have both excellent mechanical performance and self-healing efficiency. Such hydrogels can be further developed into 3D printable inks by controlling the degree of crosslinking and printed into pre-designed sizes and shapes. The printed hydrogels were treated with HI vapor to reduce GO partially and to obtain PAA-rGO-Ca^{2+} conductive hydrogels. With outstanding mechanical behavior, excellent self-healing efficiency and good conductivity, the developed PAA-rGO-Ca^{2+} hydrogels are promising in such applications as wearable biosensors that can accurately detect not only different human activities such as finger movements, inhaling and exhaling activities, sweat and pulse rate but also can be used as an electronic nose that can precisely detect ammonia which is a notorious toxic industrial pollutant and has serious adverse effects on human's well-being.

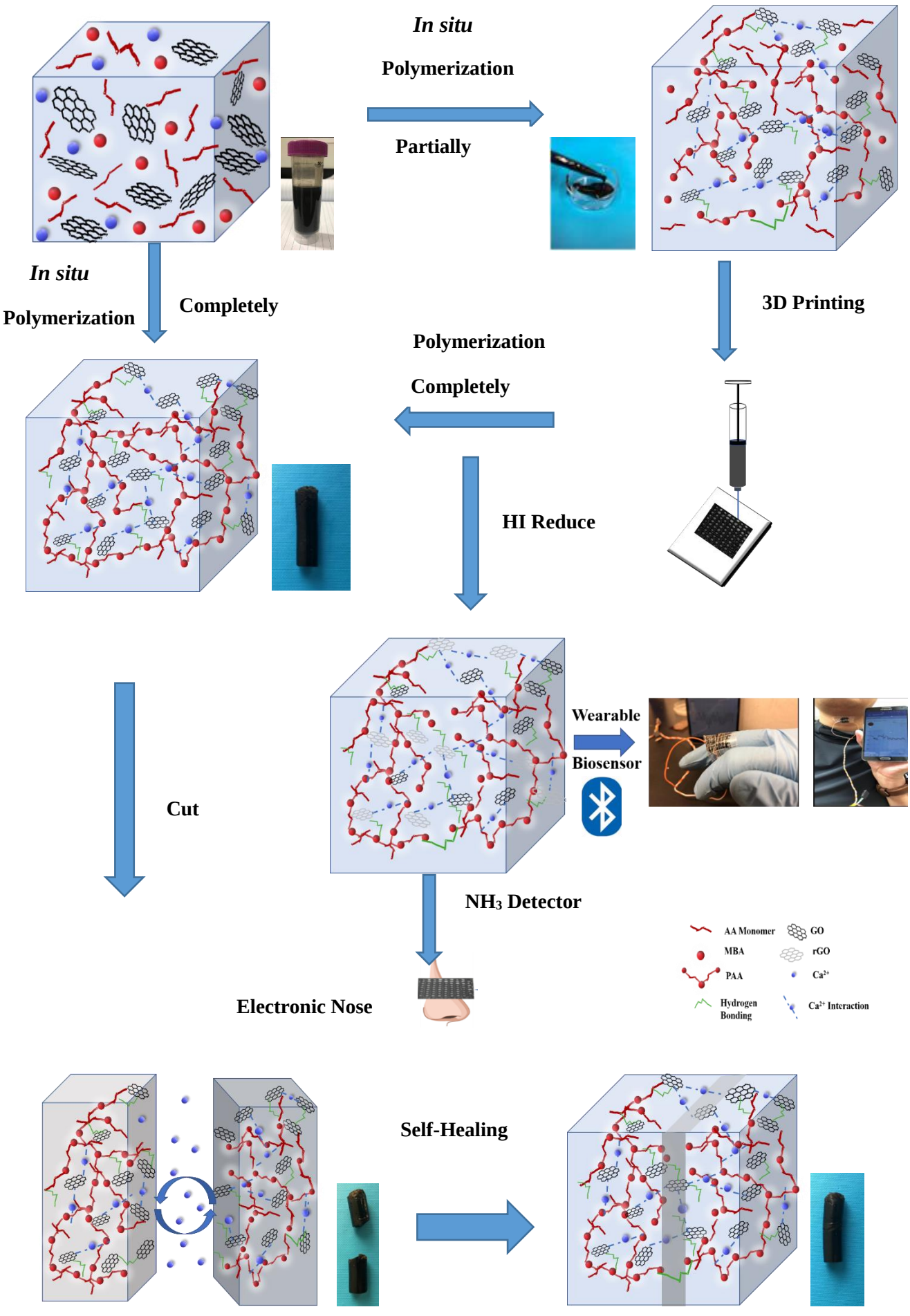
In situ
Polymerization
Partially
In situ
Polymerization
Completely
3D Printing
Polymerization
Completely
HI Reduce
Cut
Wearable
Biosensor
NH3 Detector
Electronic Nose
AA Monomer
GO
MBA
rGO
PAA
Ca2+
Hydrogen Bonding
Ca2+ Interaction
Self-Healing

Figure 1. Schematic illustration. GO nanofillers were dispersed in deionized water and mixed with AA solution, then MBA, APS for in situ polymerization and $CaCl_2$ were added to crosslink COO^- groups on both PAA and GO. The PAA network provides a strong skeleton for the hydrogel while the reversibly crosslinked GO network can help dissipate energy upon loading and recover its original shape and properties after damages.

3.2 Materials

Acrylic acid (AA), calcium chloride ($Cacl_2$),N,N' methylenebisacrylamide (MBA), Ammonium persulfate(APS), Urea powder, Ethylenediaminetetraacetic acid (EDTA) and Hydroiodic acid (HI) were bought from Sigma-Aldrich, Canada. Graphene oxide powder was provided by Wuxi Chemical company, China. All materials were used as received otherwise state.

3.3 Preparation of PAA-GO-Ca^{2+} Hydrogel

PAA-GO-Ca^{2+} composite hydrogels were synthesized by adding Ca^{2+} into the 20% acrylic acid (AA) solution in the presence of chemical crosslinker MBA, photoinitiator APS and different amount of GO nanoparticles. Specifically, neutralized AA was diluted to 20% solution by adding deionized water (DI water) followed by a thorough mix with dispersion of different amount of GO (calculated as a mass ratio to PAA as 3.0%, 5.0%, and 8.0%) then different amount Ca^{2+} crosslinker (calculated as a mass ratio to the total amount of GO and PAA, 5%, 8%, 10%, and 15%) was introduced to the mixture, followed by adding 0.075wt% chemical crosslinker MBA and 0.1wt% photoinitiator APS. The mixture was allowed 48 hours at room temperature for complete curing.

3.4 Material Characterization

3.4.1 Fourier-transform Infrared (FTIR) Spectra Characterization

FTIR characterization was carried out on an FTIR spectrometer (Bruker IFS 66v/s, German) within limits between 4000–400 cm^{-1}. Freezing-dried samples were divided into pristine PAA hydrogel, PAA-GO hydrogel with 5% GO and PAA-rGO-Ca^{2+} hydrogel with 5% GO and 10% Ca^{2+}.

3.4.2 Scanning Electron Microscope (SEM) Characterization

SEM characterization was performed on a model of Quanta FEG 650 scanning electron microscope with an operation voltage of 20eV. The PAA-GO-Ca^{2+} hydrogel sample with 3%, 5%, and 8 % GO and a fixed10% Ca^{2+} was lyophilized, coated with a thin layer of gold and then loaded onto a metal holder for examination under the microscope.

3.4.3 Swelling Kinetics Performance

To investigate the swelling kinetics behavior of PAA-GO-Ca^{2+} hydrogel, samples were prepared as $1\times1\times1$ cm^3 and lyophilized before immersed into excess water at room temperature for 150 minutes and were taken out for weighting at every 15-minute interval. The swelling ratio (SR) was calculated as $SR=(W_t - W_d)$ where W_t represents the weight of hydrogel after swelling water at different times while W_d represents the weight of the dry hydrogel. Pristine PAA hydrogel samples experienced the same experimental procedure as a control group.

3.5 Mechanical Properties Testing

Mechanical evaluations were conducted with an Instron 3366 Electronic Universal Testing Machine. All mechanical tests were performed at least five times with samples prepared with the same protocols. Average values and standard deviations for all sample groups were calculated for statistical analysis and were plotted into graphs by Origin Lab software.

3.5.1Tensile Test

The sample sizes for tensile tests were 50 mm in length, 5mm in width and 2mm in the thickness. All samples were tested at a crosshead speed of 10mm/min at room temperature. The tensile stress (σ) was calculated as $\sigma = F/(W*T)$, where F represents the load, W and T represent the original width and thickness of the tested specimen. The tensile strain (ε) was defined as the ratio of the change in length $L-L_0$ to the original length L_0, or $\varepsilon= (L-L_0)/L_0$. The fracture toughness was

characterized by fracture energy (U, MJ/m^3) which was calculated by the area under the stress-strain curve or $U= \int \sigma \, d\varepsilon$.

3.5.2 Cyclic Tensile Evaluation

Cyclic tensile tests were conducted with a maximum strain of 800% on samples with the same sample sizes at the same test speed as described above. The dissipated energy ΔU was defined as the hysteresis loop area encompassed by the loading-unloading curve: $\Delta U = \int \sigma_{loading} \, d\varepsilon - \int \sigma_{unloading} \, d\varepsilon$.

3.5.3 Compression Tests and Cyclic Compression Tests

Compression and cyclic compression experiments were carried out on samples with a diameter of 8 mm and a height of 5mm under a maximum compression strain of 80% at a speed of 10mm/min. The calculation methods for dissipated energy during the compression cycles are the same with that of the cyclic tensile tests.

3.6 Rheology Evaluation

Rheology measurements of the hybrid hydrogels were carried out with a TA DHR-2 rheometer using a cylinder sample of the diameter of 8 mm. Hydrogel Samples with different GO contents (0%,3%,5% and 8%) and different Ca^{2+}(5%, 8%, 10% and 15%) were respectively prepared for optimize parameters. Hydrogel sample with 5% GO, and 10% Ca^{2+} was manufactured for rheology test to evaluate self-healing property.

3.7 Evaluation of Self-healing Properties

As-prepared rectangle hydrogels were bisected and subsequently allowed to heal in a covered plastic dish to prevent water loss. After healing for certain times, the healed hydrogels were tested again for their mechanical properties.

3.8 Mechanism of Self-healing Property

0.1M EDTA was dissolved into DI water, and then NaOH was added gradually to adjust the PH to around 8.5. Desired amount urea was dissolved into DI water to make the concentration of the 1M urea solution. As a control group, the same amount purified water was used for treatment. The PAA-GO-Ca^{2+} hydrogel samples were immersed into the above three solutions respectively for 30 minutes followed by testing of their self-healing capacities.

3.9 3D printed PAA-GO-Ca^{2+} Hydrogels

A mixed solution 20% PAA, 5% GO, and 10% Ca^{2+} was pre-cured for 12-hour at room temperature to produce 3D printable ink with appropriate viscosity. Then the ink was loaded into an extrusion syringe on a costumer-built 3D printer for printing through a 20G flat tip needle. Pre-designed 3D shapes can be printed onto a glass slide. Then the 3D printed structure was removed from the substrate and kept in covered plastic dishes at room temperature for an additional 36 hours for a complete crosslinking.

3.10 Prototype Wearable Biosensors Composed of 3D Printed PAA-rGO-Ca^{2+} Hydrogels

Completely crosslinked 3D printed PAA-GO-Ca^{2+} hydrogels mesh were treated by HI vapor, which is an efficient, reducing agent (*176*), for 3 hours to reduce GO nanoparticles on the surface of the hydrogels to improve its conductivity while maintaining its excellent mechanical performance. The partially reduced 3D printed hydrogels were thoroughly washed using deionized water to remove excessive HI followed by removing excess water using a dryer. Then the 3D printed film was connected to a chip which can decode mechanical, biological and chemical signals to electric signals that can be shown on the screen of a smartphone via Bluetooth. The hydrogel-based sensing system was attached with a commercially available bandage to an index finger to detect finger movement and to a person's throat to evaluate breath activities.

3.11 PAA-rGO-Ca^{2+} Hydrogel-based Sensor for Ammonia Vapor Detection

PAA-GO-Ca^{2+} hydrogel's ability to absorb ammonia vapor and changing sensor's response was evaluated by placing the sensor on the top of ammonia hydroxide solution with different

concentrations in a closed environment. For each concentration, the sensor was placed over ammonia vapor for approximately 20 minutes until the conductivity changes reached a steady level, which was last for an additional 20 minutes. In each group, the concentrations of gaseous NH_3 were determined according to Raoult's law and Henry's law.

Chapter 4. Results and Discussion

4.1 Results for Hydrogel Materials Characterization

The PAA-GO-Ca^{2+} hydrogels developed are expected to have both excellent mechanical properties and remarkable self-healing efficiency, which were endowed by the two types of physical interactions: the hydrogen bodings between the oxygen-containing functional groups and the Ca^{2+} ionic interaction with COO^- groups. FTIR characterizations were conducted to verify the existence of these two physical interactions. As shown in Figure 2, the FTIR spectrum of GO powder shows various oxygen-containing functional groups including O-H banding at 3495 cm^{-1}, C-O at 1228 cm^{-1}, and acidic C=O at 1780 cm^{-1}, while 1625 cm^{-1} was assigned to the C=C (*177*, *178*). The band at 1697 cm^{-1} was attributed to the carboxylic groups in the PAA side chains (*179*). It can be seen that in the FTIR spectrum of PAA-GO-Ca^{2+} hydrogel, some of the bands that belong to GO powder and PAA were significantly decreased (3531 cm^{-1} and 1228 cm^{-1}) and some even totally disappeared (1780 cm^{-1} and 1697 cm^{-1}) (*180*). However, there was a new band in the PAA-GO-Ca^{2+} sample, 1541 cm^{-1} that can be assigned to COO^-. The decrease in oxygen-containing groups indicates hydrogel bonding was formed when PAA and GO were integrated. The COOH and acidic CO bands disappeared, indicating the presence of electrostatic interaction between COO^- and Ca^{2+} when Ca^{2+} was introduced as an ionic crosslinker.

To further reveal the crosslinking structural feature of PAA-GO-Ca^{2+} hydrogel and compare it to pristine PAA hydrogel, the swelling performance was systematically conducted. It is believed that the swelling behavior of hydrogel depends heavily on the crosslinking density of the hydrogel networks (*181, 182*). As shown in Figure 3, PAA hydrogel presents a much faster rate of absorbing water ability than PAA-GO-Ca^{2+} hydrogel in accordance with the fact that PAA hydrogel is known for its high water absorbing ability (*183, 184*). Herein, after introducing GO as additional crosslinking sites and Ca^{2+} ionics as a second crosslinker, the crosslinked density of PAA-GO-Ca^{2+}

hydrogel becomes way too much than pristine PAA hydrogel, resulting in the reduced ability to absorb water.

SEM images also show the fine incorporation of GO with PAA polymer chains with the help of Ca^{2+} as an effective crosslinker for COO^- and the abundant hydrogen-containing functional groups which can generate adequate hydrogen bonds. All the SEM pictures with a lower magnification indicate that the interior microstructure of all hydrogels samples are well-defined and show a flexible porous structure with size ranging from micrometers to nanometers. It is indicated in the pictures with higher magnification that when incorporated GO nanoparticles with PAA and adding Ca^{2+}, the PAA polymer chains that used to be smooth, as shown in Figure 4A right, become rough as shown in Figure 4B, C and D, indicates that GO nanosheets were completely and perfectly covered the polymer chains due to hydrogen bondings and ionic interactions, no bare GO were exposed in the gel structure.

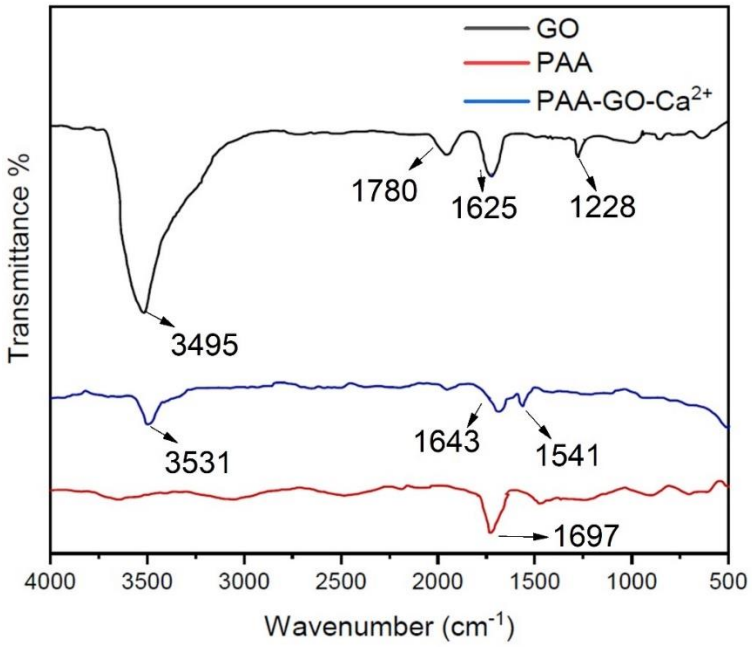

Figure 2. FTIR spectra of pristine PAA hydrogel, PAA-GO hydrogel and PAA-GO-Ca^{2+} hydrogel.

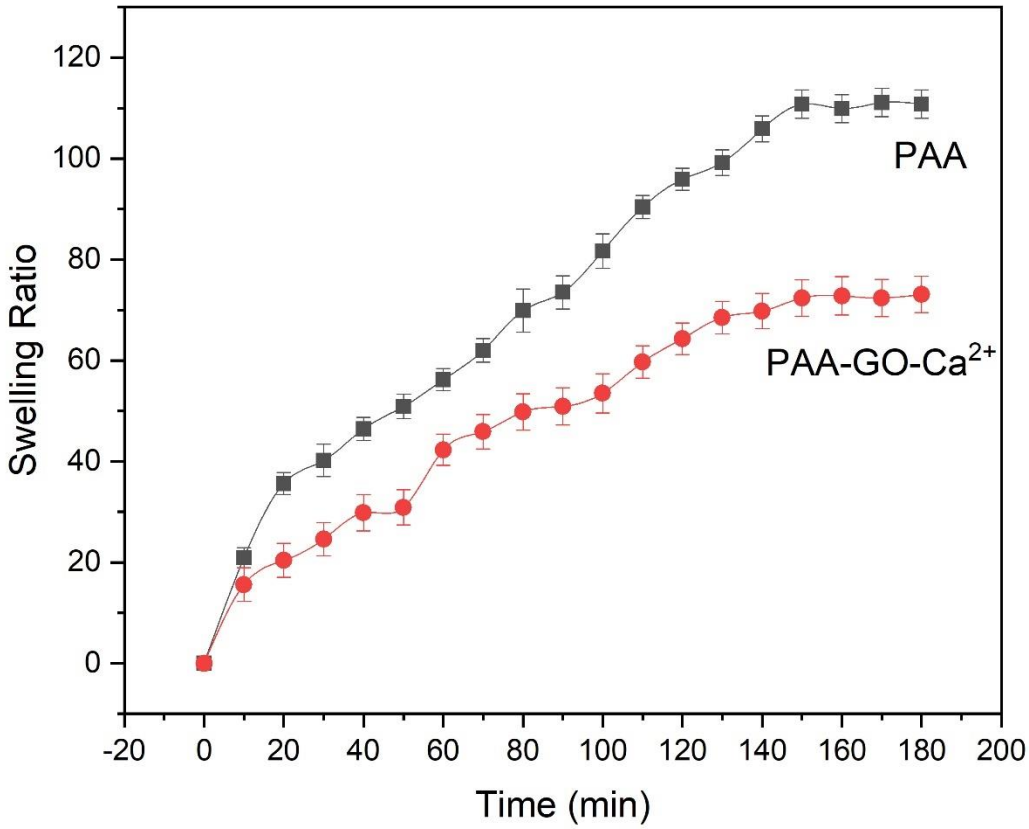

Figure 3. Swelling kinetics behavior of PAA and PAA-GO-Ca^{2+}hydrogels at room temperature.

A

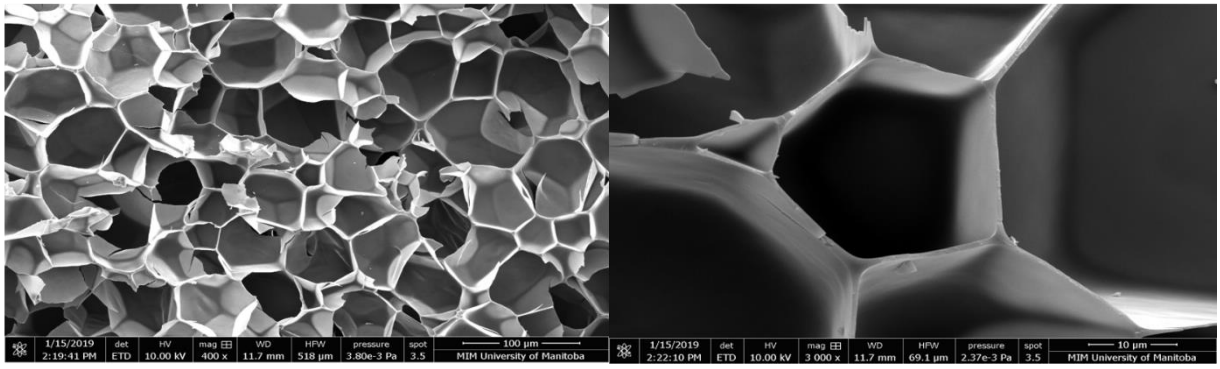
1/15/2019 2:19:41 PM det ETD HV 10.00 kV mag 400 x WD 11.7 mm HFW 518 µm pressure 3.80e-3 Pa spot 3.5 100 µm MIM University of Manitoba
1/15/2019 2:22:10 PM det ETD HV 10.00 kV mag 3 000 x WD 11.7 mm HFW 69.1 µm pressure 2.37e-3 Pa spot 3.5 10 µm MIM University of Manitoba

B

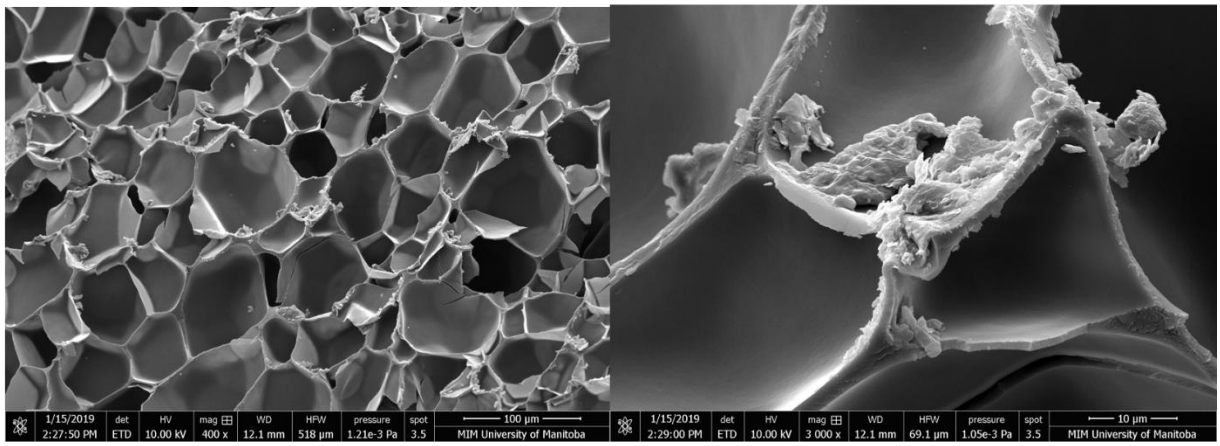
1/15/2019 2:27:50 PM det ETD HV 10.00 kV mag 400 x WD 12.1 mm HFW 518 µm pressure 1.21e-3 Pa spot 3.5 100 µm MIM University of Manitoba
1/15/2019 2:29:00 PM det ETD HV 10.00 kV mag 3 000 x WD 12.1 mm HFW 69.1 µm pressure 1.05e-3 Pa spot 3.5 10 µm MIM University of Manitoba

C

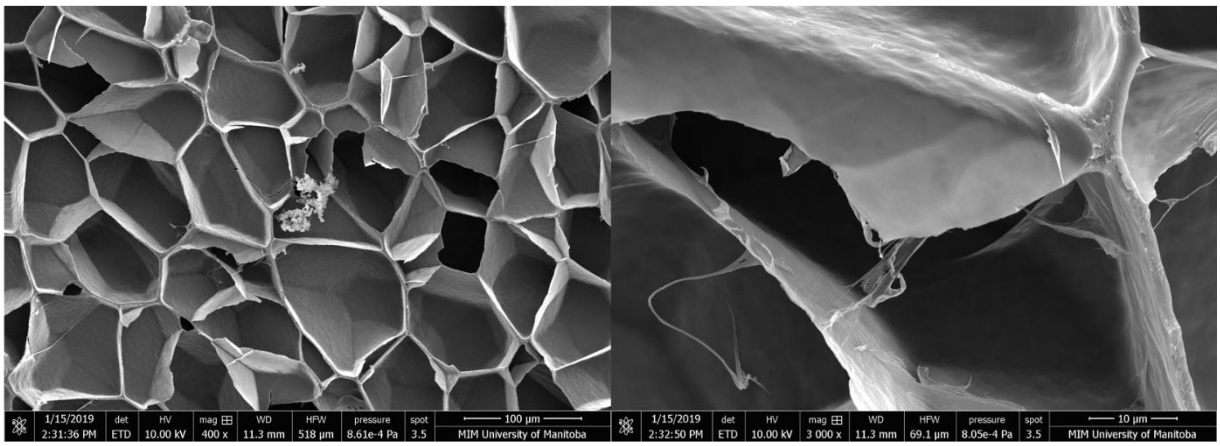
1/15/2019 2:31:36 PM det ETD HV 10.00 kV mag 400 x WD 11.3 mm HFW 518 µm pressure 8.61e-4 Pa spot 3.5 100 µm MIM University of Manitoba
1/15/2019 2:32:50 PM det ETD HV 10.00 kV mag 3 000 x WD 11.3 mm HFW 69.1 µm pressure 8.05e-4 Pa spot 3.5 10 µm MIM University of Manitoba

D

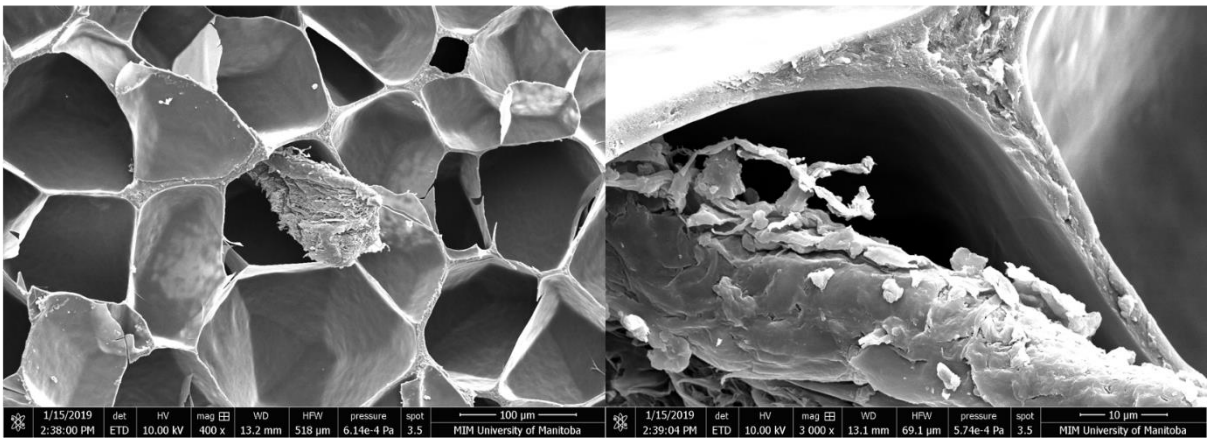

Figure 4. SEM images of pure PAA hydrogel and PAA-GO-Ca^{2+}hydrogels with different GO ratio of 3%,5% and 8%. All the images on the left are with a lower magnification of 400 times and all the images on the right are with a higher magnification of 3000 times.

4.2 Results for Tensile Tests

Extraordinary mechanical properties can only be achieved in the developed hydrogel by an optimum balance between the hydrogen bonding and ionic interaction that were introduced into the PAA hydrogel network. The density of hydrogen bonding can be tuned by controlling GO content, and the density of ionic interaction can be controlled by Ca^{2+} amount. Therefore, massive experiments with different amount of GO and Ca^{2+} were conducted to investigate the effects of these two physical bondings on the mechanical properties of the hydrogels. The content of the chemical crosslinker MBA was fixed at 0.075wt% in all experiments to exclude the effect of the chemical crosslinker.

4.2.1 Results for Tensile Tests with Different GO Contents

Rectangular samples for tensile tests with different GO (0, 3%, 5%, 8%) but the same Ca^{2+} content of 10% content were performed to determine the impact of GO content on mechanical properties of hydrogels. Typical strain-stress curves of hydrogels with different GO contents are presented in Figure 5A. It is obvious that with the increase in GO content, both the tensile strength and elongation increase dramatically until the GO content reaches 5%, when the hydrogels (PAA-$GO_{5\%}$)

were capable of more than triple their elongation at break as compared to pristine PAA hydrogels, from the strain at break of about 9 to nearly 25, and the hydrogels improved their tensile strength by 950%, from 70.53KPa to 741.90KPa. Further increase in GO content, however, leads to a substantial decrease in both elongation stress and strain, although a continuous increase in Young's modulus is still observed as shown in Figure 5B. This is due to the fact that GO tend to amalgamate easily at a high concentration especially when there are abundant crosslinking sites, e.g., calcium ions. Therefore, a moderate GO content of 5% has been found to optimize the mechanical stretchability and toughness of the PAA hydrogels.

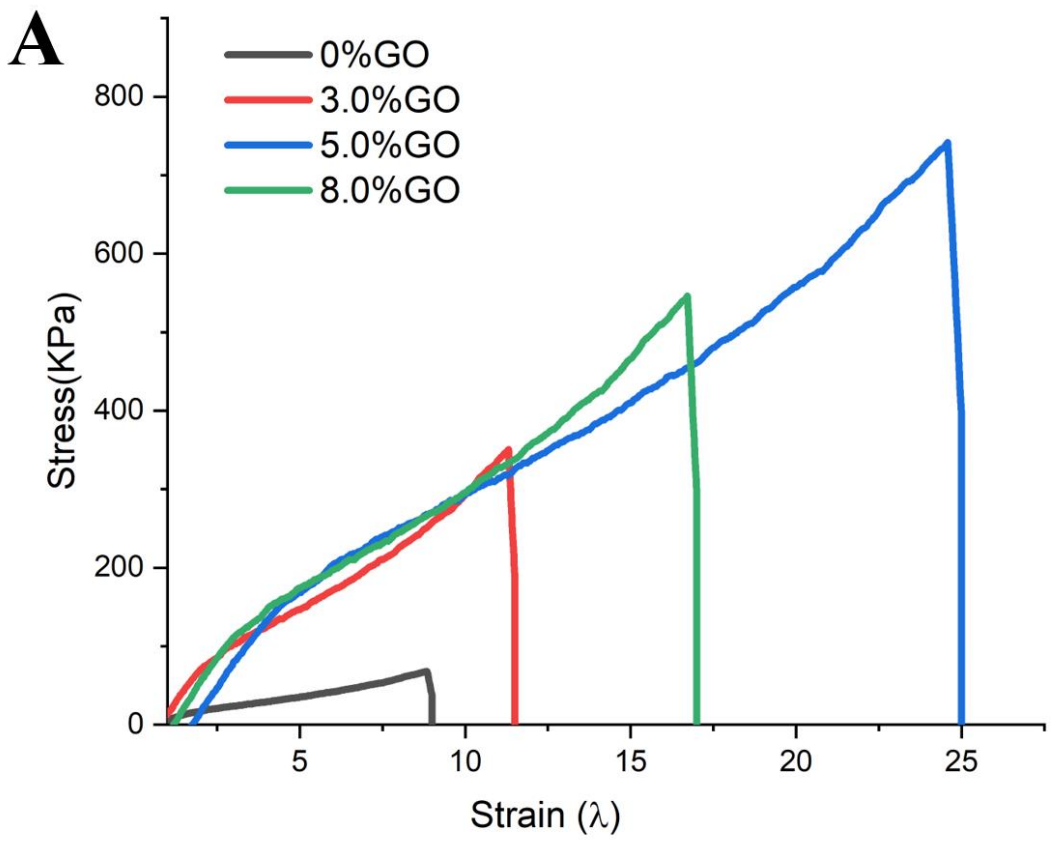

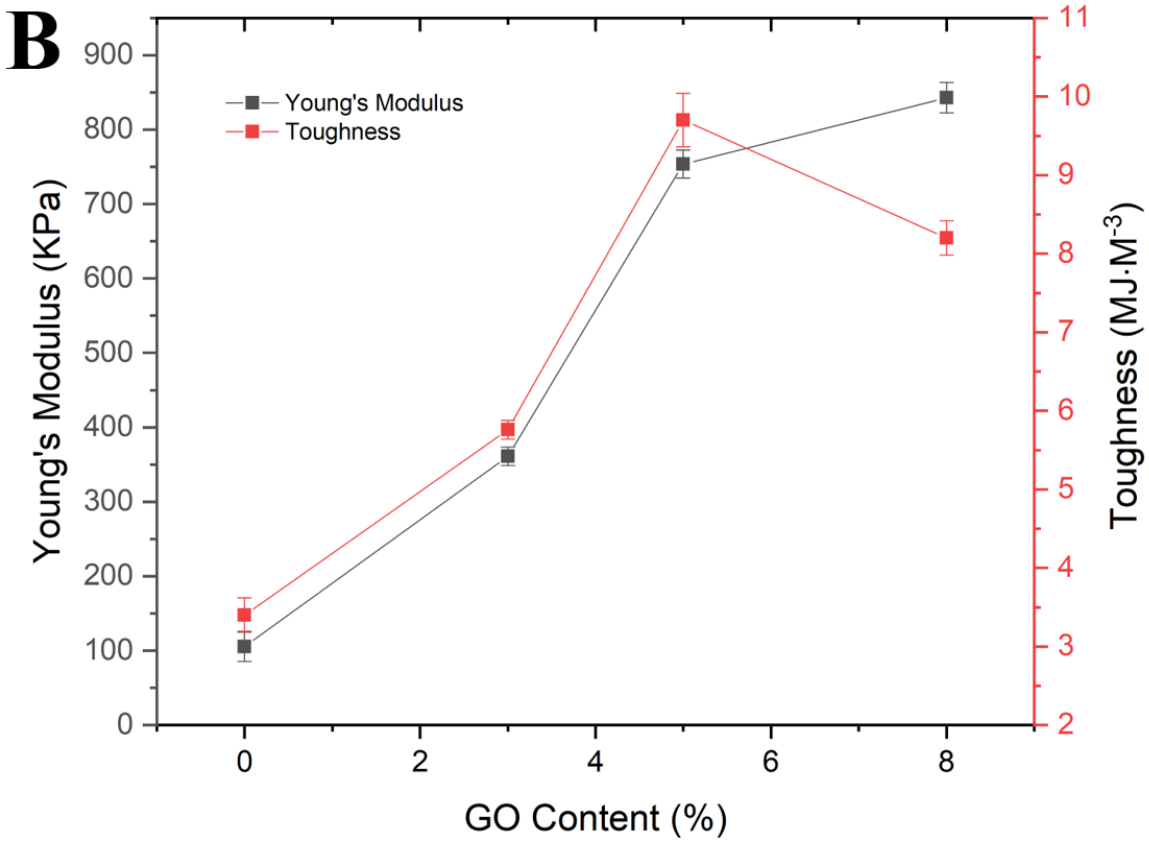

Figure 5. A) Stress-strain curves for tensile tests on hydrogels with different GO contents. B) Young's modulus and toughness.

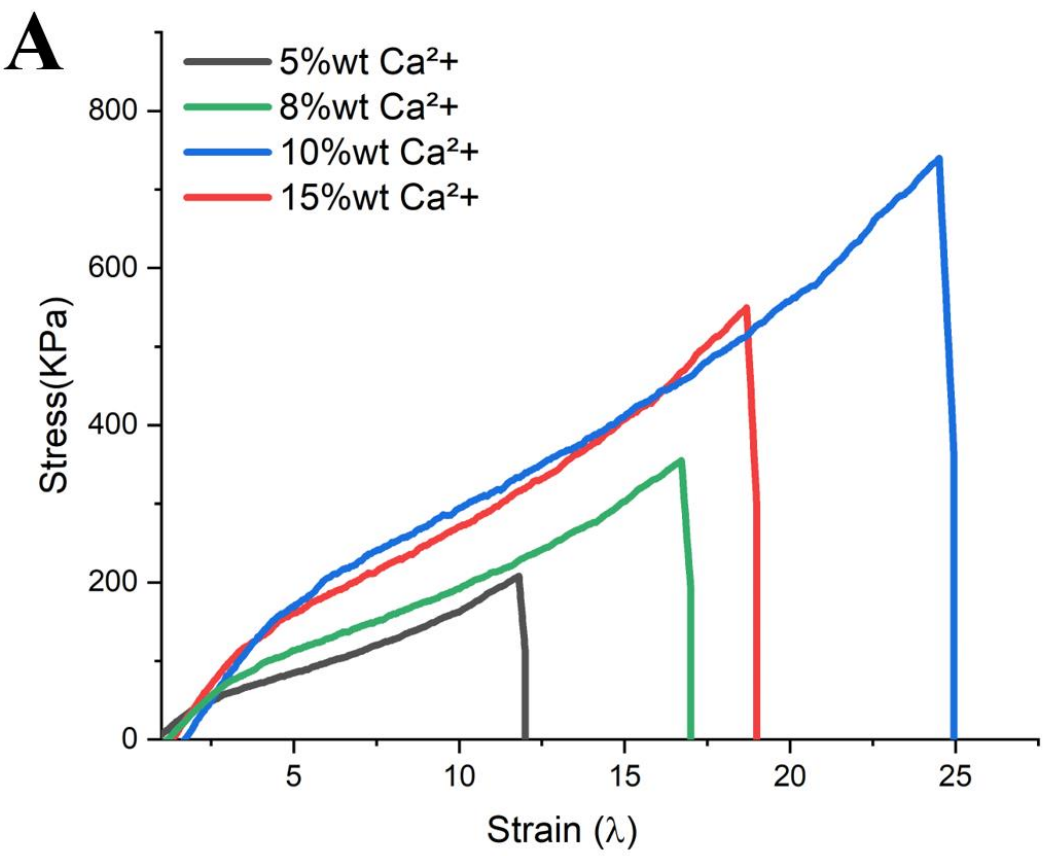
A
5%wt Ca²+
8%wt Ca²+
10%wt Ca²+
15%wt Ca²+
Stress(KPa)
800
600
400
200
0
5
10
15
20
25
Strain (λ)

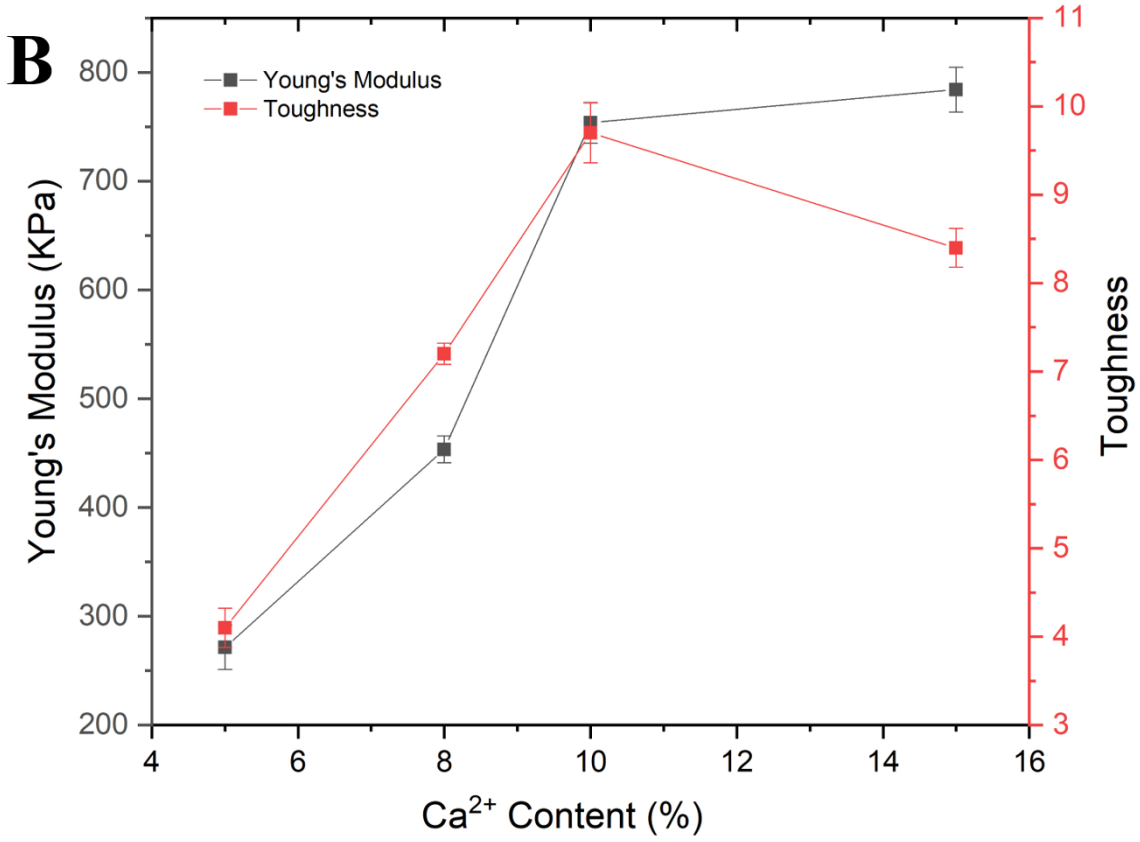

Figure 6. A)Tensile tests on hydrogels with different amounts of Ca^{2+} crosslinker. B) Young's modulus and toughness for hydrogels with different amounts of Ca^{2+} crosslinker.

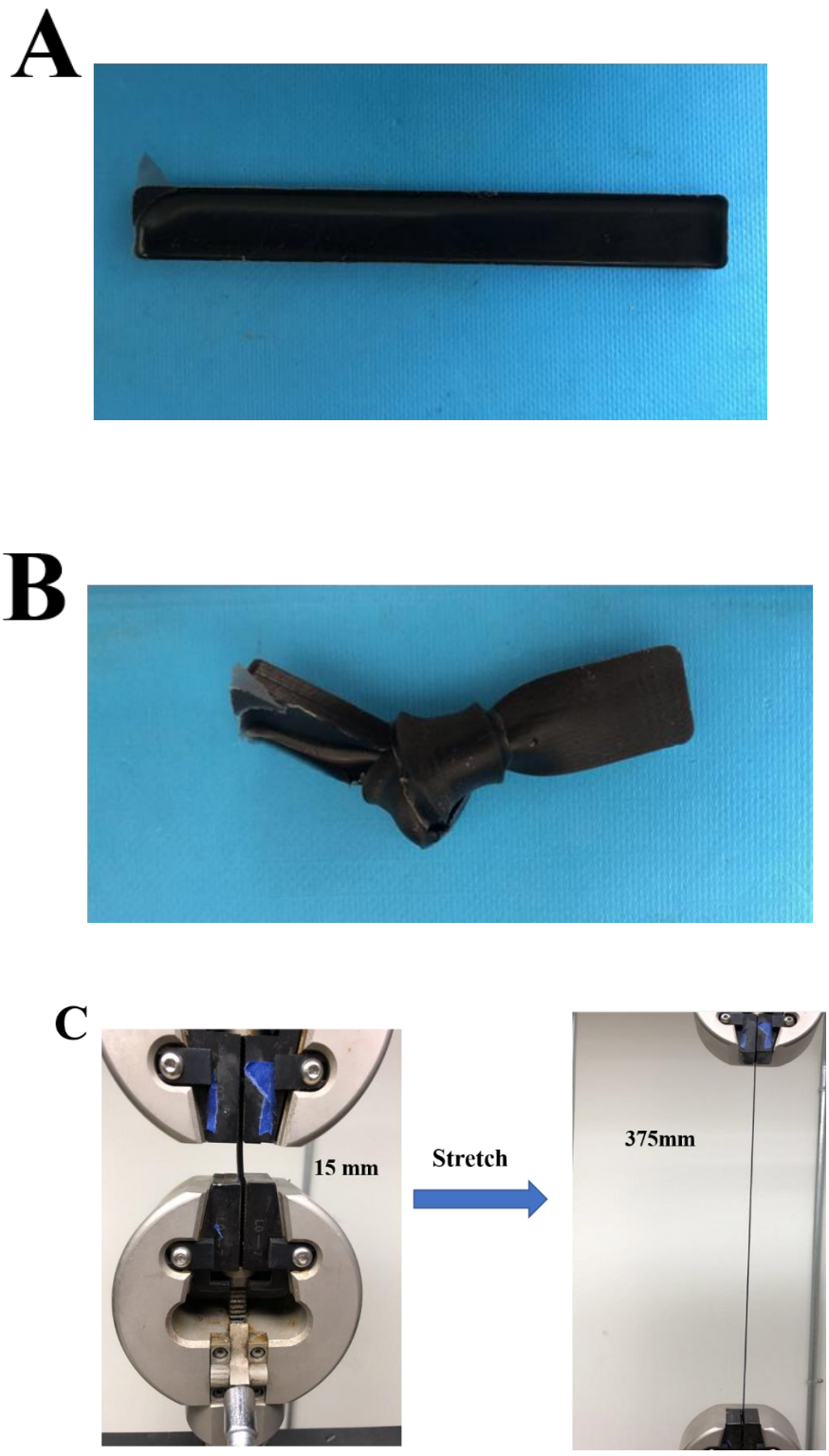

Figure 7. A) Picture of PAA-GO-Ca^{2+}hydrogel. B) A strip of PAA-GO-Ca^{2+} hydrogel in a knot. C) The PAA-GO-Ca^{2+} hydrogel sample fixed between two clips of a tensile tester with a lap distance of 15mm.Tested sample can be extended to 375mm which is 25 times longer than the original length.

4.2.2 Results for Tensile Tests with Different Ca^{2+} Contents

Another important factor that may contribute to the excellent mechanical behavior is the contents of Ca^{2+}. Samples were prepared with the same GO content of 5% but different amount of Ca^{2+} of 5%, 8%,10%,and 15%. Their stress-strain curves are illustrated in Figure 6A. As shown in Figure 6A with the increase of Ca^{2+} from 5% to 10%, the elongation at break, Young's modulus, tensile strength and toughness of the hydrogels experience remarkable increases. When the Ca^{2+} content is above to 15%, however, only Young's modulus of the hydrogels remain a continuous increase and all other properties degrade. The mechanism is that the higher the Ca^{2+} contents, the higher the crosslinking density, an increasing in crosslinking density at certain range leads to enhanced mechanical properties of hydrogels, but excessive crosslinking density beyond a certain point may overly increase the stiffness (i.e., Young's modulus) but reduce the stretchability and consequently lead to a decrease in toughness, as shown in Figure 6B.

In a polymer hydrogel system, the stretchability and stiffness are usually inversely related, depending on the degree of crosslinking in the polymer network. A higher crosslinking density can improve the stiffness but sometimes may sacrifice the stretchability of the hydrogel. As a result, most traditional hydrogels are either stretchable but soft with low modulus, or hard but brittle with a relatively high modulus. In this work, we attempted to find appropriate levels of crosslinking in order to optimize the mechanical properties of PAA hydrogels. It has been discussed above that GO content is a critical factor for crosslinking density because GO can provide both abundant oxygen-containing groups for hydrogen bonding, and sufficient carboxyl groups for ionic crosslinking, as shown in Figure 5B. With the increase of GO content in the PAA hydrogel system, the stiffness of the hydrogel went all the way up with the increase in crosslinking density; however, the stretchability went up initially with the increase in GO content but dropped after the GO content exceeded 5%, because an overly high crosslinking density can bring down the stretchability and thus lead to a decrease in toughness.

Ca^{2+} is another important factor for the crosslinking density of hydrogels. According to Figure 6B, Young's modulus underwent steady increase with the addition of Ca^{2+}, but the stretchability and toughness experienced a significant drop when the Ca^{2+} content was beyond 10%, indicating that 10% Ca^{2+} can provide the best crosslinking density which can improve stiffness without deteriorating stretchability and toughness of the hydrogel. Therefore, we chose the hydrogel with 5% GO content and 10% Ca^{2+} for further studies on its application in wearable biosensors. The resulting PAA-GO-Ca^{2+} hydrogel has a uniform shape as shown in Figure 7A and can easily withstand massive deformation like twisting as shown in Figure 7B. It can also be stretched to as much as 25 times of its original length as illustrated in Figure 7C.

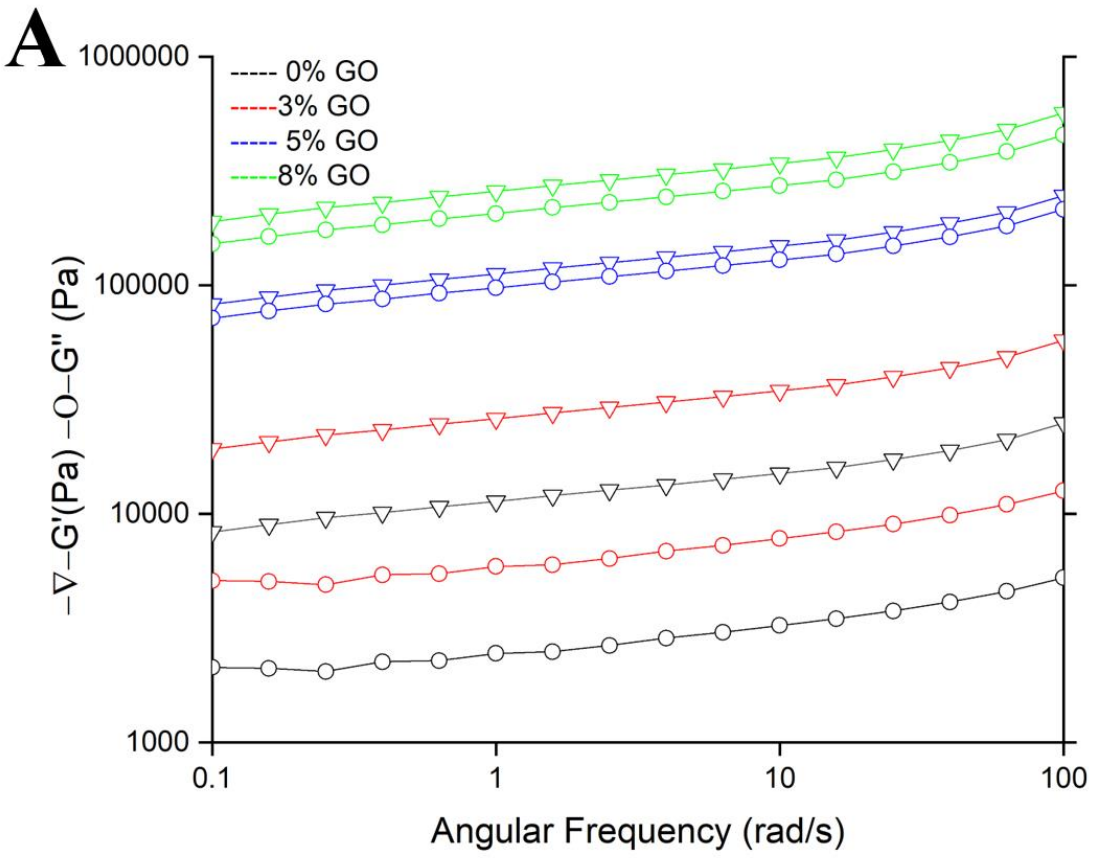

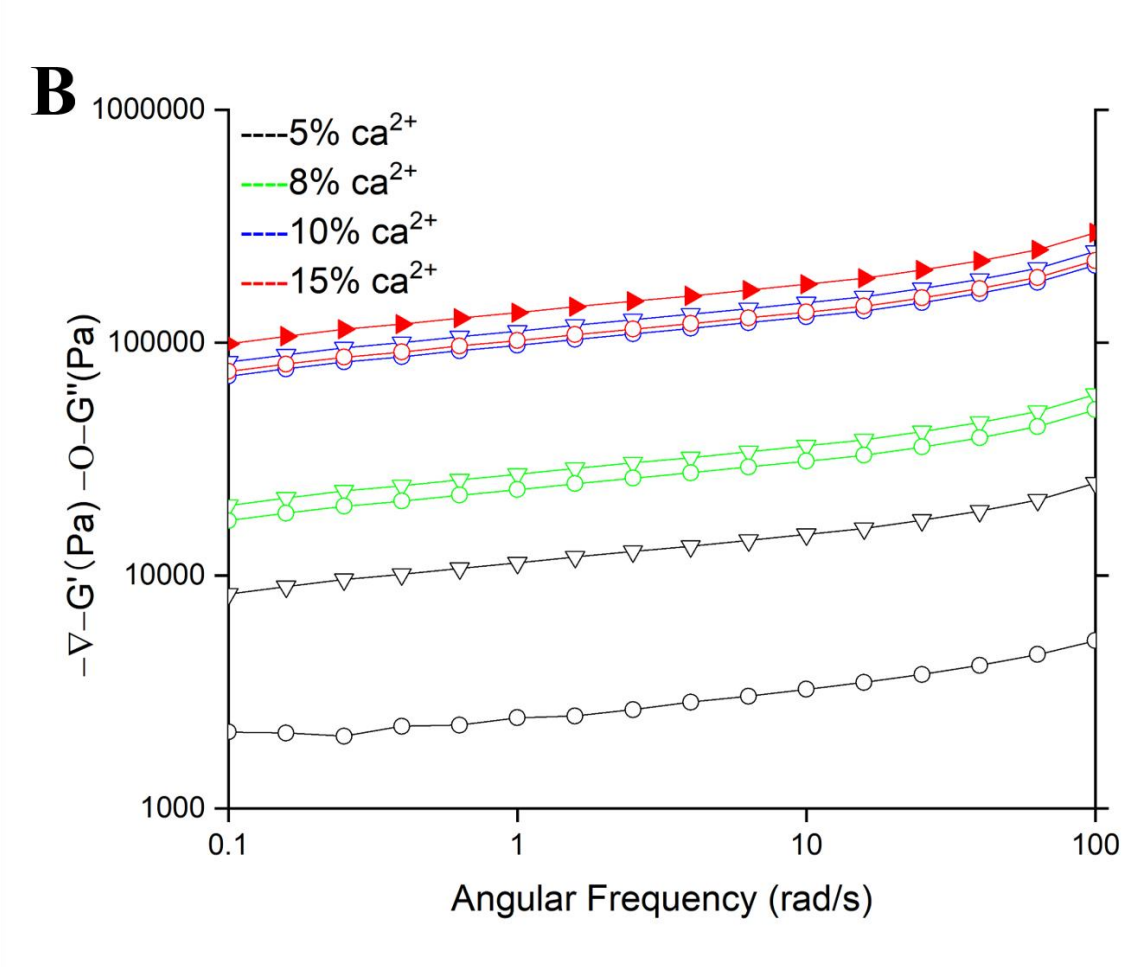

Figure 8. Rheology tests for hydrogels with different GO and Ca^{2+} contents. All tests were carried out with a fixed strain of 0.5% and changing angular frequencies ranging from 0.1 to 100rad/s. A) Samples with different GO contents and B) with different Ca^{2+} content.

4.3 Results of Rheology Tests

Rheology tests were also performed to better understand the effect of GO and Ca^{2+} contents on the mechanical properties of hydrogels. The oscillation strain dependence of the storage modulus G' and loss modulus G'' were tested at a fixed strain 0.5% which ensured enough sensitivity but still the availability of the linear viscoelasticity. All tests were carried out at a changing angular frequency ranging from 0.1 to 100 rad/s. As shown in Figures 8A and 8B, G' is always higher than G'', indicating complete crosslinking networks formed in all samples. To understand the effect of GO contents on hydrogels' mechanical behaviors, Ca^{2+} was fixed at 10% for samples with different GO contents. The higher the GO contents, the higher the modulus values, which agrees with the

results from the tensile tests. Similarly, the GO content was fixed at 5% for samples with varied Ca^{2+} contents. It is shown that a higher Ca^{2+} content gives rise in both G' and G'', which agrees well with the results in tensile tests.

4.4 Results of Cyclic Tensile Tests

In addition to high toughness and excellent stretchability, the PAA-GO-Ca^{2+} hydrogels also possess a superb energy dissipation recovery, which was evaluated by loading-unloading cyclic tensile tests. As the results are shown in Figure 9A. A sample was stretched eight times of its original length during loading. Upon unloading, the hydrogel shows a relatively large hysteresis loop with dissipated energy of ~ 0.67MJm^{-3}. If the second loading-unloading cycle was performed right after the first cycle without any recovery time, the hysteresis loop was much smaller with dissipated energy of 0.22 MJm^{-3}. If the tested sample was allowed to recover for 5 minutes after the first cycle, there is an obvious recovery in the dissipated energy to ~ 0.56 MJm^{-3}. As shown in Figure 9B, more recovery time leads to a better energy dissipation recovery: when the recovery time was 10 minutes, the energy dissipation reached 0.63 MJm^{-3}; and when the recovery time was 15 minutes, the energy dissipation had an almost full recovery to ~ 0.65 MJm^{-3} , which was a 97.01% of recovery .

Cyclic tensile tests were further conducted on PAA-GO-Ca^{2+} hydrogels with a 15-minute recovery time allowed between each two loading-unloading cycles. The stress-strain curves are shown in Figure 10A. The recovery rates of both Young's modulus and dissipated energy (Figure 10B) were calculated to show the PAA-GO-Ca^{2+} hydrogels' recovering capacity in both stiffness and toughness after different loading cycles. It can be seen that the PAA-GO-Ca^{2+} hydrogel recovered 93.4% of its stiffness and 92.3% of its toughness after 5 loading-unloading cycles. The hydrogel maintained 83.2% of its Young's modulus and 57.4% of its toughness after 15 loading-unloading cycles, indicating its excellent fatigue resistance and outstanding recovery capacity after deformation.

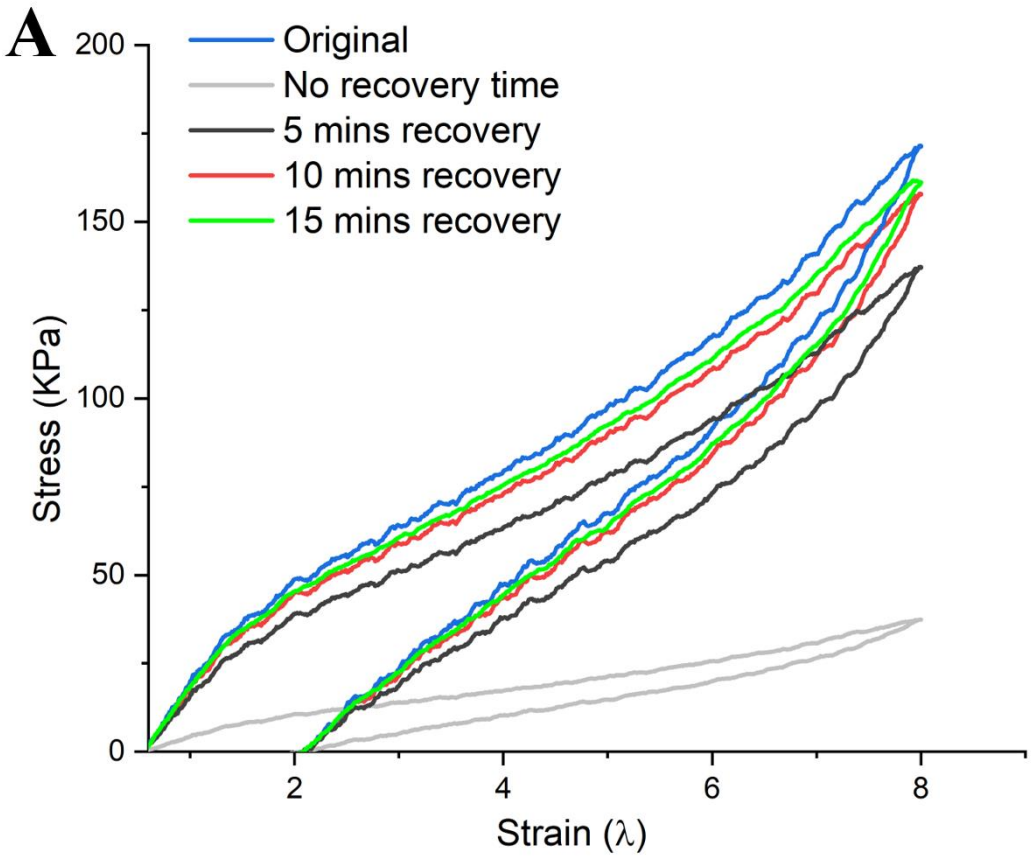
A
Original
No recovery time
5 mins recovery
10 mins recovery
15 mins recovery
Stress (KPa)
200
150
100
50
0
2
4
6
8
Strain (λ)

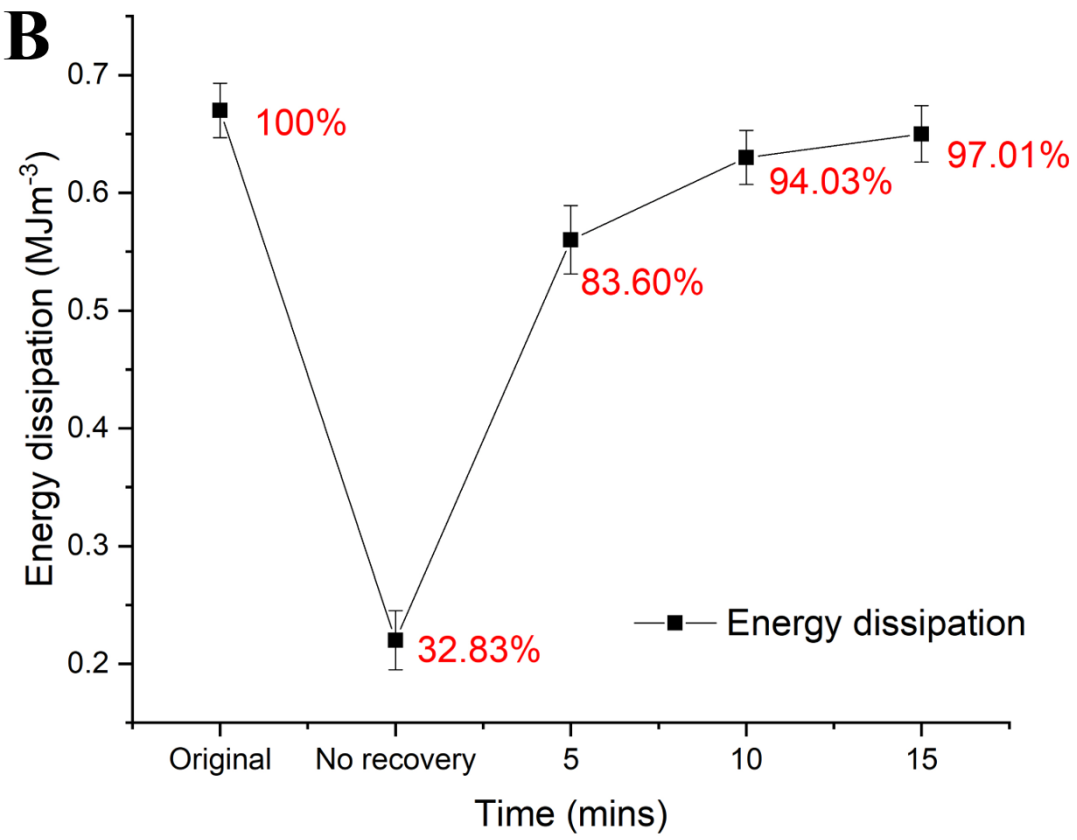

Figure 9.Cyclic tensile tests on PAA-GO-Ca^{2+} hydrogels with 5% GO, and 10% Ca^{2+}, the maximum strain was 8 times of the original length. A) Hysteresis loops obtained from cyclic tests on hydrogels with different recovery times (0, 5, 10,15 minutes). B) The rate of dissipated energy recovery vs. time of recovery.

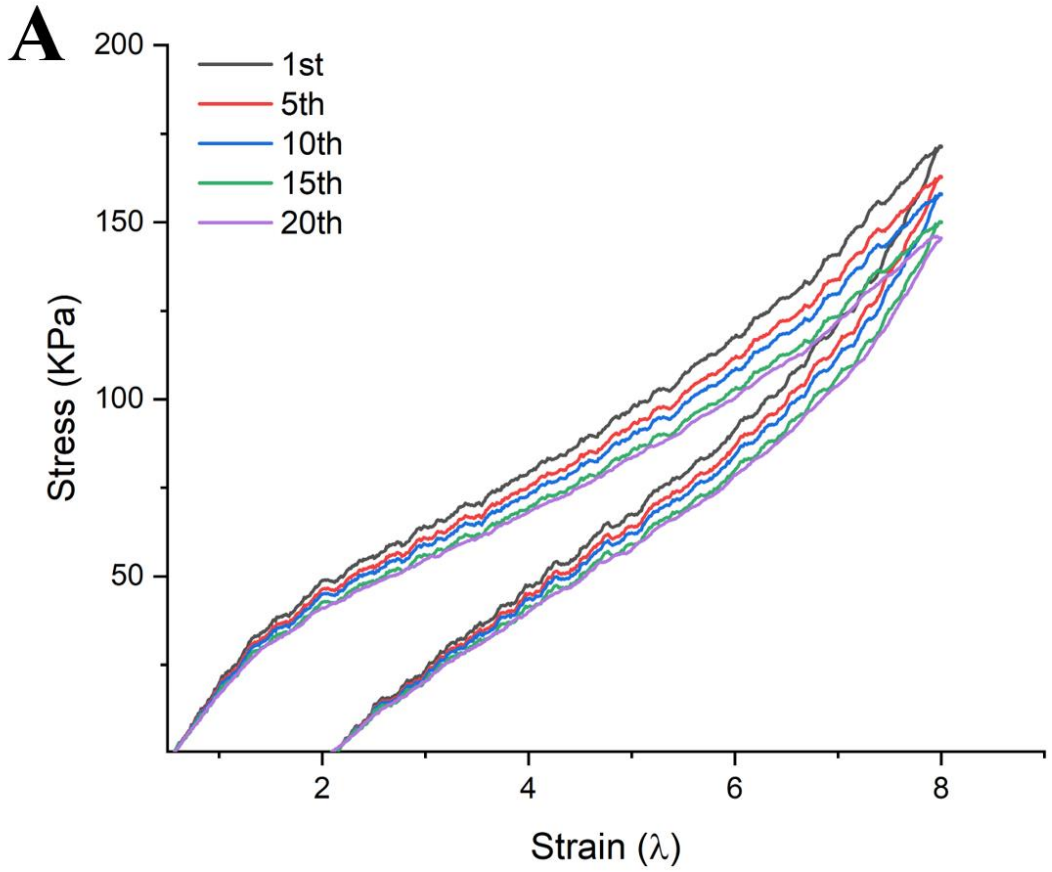
A
200
150
100
50
Stress (KPa)
1st
5th
10th
15th
20th
2
4
6
8
Strain (λ)

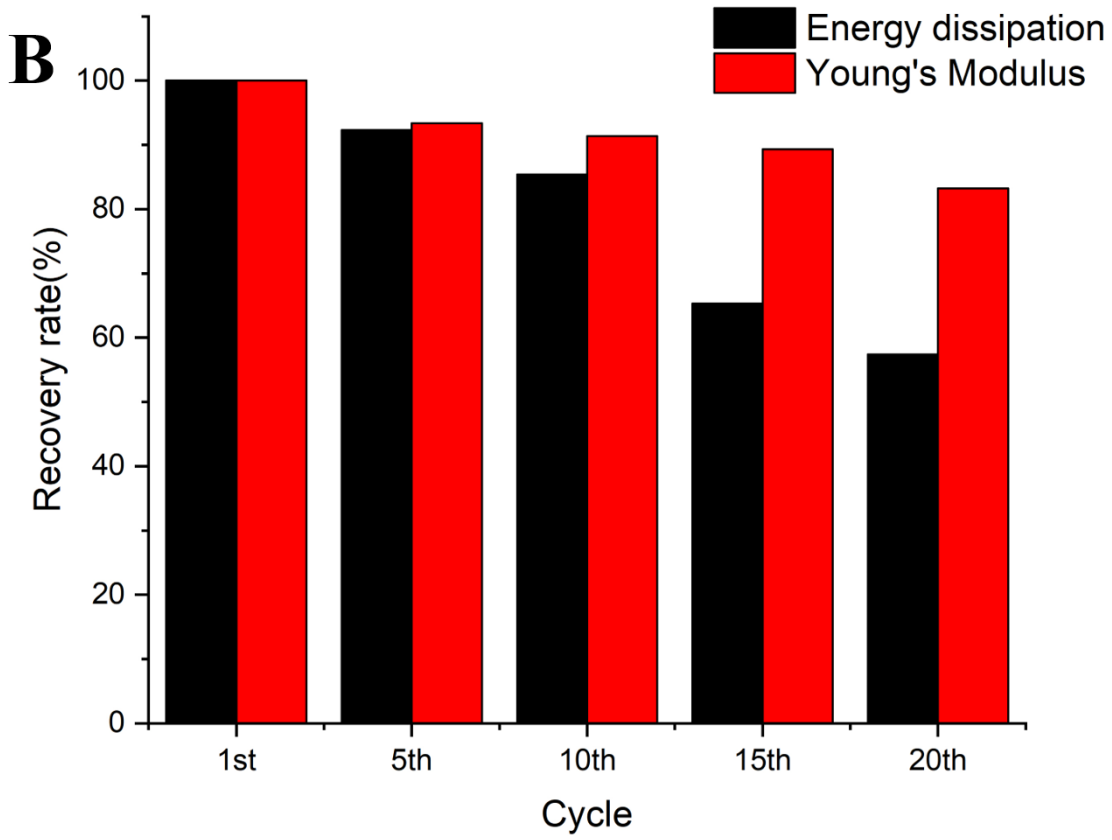

Figure 10. A) Up to 20 times of cyclic tests on PAA-GO-Ca^{2+} hydrogels with a 15-minute break between each two cycles. B)Recovery rates of energy dissipation and Young's modulus after different cycles

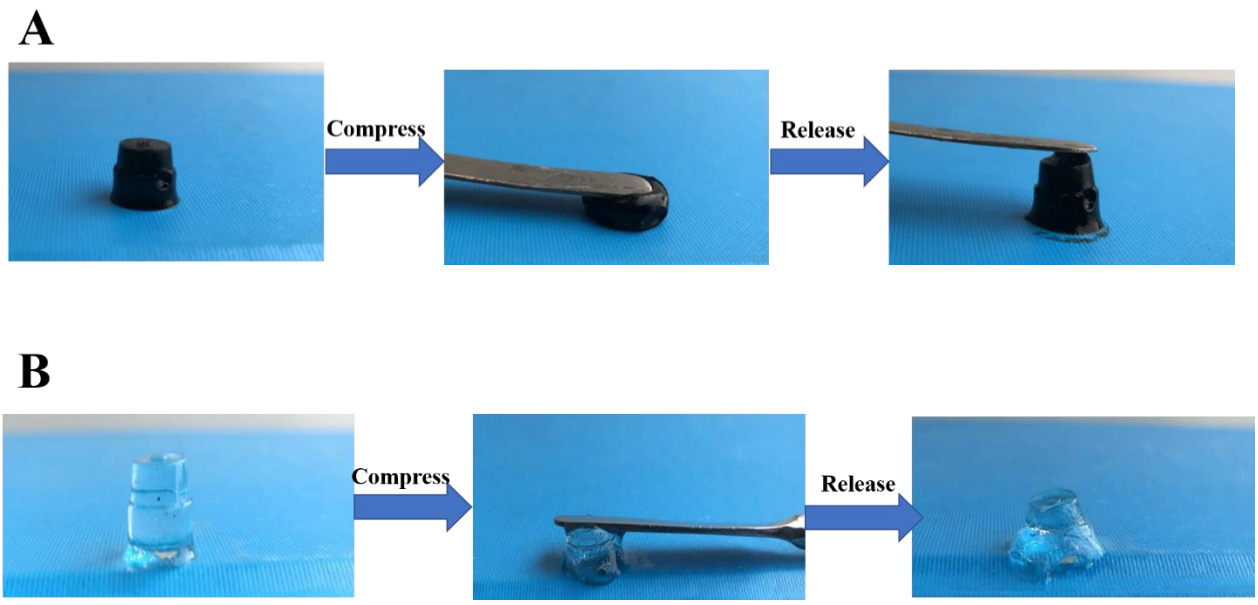

Figure 11. A) A PAA-GO-Ca^{2+} hydrogel fully restores its original shape when a compressive load is released. B) A pristine PAA hydrogel cannot restore its original shape after a compressive load is released.

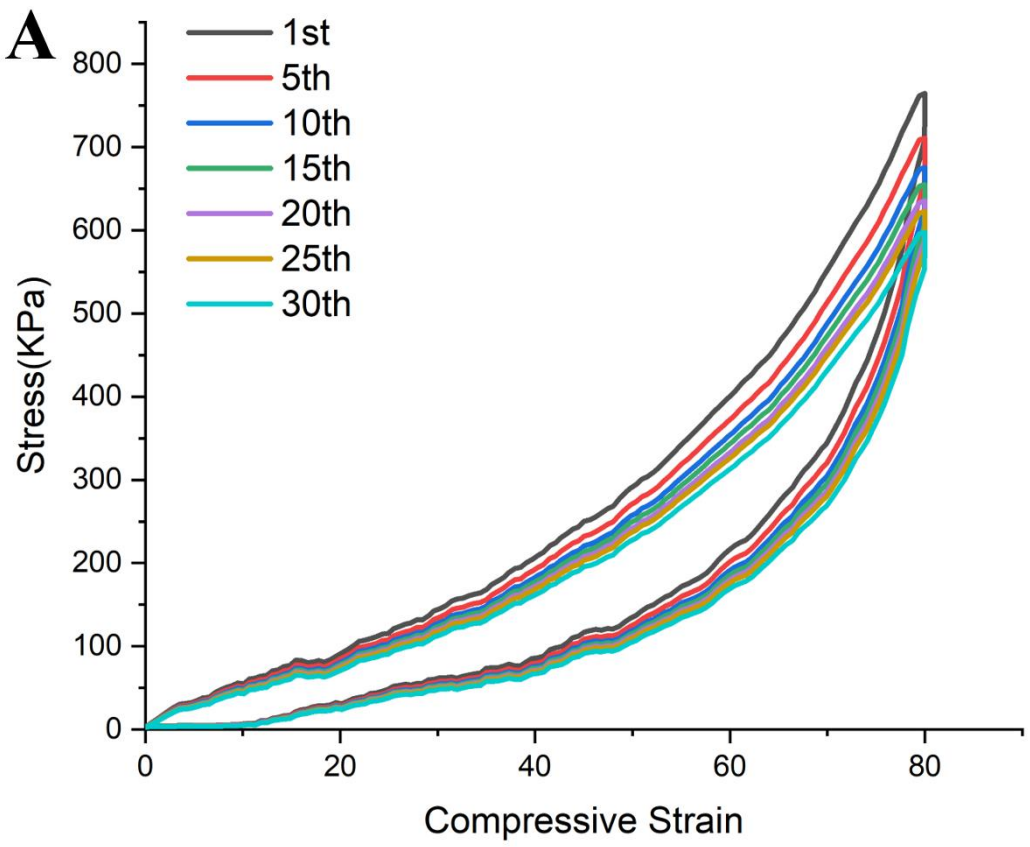

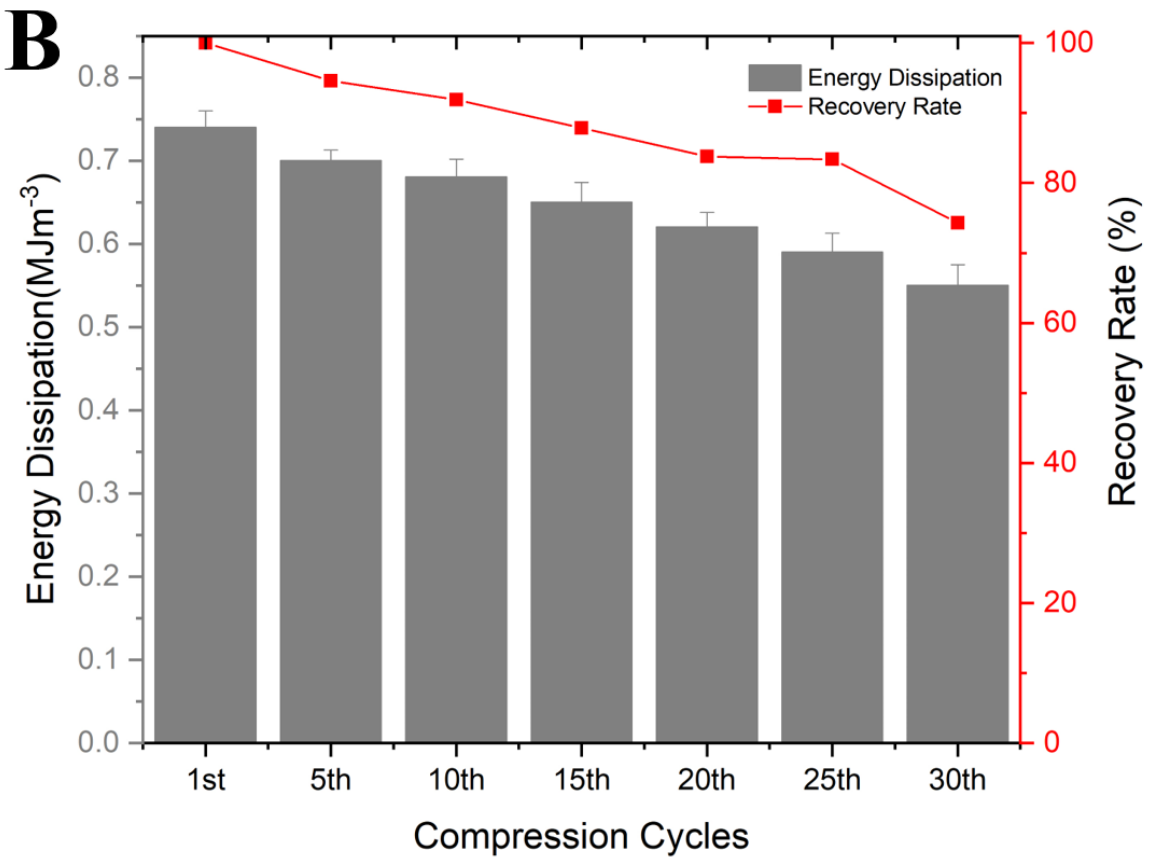

Figure 12. Results for cyclic compression tests A) Stress-strain curves of cyclic compression tests. B) Energy dissipation and its recovery rate in cyclic compression tests on PAA-GO-Ca^{2+} hydrogels. PAA-GO-Ca^{2+} hydrogels with 5% GO, and 10% Ca^{2+} were used in cyclic compression tests with a maximum strain of 80%.

4.5 Results for Cyclic Compression Tests

Cyclic compression tests were conducted to evaluate the compressive fatigue resistance and recovery of the developed hydrogels. As shown in Figure 11A, the PAA-GO-Ca^{2+} hydrogel is highly compressive and fully restores its original shapes upon the removal of strain. PAA pristine hydrogel, in contrast, demonstrates permanent deformation after removal of the compression load, indicating a great improvement in compressive resistance for PAA-GO-Ca^{2+} hydrogels. Compressive loading-unloading tests were repeated 30 times on a sample at a strain of 80% with a 60 seconds break between each two cycles. The typical compression stress-strain curves for all

cycles are shown in Figure 12A, which shows almost full recovery of the hydrogel to its original shape after a different number of test cycles, indicating recoveries of all the elastic deformations. It can be seen from Figure 12B that the energy dissipation decreases from 0.74 to 0.55KJm^{-3} but still retains a 74.32% recovery rate after 30 test cycles, indicating that the PAA-GO-Ca^{2+} hydrogel can sustain massively compressive stresses repeatedly. All in all, it is evident from these mechanical test results that the developed PAA-GO-Ca^{2+} hydrogel is a high-performance material with a combination of high stiffness, high toughness, superelasticity, and excellent resistance to both tensile and compressive fatigue.

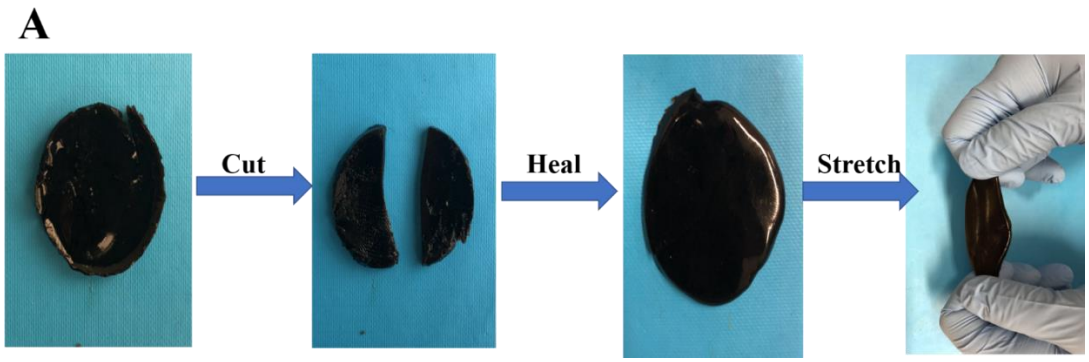

B



Figure 13. A) Self-healing test on a PAA-GO-Ca^{2+} hydrogel (5% GO and 10% Ca^{2+}) in a disk shape, which was bisected and subsequently allowed to heal. B)Microscope image of the healed hydrogel, the dark area represents the trace of cut after healing and reconnection.

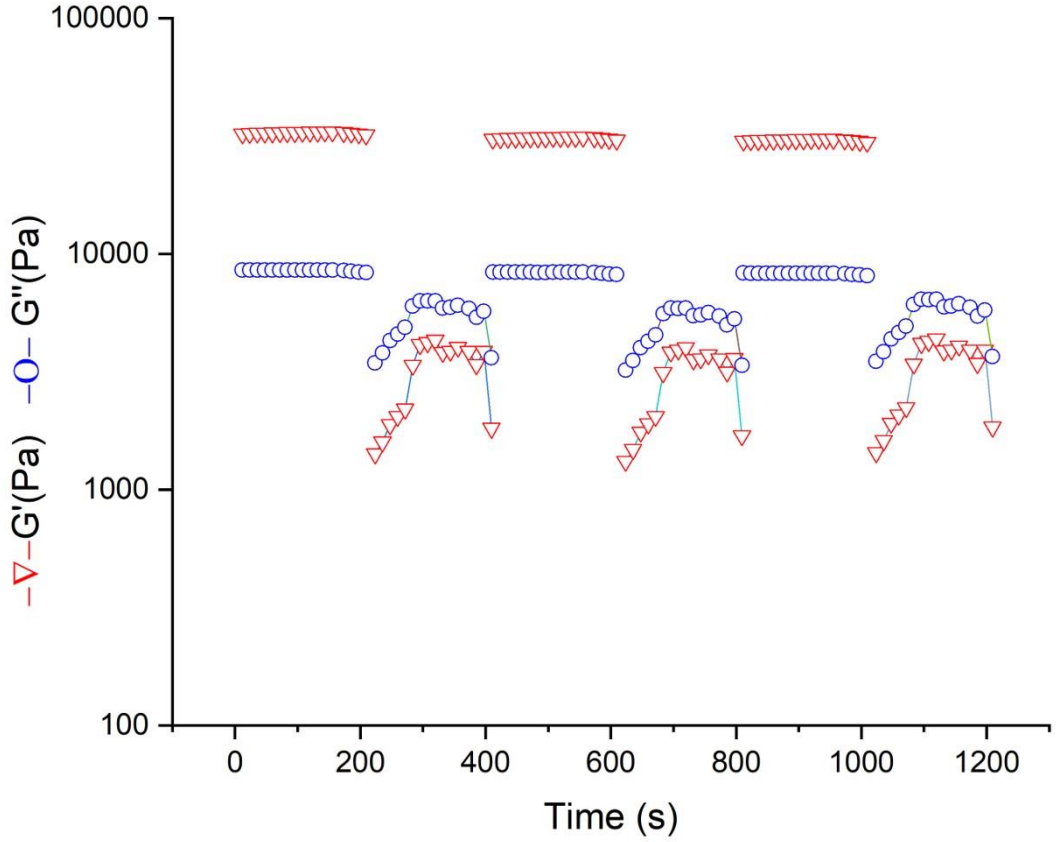

Figure 14. Rheology tests: G' and G'' were measured when alternative strain switched from a small strain of 1% (λ=1%) to a large strain of 400% (λ=400%) at a fixed frequency of 10 rads^{-1}. Each strain was kept for 200s.

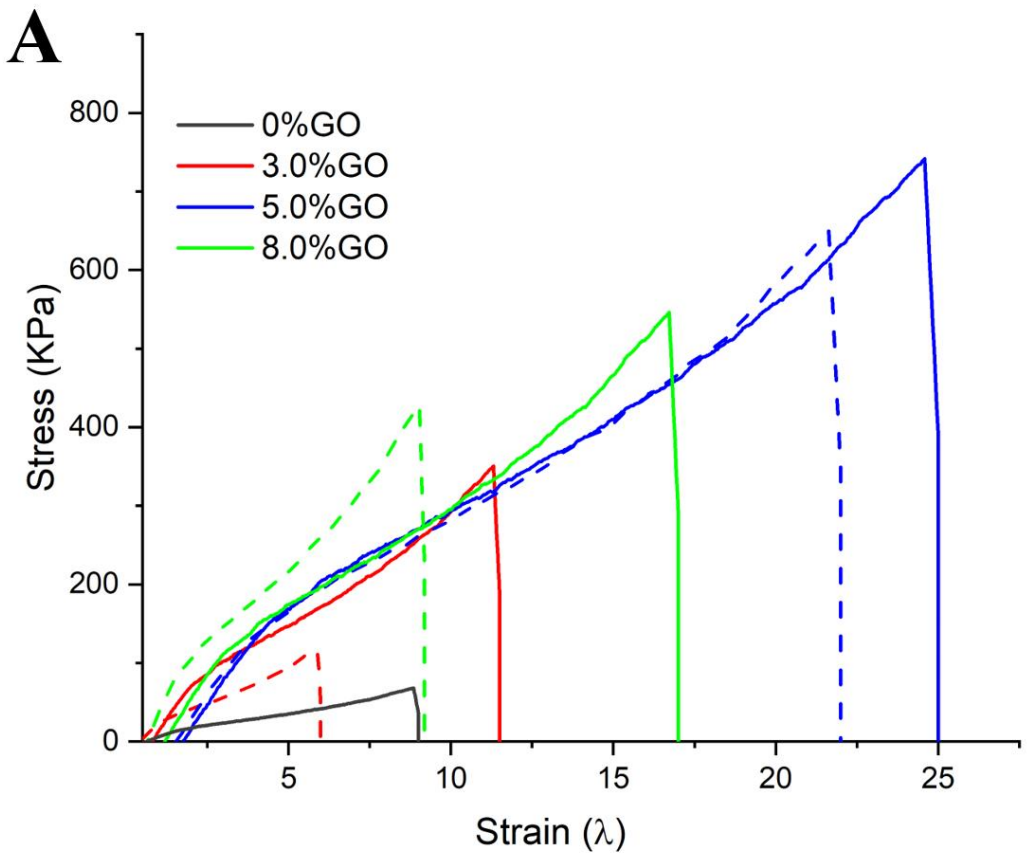
A
0%GO
3.0%GO
5.0%GO
8.0%GO
Stress (KPa)
800
600
400
200
0
5
10
15
20
25
Strain (λ)

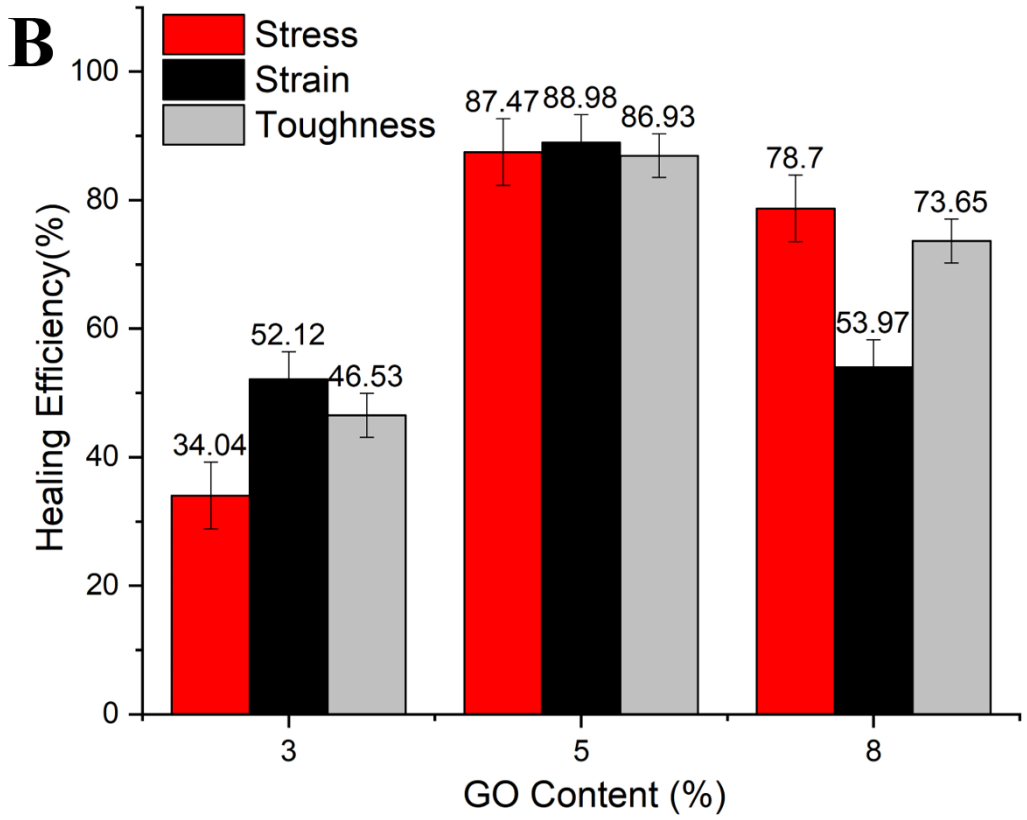

Figure 15. (A) Self-healing mechanical behavior of hydrogels with different GO ratio (B) Corresponding healing efficiency in tensile stress, tensile strain and toughness.

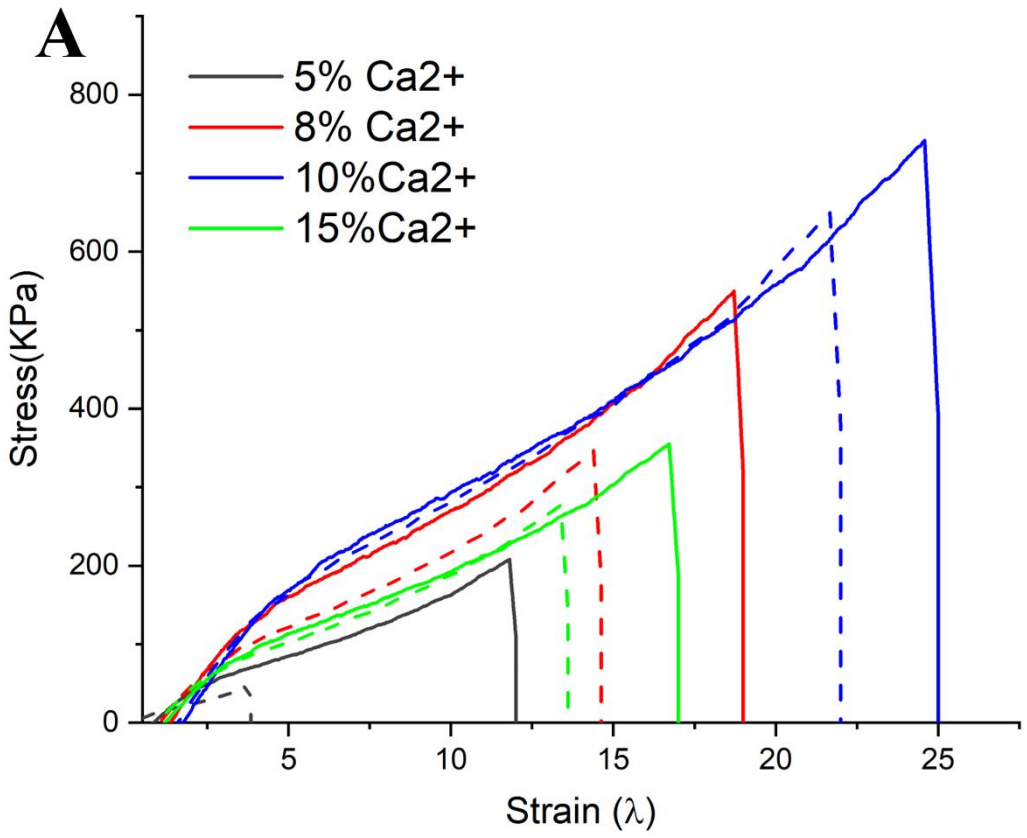
A
5% Ca2+
8% Ca2+
10%Ca2+
15%Ca2+
Stress(KPa)
800
600
400
200
0
5
10
15
20
25
Strain (λ)

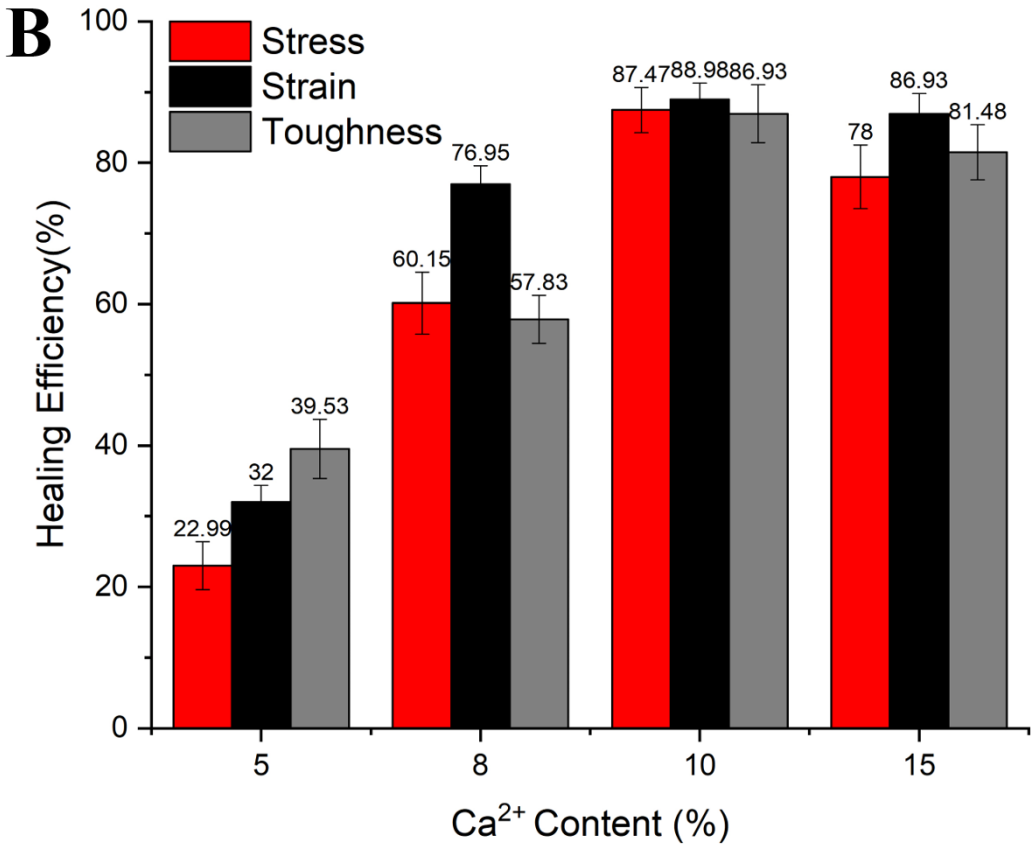

Figure 16. (A) Self-healing mechanical behavior of hydrogels with different Ca^{2+} ratio (B) Corresponding healing efficiency in tensile stress, tensile strain and toughness.

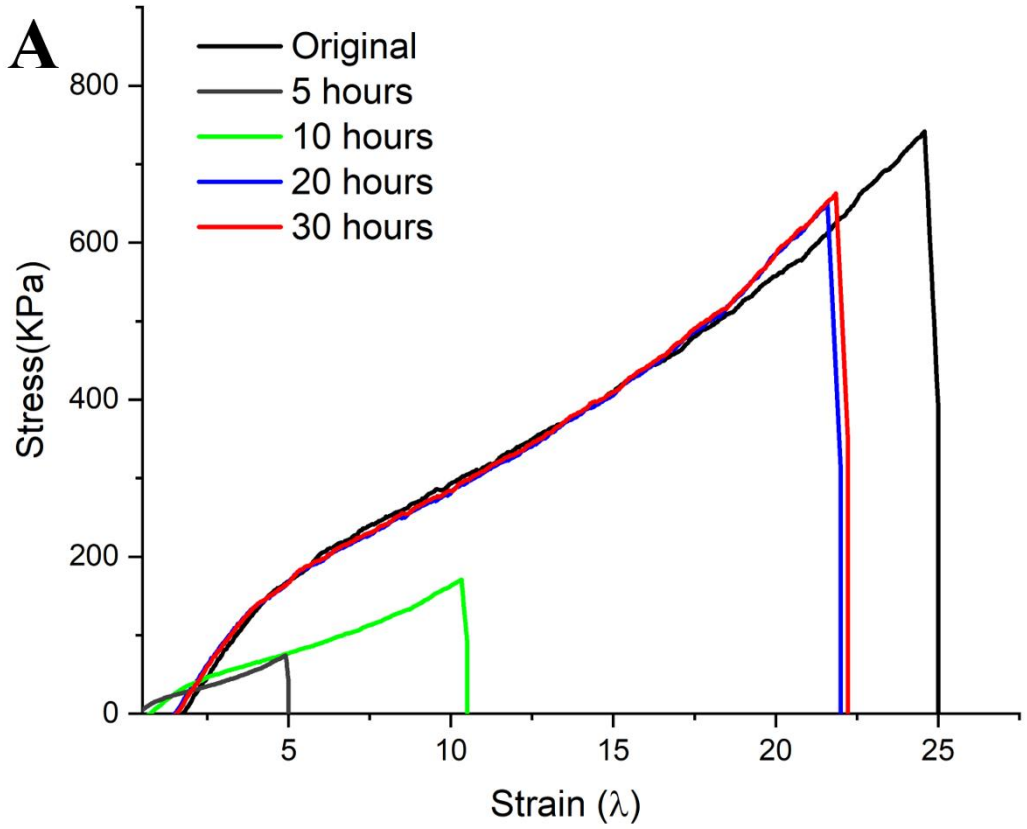
A
Original
5 hours
10 hours
20 hours
30 hours
Stress(KPa)
800
600
400
200
0
5
10
15
20
25
Strain (λ)

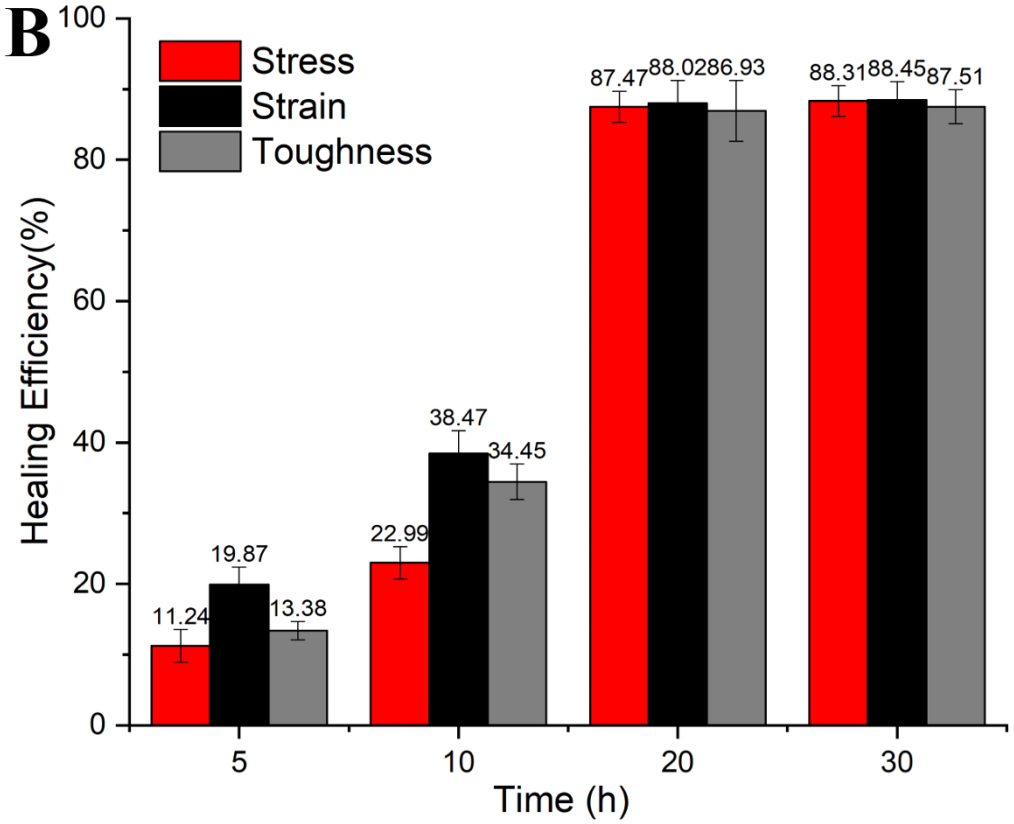

Figure 17. (A) Self-healing mechanical behavior of hydrogels with time. (B) Corresponding healing efficiency in tensile stress, tensile strain and toughness.

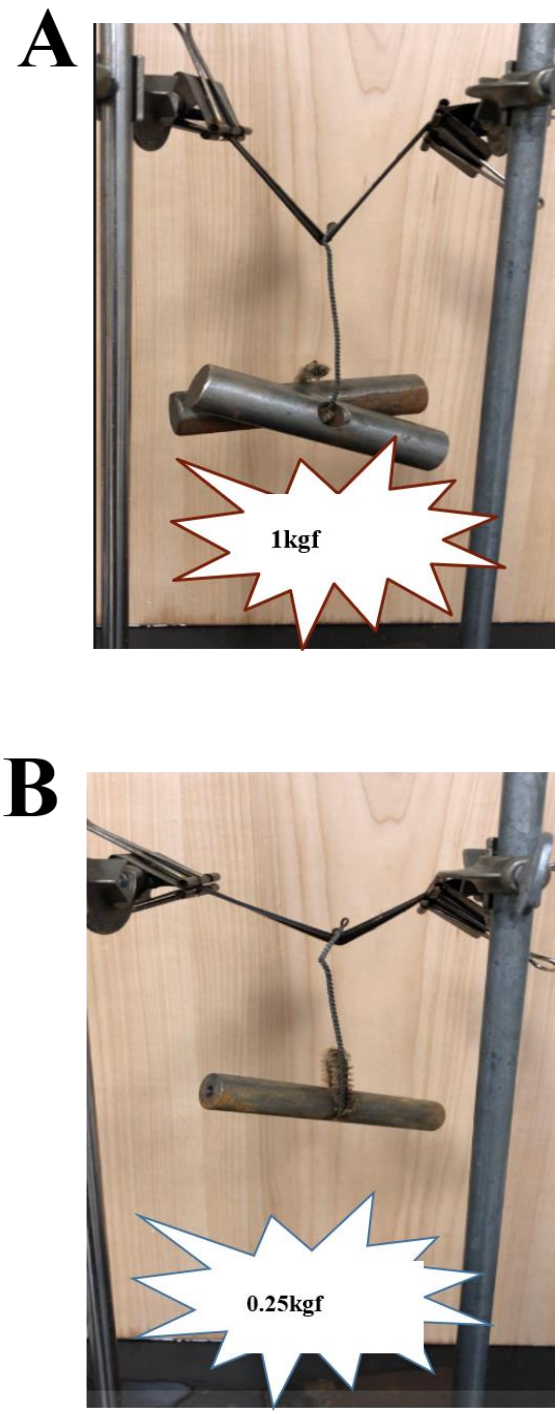

Figure 18. A) An original hydrogel sample can bear a weight of 1kgf B) A self-healed sample can also bear 0.25 kgf.

4.6 Self-healing Tests

The developed PAA-GO-Ca^{2+} hydrogels were evaluated regarding their self-healing capacity. As shown in Figure 6A, a hydrogel sample in a disk shape was cut into two halves and the two cut

surfaces were allowed to get back in touch to heal for 20 hours. It can be observed (Figure 13A) that the two halves reunited without any visible scar, and the healed hydrogel can sustain considerable stretch without breaking. Microscope image of the healed surface (Figure 13B) shows a dark area where the hydrogel was bisected and subsequently healed. Rheology recovery tests were also performed to evaluate PAA-GO-Ca^{2+} hydrogel's self-healing behaviors. As shown in Figure 14, the oscillatory shear strain of a small one (1%) and a large one (400%) were alternatively applied with each strain kept for 200s. When the first small stain was applied, both G' and G'' appeared steady with a higher G' than G'' which indicates a stable solid-like status. When the oscillatory stain was dramatically increased to 400%, both G' and G'' showed fluctuations, with G'' exceeding G' which indicates a more liquid-like status. When the large strain was replaced by the small strain again, both G' and G'' returned to their initial values quickly. These results demonstrate that the PAA-GO-Ca^{2+} hydrogel has an extraordinary ability to recover its original status when it is subjected to large stains.

For a better understanding of the self-healing capacity of PAA-GO-Ca^{2+} hydrogels, we investigated the influence of different factors including both GO and Ca^{2+} contents and healing time on the self-healing efficiency, as described below.

4.6.1 Influence of GO Amount on Self-healing Efficiency

The amount of Ca^{2+} was fixed at 10% when the effect of GO content on hydrogel self-healing efficiency was studied. The hydrogel was cut into two halves, and the two cut surfaces were then gently pushed together to allow healing for 20 hours. The stress-strain curves in Figure 15A illustrate mechanical performances of the original hydrogel and healed hydrogels with different GO contents. It is observed that pristine PAA hydrogel can not self-heal after being cut, indicating that only the Ca^{2+} interaction between PAA chains is not sufficient for self-healing. However, when 3% of GO nanoparticles were introduced, an obvious self-healing phenomenon was observed, as shown in Figure 15B, with a stress healing efficiency of 34,04%, a strain healing efficiency of 52.12%, and

a toughness healing efficiency of 46.53%. Another increasing in the GO content endows the hydrogel with a better self-healing efficiency: when the GO content was 5%, the healing efficiency of stress increased to 87.47%, strain to 88.98% and toughness to 86.93%. A further increase in GO content to 8%, however, led to a drop in the self-healing efficiency, which was shown as a 78.70% in stress and 53.97% in strain respectively. Such a drop in self-healing efficiency may be attributed to the fact that a high crosslinking density impedes the mobility of PAA polymer chains and makes it much harder to heal upon damage.

4.6.2 Influence of Ca^{2+} Amount on Self-healing Efficiency

Another factor contributing to crosslinking density is the amount of Ca^{2+} crosslinker, which may also have an effect on healing efficiency. To investigate this influence, test samples were prepared with a fixed GO content of 5% but different amounts of Ca^{2+} crosslinker. As shown in Figures 16A and 16B, hydrogels with 5% Ca^{2+} had low healing efficiency, which was 22.99%, 32.00% and 39.53% healing efficiency in fracture stress, strain, and toughness respectively. An increase of Ca^{2+} contents renders a remarkable improvement in healing efficiency, as more Ca^{2+} enhances the interaction between PAA and GO. When the Ca^{2+} concentration reached 10%, the highest healing efficiency was achieved with 87.47% healing rate in stress, 88.9% in strain and 86.93% in toughness. However, an excessive Ca^{2+} content (15%) led to a decline in self-healing efficiency probably due to an overly high crosslinking density.

4.6.3 Influence of Healing Time on Self-healing Efficiency

To investigate the influence of healing time on the efficiency of self-healing, hydrogel samples with 5% GO and 10% Ca^{2+} contents were bisected and then allowed to heal for different times. As shown in Figure 17A, healing time exerts a great influence on self-healing efficiency. Figure 17B reveals that a longer healing time led to a higher self-healing efficiency. It is obvious that there is a significant increase in healing efficiency if healing time is increased: when the healing time was raised from 5 hours to 20 hours, the healing rate of stress increased from 11.24% to 87.47%, strain

from 19.87% to 88.02% and toughness from 13.38% to 86.93%. However, extending healing time for an additional 10 hours did not change much in healing efficiency, just a very slight increase to 88.31% (stress), 88.45% (strain), and 87.51% (toughness) respectively, indicating 20 hours should be the optimum healing time for obtaining an excellent healing efficiency. It can be seen that the developed hydrogel system has a remarkable healing efficiency upon damage with little loss in its excellent mechanical performance. This novel hydrogel can be applied in wearable electronic biosensors with greatly reduced repair costs and prolonged service life. It is shown in Figure 18A that the healed joint was able to bear very large stress as compared to the original hydrogel. For example, a strip of the original sample with a $10mm^2$ cross-sectional area can sustain a load of up to 1 kgf, while the healed sample with the loads hung right at the cut area was still able to sustain a load of 0.25 kgf shown in Figure 18B, indicating a remarkable self-healing efficiency.

4.7 Mechanism of Self-healing Property

We hypothesized that the major contribution to the impressive self-healing efficiency in PAA-GO-Ca^{2+} hydrogel would be the massive dynamic ionic interaction between carboxyl groups existing in both PAA polymer chains and GO nanoparticles. However, hydrogen bonding should also be taken into consideration due to the numerals oxygen-containing groups in the network such as carboxyl groups and hydroxyl groups. Therefore the developed hydrogel was immersed into three different solutions: 1) EDTA solution which is proved to be an effective chelation for Ca^{2+}, 2) urea solution which is widely used as a proper disruption for existing hydrogen bonds, and as a control group, and 3) purified water.

Figure 19A illustrates the impact of EDTA solution on the hydrogel's physical crosslinking: after immersing the hydrogel sample into the EDTA solution, the self-healed cut began to split in 10 minutes; after 20 minutes treatment, the gap became wider; after 30 minutes treatment, the two halves were separated completely,indicating that EDTA solution treatment influenced the ionic interaction between carboxyl groups when EDTA chelate Ca^{2+}.

When we investigated hydrogen bonds between those massive oxygen-containing groups, it was discovered that the hydrogen bonds were only reinforced factor for both mechanical properties as well as self-healing behavior, which is demonstrated in Figure 19B: after soaking in urea solution, the two healed halves were separated slightly after 20 minutes, and there was no obvious difference after an additional 10 minutes treatment, indicated that the urea solution had already de-crosslinked all hydrogen bonding interaction among the hydrogel's oxygen-containing functional groups.

When the hydrogel sample was immersed into pure water as a control group, as illustrated in Figure 19C, there was only a bit swelling behavior after 30 minutes with no obvious separation of the two halves. Therefore, in PAA-GO-Ca^{2+} hydrogel system it is an ionic interaction that plays a dominant role in self-healing mechanism, but hydrogen bonding also attributes to self-healing behavior.

In summary, it is evident that dynamic physical crosslinking can endow traditional hydrogels which are only crosslinked by chemical crosslinker with self-healing property. In this work, the ionic interaction of Ca^{2+} and hydrogen bonding both contribute to excellent and quick self-healing behavior, and the effect of ionic interaction is dominant but the effect of hydrogen bonding cannot be ignored as well.

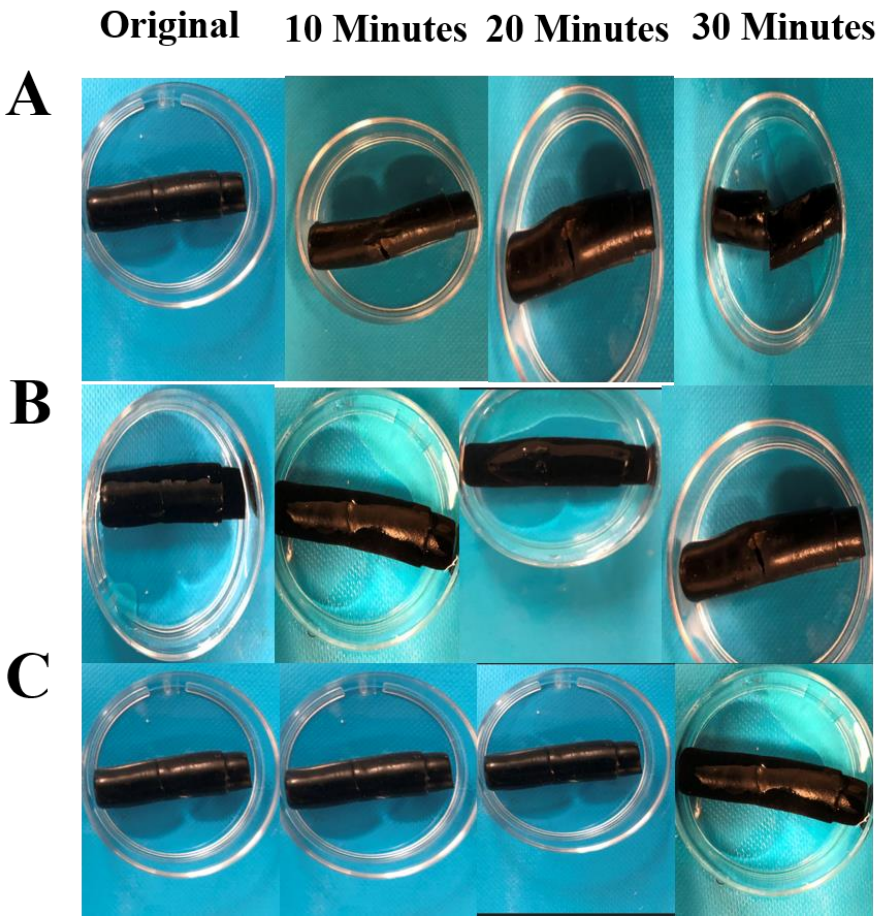

Figure 19. Self-healing mechanism. Examine the self-healing mechanism and functional roles of ionic and hydrogen bonding interactions. A) EDTA solution, B) urea solution and C) purified water as a control group.

4.8 3D Printable Hydrogels

For 3D printing, a 12-hour pre-curing process was conducted to ensure the printable ink can easily pass through the needle. As shown in Figure 20A, the printable ink can be easily loaded into a syringe and is sticky enough to maintain certain shape when being printed out from the needle. Figure 20B demonstrates the effect of shear rates on the viscosity of the PAA-GO-Ca^{2+} ink with 12-hour pre-curing, it is obvious that with the increase in shear rate, its viscosity decreases, indicating a shear-thinning behavior which is also a signal that the printable ink can pass through the needle where exerts a high shear rate, as shown in Figure 20C. After printing, the hydrogel mesh was kept in a plastic dish for an additional 36 hours to allow complete crosslinking, as shown in Figure 8D,

followed by a treatment with HI vapor to partially reduce GO on the surface of the hydrogel. Interestingly, we incorporated fluorescence with PAA-GO-Ca^{2+} hydrogel and it turned out that the fluorescence can be observed under UV light, as shown in Figure 20D insert, and there was no adverse effect on the mechanical and self-healing property. Then the hydrogel-based biosensor was used to detect different human body motions.

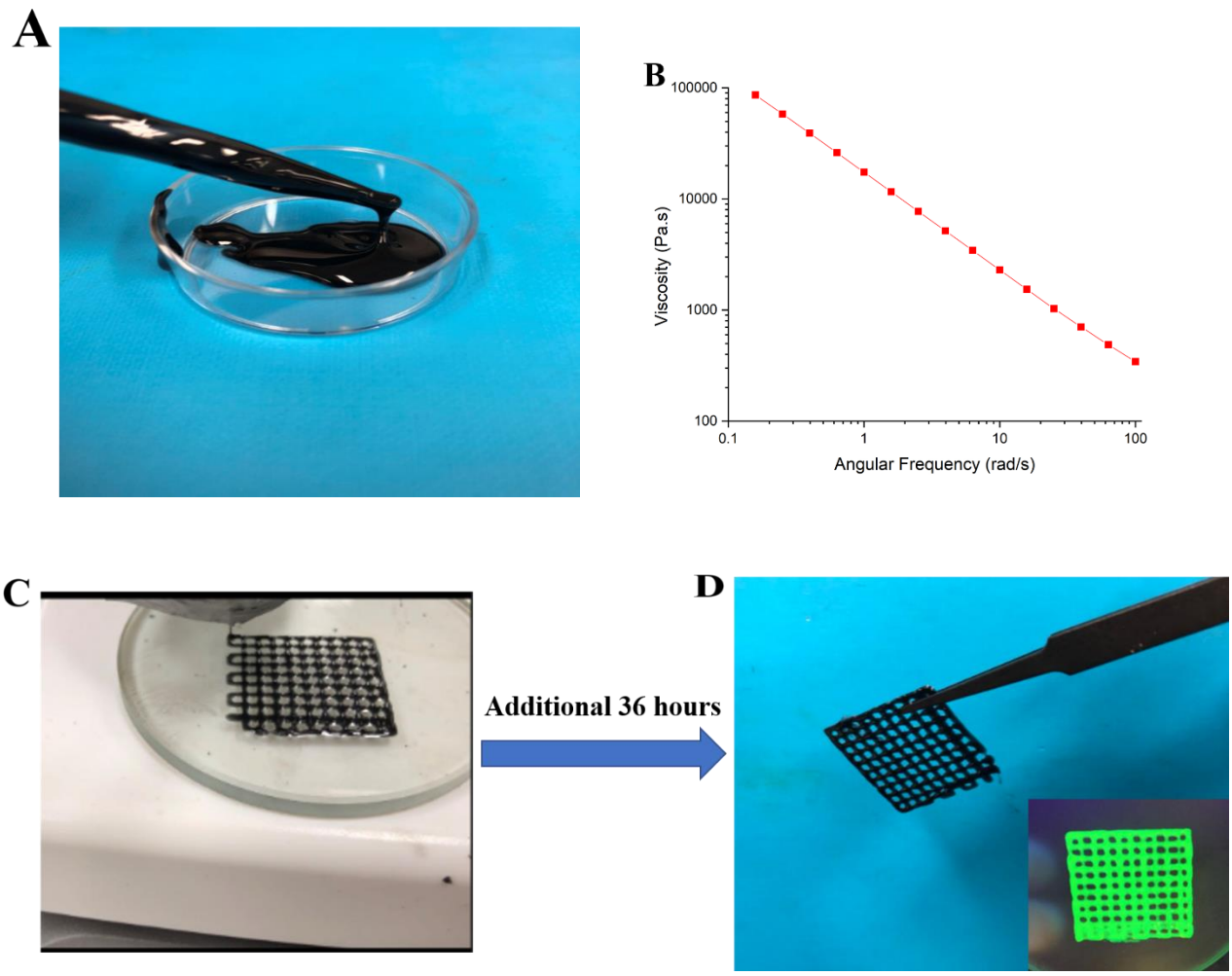

Figure 20. 3D printing. A) The PAA-GO-Ca^{2+} printable ink prepared by pre-curing hydrogel aqueous mixture for 12 hours. B) The viscosity of the ink shows a shear-thinning behavior which ensures a successful printing. C) 3D printing in progress. D) A final printed PAA-rGO-Ca^{2+} film with improved conductivity. Insert: A sample incorporated with fluorescence and observed under UV irradiation after curing completely.

The PAA-rGO-Ca^{2+} hydrogel was prepared by using HI vapor because HI has been reported as an efficiently reducing chemical for GO. In this work, instead of contacting PAA-GO-Ca^{2+} hydrogel directly with HI solution, HI vapor was used. As shown in Figure 21A, the 3D printed film was able to maintain its original shapes because of a mild HI vapor is used instead of HI solution which can destroy the hydrogels' structure. Also, HI vapor is sufficient to reduce only the GO on the hydrogel surface to maintain certain COO- groups for excellent mechanical behaviors. As shown in Figure 21B, PAA-rGO-Ca^{2+} hydrogels with different treating times in HI vapor show different resistances: where the resistance decreased sharply from 1473.23 Kohm for non-treated samples to 257.31 Kohm for samples treated with HI vapor for just 5 hours. Longer treating time can render the hydrogel a better conductivity, but the difference was not significate.

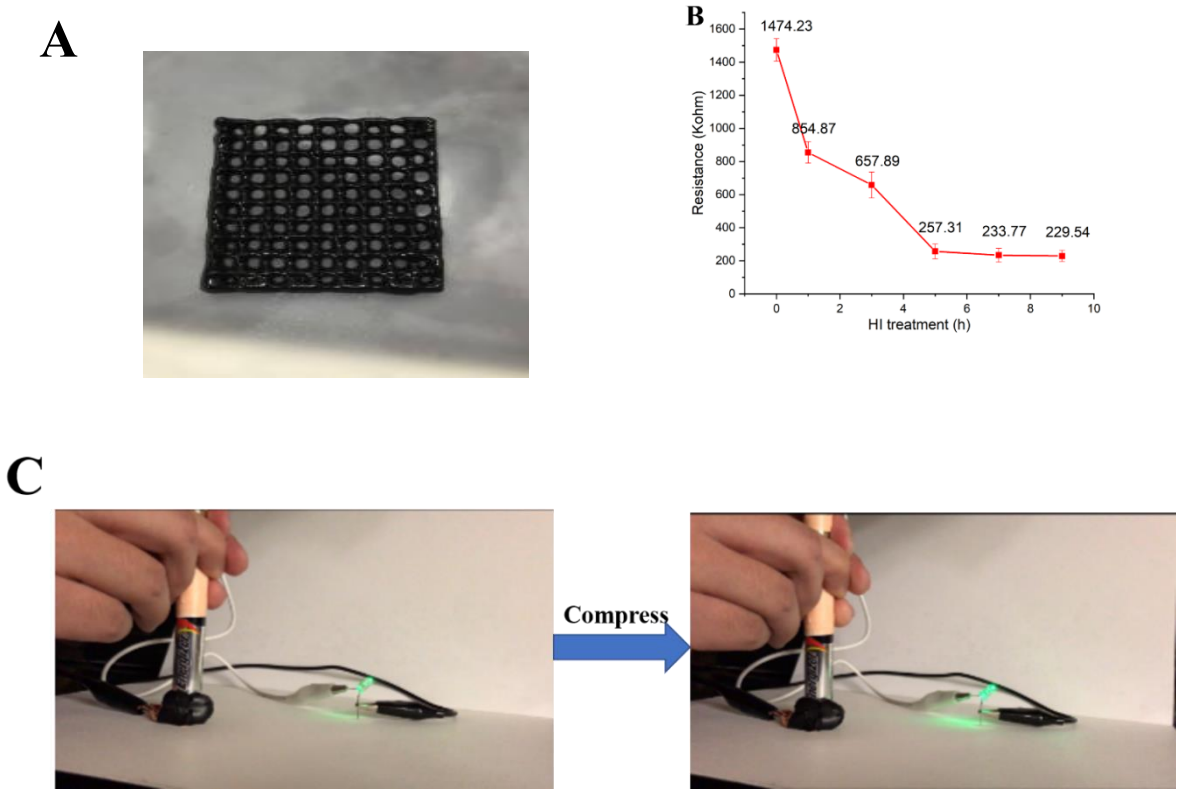

Figure 21.Conductive tests.A) 3D printed PAA-GO-Ca^{2+} hydrogel film treated by HI vapor to produce the PAA-rGO-Ca^{2+} film with enhanced conductivity. B) The conductivity of the PAA-rGO-Ca^{2+} film dramatically improved with an increase in treating time. C) Strain-dependent

conductivity: the LED light became brighter when compressing the hydrogel, which shows the conductivity is sensitive to strain.

As mentioned before, the PAA-GO-Ca^{2+} hydrogels can bear large strain(nearly 25 times than original), so it is reasonable that the PAA-rGO-Ca^{2+} hydrogels inhere this extraordinary ability, and therefore its conductivity may be strain-dependent. The strain-dependent conductivity of the hydrogels was demonstrated in Figure 21C, in which a small LED light was dim before compression, but became much brighter upon compression.

4.9 PAA-rGO-Ca^{2+} Hydrogels in Wearable Electronic Biosensor

Traditional biosensor used to detect human activities are usually high in cost, low in sensitivity, slow in response, and may be difficult to be manufactured in customized size, shape, and geometries. In addition, traditional biosensors are mostly not capable of self-repairing their damages due to fatigue which leads to frequent replacing and repairing. A novel hydrogel-based wearable electronic biosensor was engineered in this paper as a great alternative to traditional biosensors for monitoring and managing human health. This new type of biosensor not only responds quickly to large strains but also can automatically repair its fatigue and failure upon damage which greatly reduces maintenance costs.

In this project, a cell phone application was also created for this sensor to display signals corresponding to human activities. This software application can decode biological signals into electric signals and make it easy to understand one's health condition.

As shown in Figure 10A, the 3D printed film sensor was connected to the cell phone application via a Bluetooth chip. Then it was attached to a person's throat with the assistance of two-layer PDMS films to monitor and record different electrical changes related to breath variation before and after exercise. In specific as shown in Figure 22A, before exercise, the person breathed 24 times per minute while after doing some sports, the breath frequence went up to 35 times per minutes, which demonstrates the resulting hydrogel-based werable biosensor is sensitive enough to record human's

breath activity , the reason is that the resistance variations are caused by the small strain changes in the person's throat motions upon breathing. The resulting sensor was able to detect the different in pulse rate between before and after exercise, as shown in Figure 22B, the person's pulse rate was 68 times per minute in a relaxed condition while the pulse rate increased to 109 times per minutes after doing certain activities. Moreover, we demonstrated that our sensor is sensitive enough to promptly and accurately detect human sweat, which is useful to monitor individual perspirations during sports or to monitor patients' health condition. As shown in Figure 22C, the sensor was again connected with a smartphone via Bluetooth. The sensor was held in the air for two seconds; then the sensor was immersed into artificial sweat solution for another two seconds, it is clear that the resistance increased dramatically because artificial sweat solution contained sodium chloride making it an electrolyte and thus improves conductivity. After two seconds immersing into the sweat, the sensor was taken out again and held for two seconds; it can be seen from Figure 22C that the resistance decreased to nearly the same level as the beginning, as the conductivity recovered with the removal of sweat solution. The repeating process was done several times in the same time interval of two seconds.

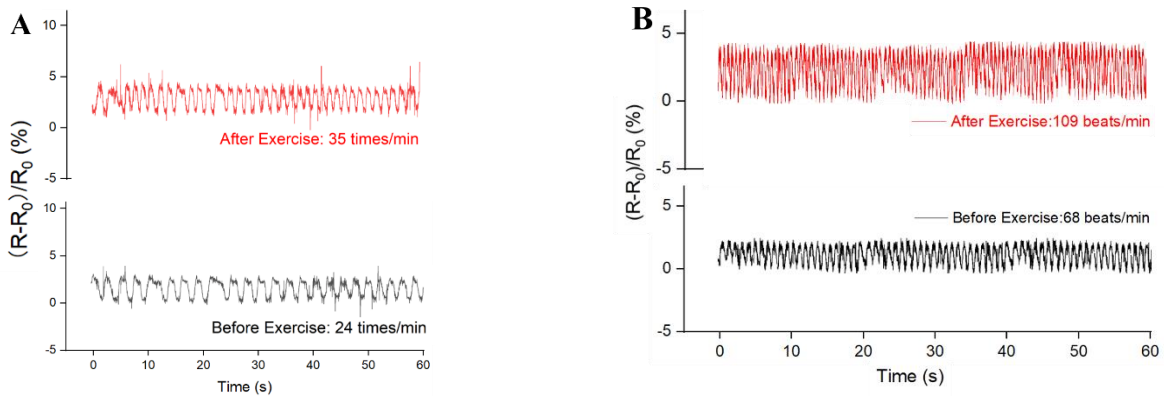

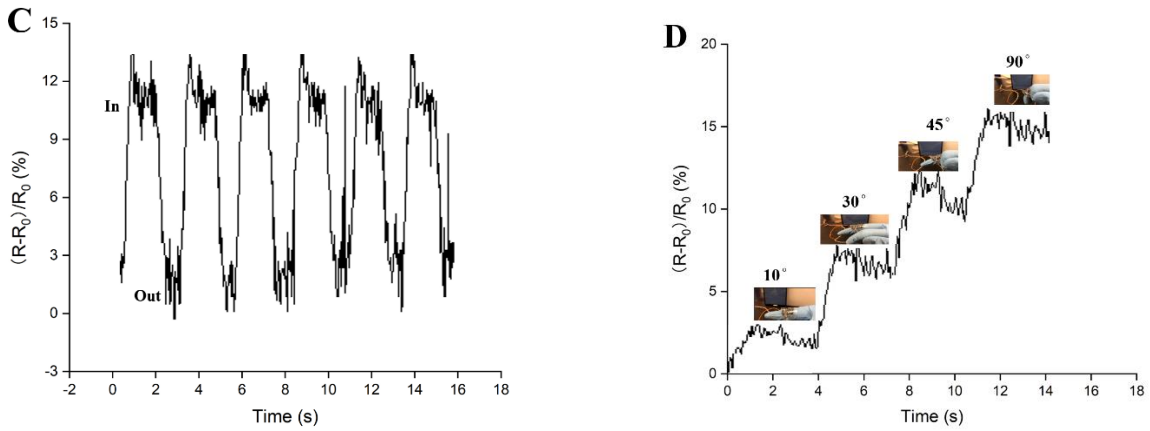

Figure 22. The resulting hydrogel-based biosensor has the potential for sports detection, such as A) breath rate differences between before and after exercise, B) pulse rate differences between before and after exercise, C) Sweat dection and D) detect different finger bending angle ranging from 10, 30, 45 and 90 degrees.

The PAA-rGO-Ca^{2+} hydrogel biosensor was also applied in detecting finger movements. Similarly, the sensor was attached on an index finger after connecting to cell phone application through bluetooth. The resistance variations were measured when bending the finger at an angle of 10°, 30°, 45° and 90°, as shown in Figure 22D, the results indicate that the sensor can detect both small and big angle changes with high accuracy as well as fast response.

4.10 Results for Detecting Ammonia

Ammonia is a notorious toxic industrial pollutant which can be harmful to human health in many ways. Graphene oxide and reduced graphene oxide have been widely investigated for applications in gas detecting. The reason for GO and rGO can sensitive to ammonia is that monolayer GO and rGO are sensitive enough to detect any adsorbed and desorbed gas due to their remarkable conductivity.The PAA-rGO-Ca^{2+} hydrogel developed in this study was also evaluated for its potential application as an ammonia sensor that can be used as artificial electronic nose that communicates with a smartphone to detect ammonia accurately as shown in Figure 23A. It can be seen from Figure 23B that when the sensor was exposed to ammonia vapor with a balanced 3 ppm,

the conductivity change rare of the sensor increased and peaked at 11.8% in 20 minutes which remained steady for the next 20 minutes indicates the sensor absorb saturated ammonia gas; Similarly, when placed the sensor closed to gaseous ammonia with 7, 13 and 30 ppm concentration, it took a similar time for the sensor to absorb the maximum ammonia gas at 17, 18 and 17.5 minutes respectively and they were able to maintain the peak number for an additional 20 minutes as well. It is suggested that the peak level of ammonia gas that is allowed in the workplace or living environment is 20 ppm (*185, 186*), any concentration beyond this number would pose a threat to human's health. Our design, the PAA-rGO-Ca^{2+} hydrogel based ammonia sensor is able to detect and response to a much smaller concentration which can be potentially applied as electronic nose to detect dangerous ammonia in the workplace or in the food manufacturing industry.

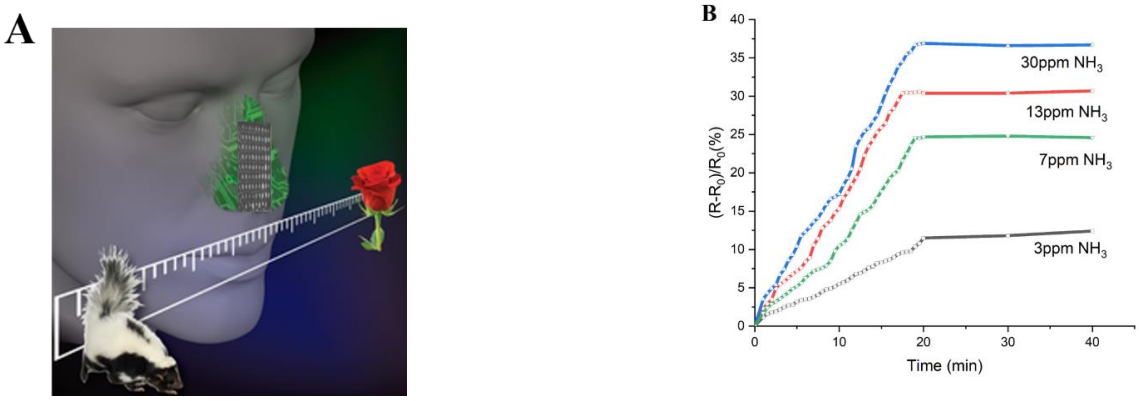

Figure 23. Ammonia detection.A) Ammonia sensor can be used as electronic nose to detect ammonia via smartphone. B) Sensors are exposed to ammonia solutions with different concentration as 3,7,13 and 300 ppm.

4.11 A Discussion on the Highlights of Our Work as Compared to Peer Research

Highly hydrophilic and biocompatible (*187*), hydrogels have found their applications in a variety of areas ranging from biomedicine (*120, 188, 189*), water purification (*190*) to electronic devices (*191*) and liquid absorbent (*192*). However, poor mechanical properties limit the applications of most hydrogels (*193*). Double-network polymer hydrogels is a type of widely studied hydrogels with enhanced mechanical properties. A double network hydrogel (DN hydrogels) is composed of two

different polymer networks usually crosslinked via different methods, typically including a densely but non-reversible crosslinked polymer network in addition to a loosely but reversible crosslinked network (*194-196*). DN hydrogels are a prevalent solution to enhance mechanical properties of hydrogels (*11, 197, 198*).

Self-healing is a natural capacity of some living organisms to repair their physical damages/injuries automatically. It has recently been introduced into functional materials/devices to endow self-repairing capacity after being damaged to reduce their maintenance costs and prolong their service times (*199-201*). However, it remains a challenge to engineer self-healing hydrogels with high efficiency in recovery of their mechanical properties before the damages. Reported strategies to achieve better self-healing property include incorporations of dynamic covalent bonds (*202, 203*), and utilization of noncovalent interactions such as hydrogen bonding (*204, 205*), π−π stacking (*206, 207*), hydrophobic associations (*208, 209*), and electrostatic interactions (*210, 211*).

Recently there have been studies on DN hydrogels with additional features like self-healing property (*212*). Chen *et al*.(*11*) fabricated a DN hydrogel, in which physically crosslinked Agar was introduced into hydrophobically associated polyacrylamide (HPAAm). The resulted Agar/HPAAm DN gels exhibited excellent mechanical strength, high toughness, and notable self-healing property. Our group (*124*) recently designed a novel DN hydrogel by introducing ferric ions to the poly(acrylic acid) network to enhance mechanical behavior as well as to achieve rapid self-healing efficiency.

An alternative and relatively simple route to enhance hydrogels' mechanical performance is to integrate nanofillers including nano clay (*129, 213*), carbon nanotube (CNT) (*214, 215*), and graphene-based nanoparticles (*216, 217*) into hydrogels. These nanofillers may also endow the composite hydrogels with multiple functions like self-healing (*132, 218*) conductivity(*219, 220*), and high stiffness along with toughness (*132, 221*). Among these nanofillers, graphene-based materials including graphene oxide (GO) and reduced graphene oxide (rGO) have been widely

utilized in fabricating composite hydrogels owing to their excellent chemical stability, superior thermal conductivity and ultra high mechanical properties. Yu *et al.* (*132*) intertwined GO and/poly(acryloyl-6-aminocaproic acid) (PAACA) using ionic crosslinkers to fabricate GO/PAACA composite hydrogels with superior mechanical strength and good self-healing ability. Yan *et al.*(*133*) introduced rGO nanoparticles into cellulose ester based hydrogels to prepared rGO/cellulose conductive hydrogel films which have potential applications in electrodes for supercapacitors due to its excellent capacitance even at a high current density.

To provide a brief comparison of our work with existing reports, Table 1 lists references on composite hydrogels enhanced with GO or rGO, as a comparison with our work. Progress has been made for nanocomposite hydrogels with improved mechanical strength and self-healing property, but the tensile strengths for most recoverable hydrogels after healing is below 300KPa and the self-healing efficiencies are mostly below 80%. Self-healing hydrogels based on other design strategies with good recovery mechanical properties can also be found in Table 2 as a comparison with our work.

Table 1 A review on typical multifunctional hydrogels reinforced by introducing GO/rGO in recent years

Nanoparticle Type	Composition	Properties	Application	Ref.
GO & rGO	PAA,Ca^{2+} MBA	Touness:9.73 MJm^{-3} Young's Modulus:753KPa 86.93% in toughness self-healing	Wearabble electronic biosensor	Our work
GO&rGO	GO dispersion	Tensile strength:582 MPa Fracture energy: 18.29 MJm^{-3}	Strain sensor	(*222*)
GO	Gelatin-MA	Biocompatible	Cell culture	(*223*)
GO	PVA	PH sensitive	PH detection	(*224*)
GO	PEGDA	Oil decontamination	Contamination removal	(*225*)
GO	Adenosine	Target response	Antibiotics detection	(*43*)
GO	CMC,AM	High adsorption	Dye removal	(*226*)

Table 2. A review on recent breakthrough in hydrogels with selfhealing ability

Materials	Mechanism	Mechanical Properties	Self-healing Properties	Ref.
PAA-GO-Ca^{2+}	Colavent bonds Ionic bonds and Hydrogen bonds	Toughness ~9.73MJm^{-3} Stiffness ~753.667KPa	86.93% in toughness	our work
PAA,chitosan	Ionic interaction	Ultrastrechable~1500%	100% recovery in 2min	(*170*)
PAA,Alginate	Ionic interaction		83%in G' in 20min	(*227*)
TA	Dynamic interaction	Toughness~5.60MJm^{-3}	88% in tensile strengh	(*228*)
CNCs, PAA		Fracture strain~2952%		
Ad-AAm,AAC	Ionic interaction	Fracture stress:40KPa,	70% after 120 mins	(*229*)
PCD		Fracture strain:600%		
PAM-co-PAA		Toughness:1.25MJm^{-3}	37% after 12 hours	(*118*)
PVA	Hydrogen bonds			

PAA:Poly(acrylic acid), GO: graphene oxide

TA:Tannic acid Ad-AAm:N-adamantylacrylamide (Ad-AAm),AAC:Acrylic acid

PCD: polycyclodextrin

Three-dimensional (3D) printing, or additive manufacture, provides a promising solution to print various raw materials into complex 3D structures with pre-designed patterns. It is desirable to design and fabricate hydrogel-based wearable electronic devices with macroporous 3D architectures. The versatility of 3D printing techniques allows for a flexible, easy and quick method to fabricate electronic devices to meet exact requirements for specific applications. However, there has been a

challenge to prepare suitable and printable ink used for 3D printing. Table 3 provides a brief list on existing 3D printable inks for hydrogel fabrications, as a comparison with our work.

Table 3. 3D printable ink for hydrogels' manufacturing.

Ink formulation	Viscosity is increasing mechanism	Application	Ref.
PAA,GO,Ca^{2+}	Control crosslinking degree	Biosensor	Our work
PEGDA, Alginate	Alginate	Tissue engineering	(*129*)
PAA,Chitosan,PPy	Chitosan	Wearable sensor	(*170*)
Gelatin	Control concentration	Cell culture	(*230*)
Collagen, Chitosan,	Crosslink GO with Ca^{2+}	Cell culture	(*231*)

Chapter 5 Conclusion and Future Work

In this work, we developed a 3D printable, conductive PAA-GO-Ca^{2+} hydrogel with both covalent and physical dual-crosslinked networks which demonstrate both excellent mechanical properties and outstanding self-healing capacity, making it promising for applications in biosensors.

In order to optimize the parameters in the hydrogel fabrication, we studied the influence of GO and Ca^{2+} contents on the mechanical properties of the hydrogels. It was found that both GO and Ca^{2+} contents can have important impacts on hydrogels' mechanical performance includes tensile stress, tensile strain, toughness and stiffness as a result of crosslinking density. The results suggest that 5% GO and 10% Ca^{2+} produce hydrogels with the best mechanical properties including an ultrahigh strain of 2500%, high toughness of 9.73 MJm^{-3} and high stiffness (Young's modulus:~753.667KPa), which were further proved by rheology tests.

In addition, the dynamic interactions including hydrogen bonding and ionic interactions in the PAA-GO-Ca^{2+} hydrogel system endow its excellent self-healing ability. Different factors that may affect the self-healing efficiency of the hydrogels, such as healing time, GO and Ca^{2+} contents, were investigated. The resulted PAA-GO-Ca^{2+} hydrogel has excellent self-healing ability with ~87.47% recovery in tensile strength, 88.02% in tensile strain and 86.93% in toughness respectively. The mechanisms of self-healing in the developed hydrogels were further studied by EDTA treating that chelates Ca^{2+} and urea treating that destroys hydrogen bonds.

To enable 3D printing of the hydrogels, the crosslinking degrees of the hydrogels were tuned to achieve desired printable viscosity, followed by HI vapor treating which can improve hydrogels' conductivity from 1474.23 Kohm to 229.54 Kohm. Then the hydrogel was developed into wearable biosensors for detecting different signals, such as various human activities like breathing, cough, pulse rate and sweat rate, and electronic noses to detect toxic gas like ammonia.

Improving hydrogels' mechanical properties has been an important topic in biomaterial engineering to enable their applications in a wider variety of applications. There has also been a trend to

explore new applications for hydrogels by endowing hydrogels with such unique properties as self-healing efficiency, conductivity, self-adhesive ability, and combinations of several advanced functions to further enhance the functionalities, lower the cost and prolong service lifetime of the hydrogels. These efforts can be the focus of future research and development of the current work.

Reference

1. Z. Fan *et al.*, A novel wound dressing based on Ag/graphene polymer hydrogel: effectively kill bacteria and accelerate wound healing. *Advanced Functional Materials* **24**, 3933-3943 (2014).
2. H. J. Jung, M. Abou-Jaoude, B. E. Carbia, C. Plummer, A. Chauhan, Glaucoma therapy by extended release of timolol from nanoparticle loaded silicone-hydrogel contact lenses. *Journal of controlled release* **165**, 82-89 (2013).
3. Y. Jiang, J. Chen, C. Deng, E. J. Suuronen, Z. Zhong, Click hydrogels, microgels and nanogels: emerging platforms for drug delivery and tissue engineering. *Biomaterials* **35**, 4969-4985 (2014).
4. C. S. Boland *et al.*, Sensitive, high-strain, high-rate bodily motion sensors based on graphene–rubber composites. *ACS nano* **8**, 8819-8830 (2014).
5. C. Mattmann, F. Clemens, G. Tröster, Sensor for measuring strain in textile. *Sensors* **8**, 3719-3732 (2008).
6. T. Yamada *et al.*, A stretchable carbon nanotube strain sensor for human-motion detection. *Nature nanotechnology* **6**, 296-301 (2011).
7. D. Zhai *et al.*, Highly sensitive glucose sensor based on Pt nanoparticle/polyaniline hydrogel heterostructures. *ACS nano* **7**, 3540-3546 (2013).
8. Y. Wang, X. Yang, L. Qiu, D. Li, Revisiting the capacitance of polyaniline by using graphene hydrogel films as a substrate: the importance of nano-architecturing. *Energy & Environmental Science* **6**, 477-481 (2013).
9. H. Bai, K. Sheng, P. Zhang, C. Li, G. Shi, Graphene oxide/conducting polymer composite hydrogels. *Journal of Materials Chemistry* **21**, 18653-18658 (2011).
10. C. Fan, L. Liao, C. Zhang, L. Liu, A tough double network hydrogel for cartilage tissue engineering. *Journal of Materials Chemistry B* **1**, 4251-4258 (2013).
11. Q. Chen *et al.*, A Novel Design Strategy for Fully Physically Linked Double Network Hydrogels with Tough, Fatigue Resistant, and Self-Healing Properties. *Advanced Functional Materials* **25**, 1598-1607 (2015).
12. A. K. Gaharwar, N. A. Peppas, A. Khademhosseini, Nanocomposite hydrogels for biomedical applications. *Biotechnology and bioengineering* **111**, 441-453 (2014).
13. K. Nishi, K. Fujii, Y. Katsumoto, T. Sakai, M. Shibayama, Kinetic aspect on gelation mechanism of tetra-PEG hydrogel. *Macromolecules* **47**, 3274-3281 (2014).
14. S. Zeng *et al.*, Electrochemical fabrication of carbon nanotube/polyaniline hydrogel film for all-solid-state flexible supercapacitor with high areal capacitance. *Journal of Materials Chemistry A* **3**, 23864-23870 (2015).
15. Y. Xu *et al.*, Flexible solid-state supercapacitors based on three-dimensional graphene hydrogel films. *ACS nano* **7**, 4042-4049 (2013).
16. J. L. Erkal *et al.*, 3D printed microfluidic devices with integrated versatile and reusable electrodes. *Lab on a Chip* **14**, 2023-2032 (2014).
17. S. A. Gowers *et al.*, 3D printed microfluidic device with integrated biosensors for online analysis of subcutaneous human microdialysate. *Analytical chemistry* **87**, 7763-7770 (2015).
18. P. Thibon, X. Le Coutour, R. Leroyer, J. Fabry, Randomized multi-centre trial of the effects of a catheter coated with hydrogel and silver salts on the incidence of hospital-acquired urinary tract infections. *Journal of Hospital Infection* **45**, 117-124 (2000).
19. E. M. Ahmed, Hydrogel: Preparation, characterization, and applications: A review. *Journal of advanced research* **6**, 105-121 (2015).
20. J. H. Holtz, S. A. Asher, Polymerized colloidal crystal hydrogel films as intelligent chemical sensing materials. *Nature* **389**, 829 (1997).
21. Q. Wang *et al.*, High-water-content mouldable hydrogels by mixing clay and a dendritic molecular binder. *Nature* **463**, 339 (2010).

22. H.-Y. Hsieh *et al.*, Gradient Strain Chip for Stimulating Cellular Behaviors in Cell-laden Hydrogel. *Journal of visualized experiments: JoVE*, (2017).
23. S. B. Sonnenberg *et al.*, Delivery of an engineered HGF fragment in an extracellular matrix-derived hydrogel prevents negative LV remodeling post-myocardial infarction. *Biomaterials* **45**, 56-63 (2015).
24. E. A. Kamoun, X. Chen, M. S. M. Eldin, E.-R. S. Kenawy, Crosslinked poly (vinyl alcohol) hydrogels for wound dressing applications: A review of remarkably blended polymers. *Arabian Journal of chemistry* **8**, 1-14 (2015).
25. X. Zhao *et al.*, Antibacterial anti-oxidant electroactive injectable hydrogel as self-healing wound dressing with hemostasis and adhesiveness for cutaneous wound healing. *Biomaterials* **122**, 34-47 (2017).
26. F. A. Maulvi *et al.*, In vitro and in vivo evaluation of novel implantation technology in hydrogel contact lenses for controlled drug delivery. *Journal of Controlled Release* **226**, 47-56 (2016).
27. C. Coles-Brennan, T. Wilson, R. Butterfield, M. Guillon, Visual performance and subjective response to digital device use with daily wear, reusable, silicone hydrogel contact lenses in a controlled environme. *Contact Lens and Anterior Eye* **41**, S3 (2018).
28. K.-H. Hsu *et al.*, Release of betaine and dexpanthenol from vitamin E modified silicone-hydrogel contact lenses. *Current eye research* **40**, 267-273 (2015).
29. W. L. Murphy *et al.* (Google Patents, 2017).
30. M. K. Lima-Tenório *et al.*, Water transport properties through starch-based hydrogel nanocomposites responding to both pH and a remote magnetic field. *Chemical Engineering Journal* **259**, 620-629 (2015).
31. J. Witono, I. Noordergraaf, H. Heeres, L. Janssen, Water absorption, retention and the swelling characteristics of cassava starch grafted with polyacrylic acid. *Carbohydrate polymers* **103**, 325-332 (2014).
32. V. K. Thakur, M. K. Thakur, Recent advances in green hydrogels from lignin: a review. *International Journal of Biological Macromolecules* **72**, 834-847 (2015).
33. Y. Hashimoto, S.-a. Mukai, S.-i. Sawada, Y. Sasaki, K. Akiyoshi, Nanogel tectonic porous gel loading biologics, nanocarriers, and cells for advanced scaffold. *Biomaterials* **37**, 107-115 (2015).
34. H. S. Song, O. S. Kwon, J.-H. Kim, J. Conde, N. Artzi, 3D hydrogel scaffold doped with 2D graphene materials for biosensors and bioelectronics. *Biosensors and Bioelectronics* **89**, 187-200 (2017).
35. S. Deepthi, K. Jeevitha, M. N. Sundaram, K. Chennazhi, R. Jayakumar, Chitosan–hyaluronic acid hydrogel coated poly (caprolactone) multiscale bilayer scaffold for ligament regeneration. *Chemical Engineering Journal* **260**, 478-485 (2015).
36. Y. Liu, C. Jiang, S. Li, Q. Hu, Composite vascular scaffold combining electrospun fibers and physically-crosslinked hydrogel with copper wire-induced grooves structure. *journal of the mechanical behavior of biomedical materials* **61**, 12-25 (2016).
37. S. Merino, C. Martín, K. Kostarelos, M. Prato, E. Vázquez, Nanocomposite hydrogels: 3D polymer–nanoparticle synergies for on-demand drug delivery. *Acs Nano* **9**, 4686-4697 (2015).
38. E. L. Schneider, J. Henise, R. Reid, G. W. Ashley, D. V. Santi, Hydrogel drug delivery system using self-cleaving covalent linkers for once-a-week administration of exenatide. *Bioconjugate chemistry* **27**, 1210-1215 (2016).
39. L. Li *et al.*, A nanostructured conductive hydrogels-based biosensor platform for human metabolite detection. *Nano letters* **15**, 1146-1151 (2015).
40. L. Li *et al.*, All Inkjet-Printed Amperometric Multiplexed Biosensors Based on Nanostructured Conductive Hydrogel Electrodes. *Nano letters*, (2018).

41. L. Liu *et al.*, One-pot synthesis of 3-dimensional reduced graphene oxide-based hydrogel as support for microbe immobilization and BOD biosensor preparation. *Biosensors and Bioelectronics* **63**, 483-489 (2015).
42. W. Cai, S. Xie, J. Zhang, D. Tang, Y. Tang, An electrochemical impedance biosensor for Hg2+ detection based on DNA hydrogel by coupling with DNAzyme-assisted target recycling and hybridization chain reaction. *Biosensors and Bioelectronics* **98**, 466-472 (2017).
43. B. Tan, H. Zhao, L. Du, X. Gan, X. Quan, A versatile fluorescent biosensor based on target-responsive graphene oxide hydrogel for antibiotic detection. *Biosensors and Bioelectronics* **83**, 267-273 (2016).
44. M. A. Darabi, A. Khosrozadeh, Q. Wang, M. Xing, Gum sensor: a stretchable, wearable, and foldable sensor based on carbon nanotube/chewing gum membrane. *ACS applied materials & interfaces* **7**, 26195-26205 (2015).
45. I. Y. Jung, J. S. Kim, B. R. Choi, K. Lee, H. Lee, Hydrogel based biosensors for in vitro diagnostics of biochemicals, proteins, and genes. *Advanced healthcare materials* **6**, 1601475 (2017).
46. N. S. Kehr, S. Atay, B. Ergün, Self-assembled Monolayers and Nanocomposite Hydrogels of Functional Nanomaterials for Tissue Engineering Applications. *Macromolecular bioscience* **15**, 445-463 (2015).
47. Y. Chen *et al.*, Injectable self-crosslinking HA-SH/Col I blend hydrogels for in vitro construction of engineered cartilage. *Carbohydrate polymers* **190**, 57-66 (2018).
48. X. Zhao *et al.*, Photocrosslinkable gelatin hydrogel for epidermal tissue engineering. *Advanced healthcare materials* **5**, 108-118 (2016).
49. S. Das *et al.*, Bioprintable, cell-laden silk fibroin–gelatin hydrogel supporting multilineage differentiation of stem cells for fabrication of three-dimensional tissue constructs. *Acta biomaterialia* **11**, 233-246 (2015).
50. N.-C. Cheng, W.-J. Lin, T.-Y. Ling, T.-H. Young, Sustained release of adipose-derived stem cells by thermosensitive chitosan/gelatin hydrogel for therapeutic angiogenesis. *Acta biomaterialia* **51**, 258-267 (2017).
51. H. Chen *et al.*, Covalently antibacterial alginate-chitosan hydrogel dressing integrated gelatin microspheres containing tetracycline hydrochloride for wound healing. *Materials Science and Engineering: C* **70**, 287-295 (2017).
52. N. Helfricht *et al.*, Probing the adhesion properties of alginate hydrogels: a new approach towards the preparation of soft colloidal probes for direct force measurements. *Soft matter* **13**, 578-589 (2017).
53. C. Bertagnolli, A. Grishin, T. Vincent, E. Guibal, Boron removal by a composite sorbent: Polyethylenimine/tannic acid derivative immobilized in alginate hydrogel beads. *Journal of Environmental Science and Health, Part A* **52**, 359-367 (2017).
54. Y. Yang, S. Song, Z. Zhao, Graphene oxide (GO)/polyacrylamide (PAM) composite hydrogels as efficient cationic dye adsorbents. *Colloids and Surfaces A: Physicochemical and Engineering Aspects* **513**, 315-324 (2017).
55. L. Han *et al.*, A Mussel-Inspired Conductive, Self-Adhesive, and Self-Healable Tough Hydrogel as Cell Stimulators and Implantable Bioelectronics. *Small* **13**, 1601916 (2017).
56. J. Chen, X. Shi, L. Ren, Y. Wang, Graphene oxide/PVA inorganic/organic interpenetrating hydrogels with excellent mechanical properties and biocompatibility. *Carbon* **111**, 18-27 (2017).
57. A. Marrella *et al.*, 3D Porous Gelatin/PVA Hydrogel as Meniscus Substitute Using Alginate Micro-Particles as Porogens. *Polymers* **10**, 380 (2018).
58. A. Vedadghavami *et al.*, Manufacturing of hydrogel biomaterials with controlled mechanical properties for tissue engineering applications. *Acta biomaterialia* **62**, 42-63 (2017).

59. S. E. Bakarich, R. Gorkin III, R. Gately, S. Naficy, G. M. Spinks, 3D printing of tough hydrogel composites with spatially varying materials properties. *Additive Manufacturing* **14**, 24-30 (2017).
60. A. Zheng *et al.*, Biocompatible silk/calcium silicate/sodium alginate composite scaffolds for bone tissue engineering. *Carbohydrate Polymers* **199**, 244-255 (2018).
61. A. Mohandas, S. Deepthi, R. Biswas, R. Jayakumar, Chitosan based metallic nanocomposite scaffolds as antimicrobial wound dressings. *Bioactive materials*, (2017).
62. P. Tirino *et al.*, Synthesis of chitosan–PEO hydrogels via mesylation and regioselective Cu (I)-catalyzed cycloaddition. *Carbohydrate polymers* **112**, 736-745 (2014).
63. L. Fan, H. Yang, J. Yang, M. Peng, J. Hu, Preparation and characterization of chitosan/gelatin/PVA hydrogel for wound dressings. *Carbohydrate polymers* **146**, 427-434 (2016).
64. X.-l. Xu *et al.*, Solution blowing of chitosan/PLA/PEG hydrogel nanofibers for wound dressing. *Fibers and Polymers* **17**, 205-211 (2016).
65. K. Wang *et al.*, Chemically crosslinked hydrogel film leads to integrated flexible supercapacitors with superior performance. *Advanced Materials* **27**, 7451-7457 (2015).
66. K. J. De France, K. J. Chan, E. D. Cranston, T. Hoare, Enhanced mechanical properties in cellulose nanocrystal–poly (oligoethylene glycol methacrylate) injectable nanocomposite hydrogels through control of physical and chemical cross-linking. *Biomacromolecules* **17**, 649-660 (2016).
67. D. Zhao *et al.*, High-Strength and High-Toughness Double-Cross-Linked Cellulose Hydrogels: A New Strategy Using Sequential Chemical and Physical Cross-Linking. *Advanced Functional Materials* **26**, 6279-6287 (2016).
68. X. Dai *et al.*, A Mechanically Strong, Highly Stable, Thermoplastic, and self-healable supramolecular polymer hydrogel. *Advanced Materials* **27**, 3566-3571 (2015).
69. F.-K. Shi, X.-P. Wang, R.-H. Guo, M. Zhong, X.-M. Xie, Highly stretchable and super tough nanocomposite physical hydrogels facilitated by the coupling of intermolecular hydrogen bonds and analogous chemical crosslinking of nanoparticles. *Journal of Materials Chemistry B* **3**, 1187-1192 (2015).
70. R. Du *et al.*, Hierarchical Hydrogen Bonds Directed Multi-Functional Carbon Nanotube-Based Supramolecular Hydrogels. *Small* **10**, 1387-1393 (2014).
71. M. Zhong, Y.-T. Liu, X.-M. Xie, Self-healable, super tough graphene oxide–poly (acrylic acid) nanocomposite hydrogels facilitated by dual cross-linking effects through dynamic ionic interactions. *Journal of Materials Chemistry B* **3**, 4001-4008 (2015).
72. M. Zhong *et al.*, Self-healable, tough and highly stretchable ionic nanocomposite physical hydrogels. *Soft Matter* **11**, 4235-4241 (2015).
73. Y. Guo *et al.*, A self-healable and easily recyclable supramolecular hydrogel electrolyte for flexible supercapacitors. *Journal of Materials Chemistry A* **4**, 8769-8776 (2016).
74. P. W. Frederix *et al.*, Exploring the sequence space for (tri-) peptide self-assembly to design and discover new hydrogels. *Nature chemistry* **7**, 30 (2015).
75. L. Li, B. Yan, J. Yang, L. Chen, H. Zeng, Novel Mussel-Inspired Injectable Self-Healing Hydrogel with Anti-Biofouling Property. *Advanced Materials* **27**, 1294-1299 (2015).
76. M. C. Koetting, J. F. Guido, M. Gupta, A. Zhang, N. A. Peppas, pH-responsive and enzymatically-responsive hydrogel microparticles for the oral delivery of therapeutic proteins: effects of protein size, crosslinking density, and hydrogel degradation on protein delivery. *Journal of Controlled Release* **221**, 18-25 (2016).
77. S. Lee, X. Tong, F. Yang, The effects of varying poly (ethylene glycol) hydrogel crosslinking density and the crosslinking mechanism on protein accumulation in three-dimensional hydrogels. *Acta biomaterialia* **10**, 4167-4174 (2014).
78. P. Lin, S. Ma, X. Wang, F. Zhou, Molecularly Engineered Dual-Crosslinked Hydrogel with Ultrahigh Mechanical Strength, Toughness, and Good Self-Recovery. *Advanced Materials* **27**, 2054-2059 (2015).

79. R. M. Desai, S. T. Koshy, S. A. Hilderbrand, D. J. Mooney, N. S. Joshi, Versatile click alginate hydrogels crosslinked via tetrazine–norbornene chemistry. *Biomaterials* **50**, 30-37 (2015).
80. X. Hu, M. Vatankhah-Varnoosfaderani, J. Zhou, Q. Li, S. S. Sheiko, Weak hydrogen bonding enables hard, strong, tough, and elastic hydrogels. *Advanced Materials* **27**, 6899-6905 (2015).
81. M. Guo *et al.*, Tough stimuli-responsive supramolecular hydrogels with hydrogen-bonding network junctions. *Journal of the American Chemical Society* **136**, 6969-6977 (2014).
82. Y. Choi *et al.*, Low-Voltage Complementary Electronics from Ion-Gel-Gated Vertical Van der Waals Heterostructures. *Advanced Materials* **28**, 3742-3748 (2016).
83. J. Visser *et al.*, Reinforcement of hydrogels using three-dimensionally printed microfibres. *Nature communications* **6**, 6933 (2015).
84. Y. Lu, Y. Wu, J. Liang, M. R. Libera, S. A. Sukhishvili, Self-defensive antibacterial layer-by-layer hydrogel coatings with pH-triggered hydrophobicity. *Biomaterials* **45**, 64-71 (2015).
85. Y. Geng *et al.*, Hydrophobic association mediated physical hydrogels with high strength and healing ability. *Polymer* **100**, 60-68 (2016).
86. H. He *et al.*, Multifunctional photo-crosslinked polymeric ionic hydrogel films. *Polymer Chemistry* **5**, 2824-2835 (2014).
87. X. Pu *et al.*, Ultrastretchable, transparent triboelectric nanogenerator as electronic skin for biomechanical energy harvesting and tactile sensing. *Science advances* **3**, e1700015 (2017).
88. S. Tosatti *et al.*, Coefficient of friction comparison of worn daily disposable silicone hydrogel contact lenses to human corneal tissue. *Contact Lens and Anterior Eye* **41**, S4-S5 (2018).
89. K. Zhang *et al.*, Strategy for constructing vascularized adipose units in poly (l-glutamic acid) hydrogel porous scaffold through inducing in-situ formation of ASCs spheroids. *Acta biomaterialia* **51**, 246-257 (2017).
90. S. Anjum, A. Arora, M. Alam, B. Gupta, Development of antimicrobial and scar preventive chitosan hydrogel wound dressings. *International journal of pharmaceutics* **508**, 92-101 (2016).
91. N. A. Peppas, D. S. Van Blarcom, Hydrogel-based biosensors and sensing devices for drug delivery. *Journal of Controlled Release* **240**, 142-150 (2016).
92. L. Sun *et al.*, A hydrogel biosensor for high selective and sensitive detection of amyloid-beta oligomers. *International journal of nanomedicine* **13**, 843 (2018).
93. S. Gu, L. Duan, X. Ren, G. H. Gao, Robust, tough and anti-fatigue cationic latex composite hydrogels based on dual physically cross-linked networks. *Journal of colloid and interface science* **492**, 119-126 (2017).
94. W. J. Zheng, N. An, J. H. Yang, J. Zhou, Y. M. Chen, Tough Al-alginate/poly (N-isopropylacrylamide) hydrogel with tunable LCST for soft robotics. *ACS applied materials & interfaces* **7**, 1758-1764 (2015).
95. Z. Li *et al.*, A novel biocompatible double network hydrogel consisting of konjac glucomannan with high mechanical strength and ability to be freely shaped. *Journal of Materials Chemistry B* **3**, 1769-1778 (2015).
96. S. Liu, W. Su, Y. Li, L. Zhang, X. Ding, Manufacturing of an electrochemical biosensing platform based on hybrid DNA hydrogel: Taking lung cancer-specific miR-21 as an example. *Biosensors and Bioelectronics* **103**, 1-5 (2018).
97. T. Kajisa, T. Sakata, Glucose-responsive hydrogel electrode for biocompatible glucose transistor. *Science and Technology of advanced MaTerialS* **18**, 26-33 (2017).
98. J. Deng, W. Liang, J. Fang, Liquid crystal droplet-embedded biopolymer hydrogel sheets for biosensor applications. *ACS applied materials & interfaces* **8**, 3928-3932 (2016).
99. Y.-N. Chou *et al.*, Ultra-low fouling and high antibody loading zwitterionic hydrogel coatings for sensing and detection in complex media. *Acta biomaterialia* **40**, 31-37 (2016).

100. S. Burrs *et al.*, A comparative study of graphene–hydrogel hybrid bionanocomposites for biosensing. *Analyst* **140**, 1466-1476 (2015).
101. K. Goh, H. Li, K. Y. Lam, Development of a multiphysics model to characterize the responsive behavior of urea-sensitive hydrogel as biosensor. *Biosensors and Bioelectronics* **91**, 673-679 (2017).
102. P. Pinyou *et al.*, Design of an Os Complex-Modified Hydrogel with Optimized Redox Potential for Biosensors and Biofuel Cells. *Chemistry–A European Journal* **22**, 5319-5326 (2016).
103. H. Xiong *et al.*, A convenient purification method for silver nanoclusters and its applications in fluorescent pH sensors for bacterial monitoring. *Biosensors and Bioelectronics* **86**, 164-168 (2016).
104. K. Goh, H. Li, K. Lam, Characterization of dual urea-and pH-induced behaviors of smart hydrogel at human physiological conditions. *Procedia Engineering* **214**, 86-92 (2017).
105. D. Puchberger, M. J. Vellekoop, Hydrogels for Imaging, Sensing and Diagnostics. *Hydrogels: Design, Synthesis and Application in Drug Delivery and Regenerative Medicine*, 140 (2018).
106. H. Yuk, T. Zhang, S. Lin, G. A. Parada, X. Zhao, Tough bonding of hydrogels to diverse non-porous surfaces. *Nature materials* **15**, 190 (2016).
107. V. X. Truong, M. P. Ablett, S. M. Richardson, J. A. Hoyland, A. P. Dove, Simultaneous orthogonal dual-click approach to tough, in-situ-forming hydrogels for cell encapsulation. *Journal of the American Chemical Society* **137**, 1618-1622 (2015).
108. L. Qiu *et al.*, Mechanically Robust, Electrically Conductive and Stimuli-Responsive Binary Network Hydrogels Enabled by Superelastic Graphene Aerogels. *Advanced Materials* **26**, 3333-3337 (2014).
109. X. Xu *et al.*, Naturally dried graphene aerogels with superelasticity and tunable Poisson's ratio. *Advanced materials* **28**, 9223-9230 (2016).
110. B. Yao *et al.*, Ultrahigh-Conductivity Polymer Hydrogels with Arbitrary Structures. *Advanced Materials* **29**, 1700974 (2017).
111. W. Zhao, L. Glavas, K. Odelius, U. Edlund, A.-C. Albertsson, Facile and green approach towards electrically conductive hemicellulose hydrogels with tunable conductivity and swelling behavior. *Chemistry of Materials* **26**, 4265-4273 (2014).
112. C. B. Highley, C. B. Rodell, J. A. Burdick, Direct 3D printing of shear-thinning hydrogels into self-healing hydrogels. *Advanced Materials* **27**, 5075-5079 (2015).
113. Q. Feng *et al.*, Mechanically resilient, injectable, and bioadhesive supramolecular gelatin hydrogels crosslinked by weak host-guest interactions assist cell infiltration and in situ tissue regeneration. *Biomaterials* **101**, 217-228 (2016).
114. L. Cai, R. E. Dewi, S. C. Heilshorn, Injectable hydrogels with in situ double network formation enhance retention of transplanted stem cells. *Advanced functional materials* **25**, 1344-1351 (2015).
115. S. Gao *et al.*, A robust polyionized hydrogel with an unprecedented underwater anti-crude-oil-adhesion property. *Advanced Materials* **28**, 5307-5314 (2016).
116. F. Yu, X. Cao, J. Du, G. Wang, X. Chen, Multifunctional hydrogel with good structure integrity, self-healing, and tissue-adhesive property formed by combining Diels–Alder click reaction and acylhydrazone bond. *ACS applied materials & interfaces* **7**, 24023-24031 (2015).
117. C. Li *et al.*, Responsive double network hydrogels of interpenetrating DNA and CB [8] host–guest supramolecular systems. *Advanced Materials* **27**, 3298-3304 (2015).
118. Z. Gong *et al.*, High-strength, tough, fatigue resistant, and self-healing hydrogel based on dual physically cross-linked network. *ACS applied materials & interfaces* **8**, 24030-24037 (2016).
119. T. Nonoyama *et al.*, Double-network hydrogels strongly bondable to bones by spontaneous osteogenesis penetration. *Advanced Materials* **28**, 6740-6745 (2016).

120. C. García-Astrain *et al.*, Biocompatible hydrogel nanocomposite with covalently embedded silver nanoparticles. *Biomacromolecules* **16**, 1301-1310 (2015).
121. A. Pourjavadi, M. Nazari, S. H. Hosseini, Synthesis of magnetic graphene oxide-containing nanocomposite hydrogels for adsorption of crystal violet from aqueous solution. *RSC Advances* **5**, 32263-32271 (2015).
122. J. Li, J. Xie, L. Gao, C. M. Li, Au nanoparticles–3D graphene hydrogel nanocomposite to boost synergistically in situ detection sensitivity toward cell-released nitric oxide. *ACS applied materials & interfaces* **7**, 2726-2734 (2015).
123. H. Chen *et al.*, A comparative study of the mechanical properties of hybrid double-network hydrogels in swollen and as-prepared states. *Journal of Materials Chemistry B* **4**, 5814-5824 (2016).
124. M. A. Darabi *et al.*, Skin-Inspired Multifunctional Autonomic-Intrinsic Conductive Self-Healing Hydrogels with Pressure Sensitivity, Stretchability, and 3D Printability. *Advanced Materials* **29**, (2017).
125. R. Xu *et al.*, New double network hydrogel adsorbent: highly efficient removal of Cd (II) and Mn (II) ions in aqueous solution. *Chemical Engineering Journal* **275**, 179-188 (2015).
126. E. S. Dragan, Design and applications of interpenetrating polymer network hydrogels. A review. *Chemical Engineering Journal* **243**, 572-590 (2014).
127. W. Xiao *et al.*, Synthesis and characterization of photocrosslinkable gelatin and silk fibroin interpenetrating polymer network hydrogels. *Acta biomaterialia* **7**, 2384-2393 (2011).
128. R. E. Webber, C. Creton, H. R. Brown, J. P. Gong, Large strain hysteresis and mullins effect of tough double-network hydrogels. *Macromolecules* **40**, 2919-2927 (2007).
129. S. Hong *et al.*, 3D printing of highly stretchable and tough hydrogels into complex, cellularized structures. *Advanced materials* **27**, 4035-4040 (2015).
130. L. Li, W. Smitthipong, H. Zeng, Mussel-inspired hydrogels for biomedical and environmental applications. *Polymer Chemistry* **6**, 353-358 (2015).
131. J. Liu *et al.*, Synthesis of graphene peroxide and its application in fabricating super extensible and highly resilient nanocomposite hydrogels. *Acs Nano* **6**, 8194-8202 (2012).
132. H.-P. Cong, P. Wang, S.-H. Yu, Stretchable and self-healing graphene oxide–polymer composite hydrogels: a dual-network design. *Chemistry of Materials* **25**, 3357-3362 (2013).
133. X. Feng, W. Chen, L. Yan, Reduced graphene oxide hydrogel film with a continuous ion transport network for supercapacitors. *Nanoscale* **7**, 3712-3718 (2015).
134. K. Yue *et al.*, Synthesis, properties, and biomedical applications of gelatin methacryloyl (GelMA) hydrogels. *Biomaterials* **73**, 254-271 (2015).
135. S. Ahadian *et al.*, Hybrid hydrogels containing vertically aligned carbon nanotubes with anisotropic electrical conductivity for muscle myofiber fabrication. *Scientific reports* **4**, 4271 (2014).
136. M. Bora, A. G. P. Kottapalli, J. Miao, M. S. Triantafyllou, Biomimetic hydrogel-CNT network induced enhancement of fluid-structure interactions for ultrasensitive nanosensors. *NPG Asia Materials* **9**, e440 (2017).
137. B. Mathieu, C. Anthony, A. Arnaud, F. Lionel, CNT aggregation mechanisms probed by electrical and dielectric measurements. *Journal of Materials Chemistry C* **3**, 5769-5774 (2015).
138. F. Inam, A. Heaton, P. Brown, T. Peijs, M. J. Reece, Effects of dispersion surfactants on the properties of ceramic–carbon nanotube (CNT) nanocomposites. *Ceramics International* **40**, 511-516 (2014).
139. Y. S. Song, J. R. Youn, Influence of dispersion states of carbon nanotubes on physical properties of epoxy nanocomposites. *Carbon* **43**, 1378-1385 (2005).
140. J. Sun *et al.*, Ultra-high dielectric constant of poly (vinylidene fluoride) composites filled with hydroxyl modified graphite powders. *Polymer Composites* **37**, 327-333 (2016).
141. L. Ma *et al.*, Enhanced Li–S batteries using amine-functionalized carbon nanotubes in the cathode. *ACS nano* **10**, 1050-1059 (2015).

142. X. Gao, A. Omosebi, J. Landon, K. Liu, Enhanced salt removal in an inverted capacitive deionization cell using amine modified microporous carbon cathodes. *Environmental science & technology* **49**, 10920-10926 (2015).
143. Z. Guan, X.-Y. Tang, T. Nishimura, Y.-M. Huang, B. J. Reid, Adsorption of linear alkylbenzene sulfonates on carboxyl modified multi-walled carbon nanotubes. *Journal of hazardous materials* **322**, 205-214 (2017).
144. T. W. Odom, J.-L. Huang, P. Kim, C. M. Lieber, Atomic structure and electronic properties of single-walled carbon nanotubes. *Nature* **391**, 62 (1998).
145. J. Kong *et al.*, Nanotube molecular wires as chemical sensors. *science* **287**, 622-625 (2000).
146. A. Vashist *et al.*, Nanocomposite Hydrogels: Advances in Nanofillers Used for Nanomedicine. *Gels* **4**, 75 (2018).
147. K. D. Behler *et al.*, Nanodiamond-polymer composite fibers and coatings. *ACS nano* **3**, 363-369 (2009).
148. Y. Zhu *et al.*, The biocompatibility of nanodiamonds and their application in drug delivery systems. *Theranostics* **2**, 302 (2012).
149. V. N. Mochalin, O. Shenderova, D. Ho, Y. Gogotsi, The properties and applications of nanodiamonds. *Nature nanotechnology* **7**, 11 (2012).
150. K. H. Nakayama, L. Hou, N. F. Huang, Role of extracellular matrix signaling cues in modulating cell fate commitment for cardiovascular tissue engineering. *Advanced healthcare materials* **3**, 628-641 (2014).
151. S. Bauer *et al.*, 25th anniversary article: a soft future: from robots and sensor skin to energy harvesters. *Advanced Materials* **26**, 149-162 (2014).
152. Y. Liu *et al.*, Highly Flexible and Resilient Elastin Hybrid Cryogels with Shape Memory, Injectability, Conductivity, and Magnetic Responsive Properties. *Advanced Materials* **28**, 7758-7767 (2016).
153. N. Annabi *et al.*, Highly Elastic and Conductive Human-Based Protein Hybrid Hydrogels. *Adv Mater* **28**, 40-49 (2016).
154. S. Liu *et al.*, Antibacterial activity of graphite, graphite oxide, graphene oxide, and reduced graphene oxide: membrane and oxidative stress. *ACS nano* **5**, 6971-6980 (2011).
155. S. Stankovich *et al.*, Synthesis of graphene-based nanosheets via chemical reduction of exfoliated graphite oxide. *carbon* **45**, 1558-1565 (2007).
156. S. Sowmya *et al.*, Tri-Layered Nanocomposite Hydrogel Scaffold for the Concurrent Regeneration of Cementum, Periodontal Ligament, and Alveolar Bone. *Advanced Healthcare Materials*, (2017).
157. M. Y. Kim *et al.*, Augmentation of tendon healing with an injectable tendon hydrogel in a rat Achilles tendon model. *Plastic and reconstructive surgery* **133**, 645e-653e (2014).
158. J. Cui, A. del Campo, Multivalent H-bonds for self-healing hydrogels. *Chemical Communications* **48**, 9302-9304 (2012).
159. H. Zhang, H. Xia, Y. Zhao, Poly (vinyl alcohol) hydrogel can autonomously self-heal. *Acs Macro Letters* **1**, 1233-1236 (2012).
160. B. Liu *et al.*, Hydrogen bonds autonomously powered gelatin methacrylate hydrogels with super-elasticity, self-heal and underwater self-adhesion for sutureless skin and stomach surgery and E-skin. *Biomaterials* **171**, 83-96 (2018).
161. Z. Wei *et al.*, Autonomous self-healing of poly (acrylic acid) hydrogels induced by the migration of ferric ions. *Polymer Chemistry* **4**, 4601-4605 (2013).
162. D. C. Tuncaboylu, M. Sari, W. Oppermann, O. Okay, Tough and self-healing hydrogels formed via hydrophobic interactions. *Macromolecules* **44**, 4997-5005 (2011).
163. A. B. Ihsan *et al.*, Self-healing behaviors of tough polyampholyte hydrogels. *Macromolecules* **49**, 4245-4252 (2016).
164. J. Chen *et al.*, High-toughness polyacrylamide gel containing hydrophobic crosslinking and its double network gel. *Polymer* **87**, 73-80 (2016).

165. F. Rengier *et al.*, 3D printing based on imaging data: review of medical applications. *International journal of computer assisted radiology and surgery* **5**, 335-341 (2010).
166. S. Bose, S. Vahabzadeh, A. Bandyopadhyay, Bone tissue engineering using 3D printing. *Materials today* **16**, 496-504 (2013).
167. G. Matzeu, L. Florea, D. Diamond, Advances in wearable chemical sensor design for monitoring biological fluids. *Sensors and Actuators B: Chemical* **211**, 403-418 (2015).
168. D. Diamond, S. Coyle, S. Scarmagnani, J. Hayes, Wireless sensor networks and chemo-/biosensing. *Chemical reviews* **108**, 652-679 (2008).
169. J. R. Windmiller, J. Wang, Wearable electrochemical sensors and biosensors: a review. *Electroanalysis* **25**, 29-46 (2013).
170. M. A. Darabi *et al.*, Skin-Inspired Multifunctional Autonomic-Intrinsic Conductive Self-Healing Hydrogels with Pressure Sensitivity, Stretchability, and 3D Printability. *Advanced Materials* **29**, 1700533 (2017).
171. J. T. Muth *et al.*, Embedded 3D printing of strain sensors within highly stretchable elastomers. *Advanced Materials* **26**, 6307-6312 (2014).
172. K. Li *et al.*, 3D printed stretchable capacitive sensors for highly sensitive tactile and electrochemical sensing. *Nanotechnology* **29**, 185501 (2018).
173. A. P. Periasamy, Y.-J. Chang, S.-M. Chen, Amperometric glucose sensor based on glucose oxidase immobilized on gelatin-multiwalled carbon nanotube modified glassy carbon electrode. *Bioelectrochemistry* **80**, 114-120 (2011).
174. A. Roda *et al.*, A 3D-printed device for a smartphone-based chemiluminescence biosensor for lactate in oral fluid and sweat. *Analyst* **139**, 6494-6501 (2014).
175. P. T. Charles *et al.*, Fabrication and characterization of 3D hydrogel microarrays to measure antigenicity and antibody functionality for biosensor applications. *Biosensors and Bioelectronics* **20**, 753-764 (2004).
176. S. Pei, J. Zhao, J. Du, W. Ren, H.-M. Cheng, Direct reduction of graphene oxide films into highly conductive and flexible graphene films by hydrohalic acids. *Carbon* **48**, 4466-4474 (2010).
177. H. P. Cong, P. Wang, S. H. Yu, Highly elastic and superstretchable graphene oxide/polyacrylamide hydrogels. *Small* **10**, 448-453 (2014).
178. J. Wang, C. Liu, Y. Shuai, X. Cui, L. Nie, Controlled release of anticancer drug using graphene oxide as a drug-binding effector in konjac glucomannan/sodium alginate hydrogels. *Colloids and Surfaces B: Biointerfaces* **113**, 223-229 (2014).
179. M. Mabrouk *et al.*, Design of a novel crosslinked HEC-PAA porous hydrogel composite for dissolution rate and solubility enhancement of efavirenz. *International journal of pharmaceutics* **490**, 429-437 (2015).
180. K. Qiao *et al.*, Effects of graphene on the structure, properties, electro-response behaviors of GO/PAA composite hydrogels and influence of electro-mechanical coupling on BMSC differentiation. *Materials Science and Engineering: C* **93**, 853-863 (2018).
181. S. J. Kim, S. J. Park, S. I. Kim, Swelling behavior of interpenetrating polymer network hydrogels composed of poly (vinyl alcohol) and chitosan. *Reactive and Functional Polymers* **55**, 53-59 (2003).
182. T. Miyata, N. Asami, T. Uragami, A reversibly antigen-responsive hydrogel. *Nature* **399**, 766 (1999).
183. E. Jabbari, S. Nozari, Swelling behavior of acrylic acid hydrogels prepared by γ-radiation crosslinking of polyacrylic acid in aqueous solution. *European Polymer Journal* **36**, 2685-2692 (2000).
184. J. E. Elliott, M. Macdonald, J. Nie, C. N. Bowman, Structure and swelling of poly (acrylic acid) hydrogels: effect of pH, ionic strength, and dilution on the crosslinked polymer structure. *Polymer* **45**, 1503-1510 (2004).
185. B. Timmer, W. Olthuis, A. Van Den Berg, Ammonia sensors and their applications—a review. *Sensors and Actuators B: Chemical* **107**, 666-677 (2005).

186. S. Bhadra, D. J. Thomson, G. E. Bridges, Monitoring acidic and basic volatile concentration using a pH-electrode based wireless passive sensor. *Sensors and Actuators B: Chemical* **209**, 803-810 (2015).
187. Z. Wei *et al.*, Novel biocompatible polysaccharide-based self-healing hydrogel. *Advanced Functional Materials* **25**, 1352-1359 (2015).
188. C. Ghobril, M. Grinstaff, The chemistry and engineering of polymeric hydrogel adhesives for wound closure: a tutorial. *Chemical Society Reviews* **44**, 1820-1835 (2015).
189. J. Duan, X. Liang, Y. Cao, S. Wang, L. Zhang, High strength chitosan hydrogels with biocompatibility via new avenue based on constructing nanofibrous architecture. *Macromolecules* **48**, 2706-2714 (2015).
190. D. J. Miller, D. R. Dreyer, C. W. Bielawski, D. R. Paul, B. D. Freeman, Surface modification of water purification membranes. *Angewandte Chemie International Edition* **56**, 4662-4711 (2017).
191. S. Lin *et al.*, Stretchable hydrogel electronics and devices. *Advanced Materials* **28**, 4497-4505 (2016).
192. J. Zhang, H. Xiao, N. Li, Q. Ping, Y. Zhang, Synthesis and characterization of super-absorbent hydrogels based on hemicellulose. *Journal of Applied Polymer Science* **132**, (2015).
193. E. A. Kamoun, E.-R. S. Kenawy, X. Chen, A review on polymeric hydrogel membranes for wound dressing applications: PVA-based hydrogel dressings. *Journal of advanced research* **8**, 217-233 (2017).
194. J. P. Gong, Y. Katsuyama, T. Kurokawa, Y. Osada, Double-network hydrogels with extremely high mechanical strength. *Advanced materials* **15**, 1155-1158 (2003).
195. J. P. Gong, Why are double network hydrogels so tough? *Soft Matter* **6**, 2583-2590 (2010).
196. X. Zhang *et al.*, Double-network hydrogel with high mechanical strength prepared from two biocompatible polymers. *Journal of applied polymer science* **112**, 3063-3070 (2009).
197. C. B. Rodell, N. N. Dusaj, C. B. Highley, J. A. Burdick, Injectable and cytocompatible tough double-network hydrogels through tandem supramolecular and covalent crosslinking. *Advanced materials* **28**, 8419-8424 (2016).
198. J.-Y. Sun *et al.*, Highly stretchable and tough hydrogels. *Nature* **489**, 133 (2012).
199. M. D. Hager, P. Greil, C. Leyens, S. van der Zwaag, U. S. Schubert, Self-healing materials. *Advanced Materials* **22**, 5424-5430 (2010).
200. V. K. Thakur, M. R. Kessler, Self-healing polymer nanocomposite materials: A review. *Polymer* **69**, 369-383 (2015).
201. N. Roy, B. Bruchmann, J.-M. Lehn, DYNAMERS: dynamic polymers as self-healing materials. *Chemical Society Reviews* **44**, 3786-3807 (2015).
202. K. Imato *et al.*, Self-healing of chemical gels cross-linked by diarylbibenzofuranone-based trigger-free dynamic covalent bonds at room temperature. *Angewandte Chemie* **124**, 1164-1168 (2012).
203. G. Deng, C. Tang, F. Li, H. Jiang, Y. Chen, Covalent cross-linked polymer gels with reversible sol− gel transition and self-healing properties. *Macromolecules* **43**, 1191-1194 (2010).
204. B. K. Ahn, D. W. Lee, J. N. Israelachvili, J. H. Waite, Surface-initiated self-healing of polymers in aqueous media. *Nature materials* **13**, 867 (2014).
205. C.-H. Li *et al.*, A highly stretchable autonomous self-healing elastomer. *Nature chemistry* **8**, 618 (2016).
206. P. Michael, D. Doehler, W. H. Binder, Improving autonomous self healing via combined chemical/physical principles. *Polymer* **69**, 216-227 (2015).
207. P. Wei, X. Yan, F. Huang, Supramolecular polymers constructed by orthogonal self-assembly based on host–guest and metal–ligand interactions. *Chemical Society Reviews* **44**, 815-832 (2015).

208. I. Jeon, J. Cui, W. R. Illeperuma, J. Aizenberg, J. J. Vlassak, Extremely Stretchable and Fast Self-Healing Hydrogels. *Advanced Materials* **28**, 4678-4683 (2016).
209. S. Owusu-Nkwantabisah, J. R. Gillmor, S. C. Switalski, G. L. Slater, An autonomous self-healing hydrogel based on surfactant-free hydrophobic association. *Journal of Applied Polymer Science* **134**, (2017).
210. W. Pu, F. Jiang, P. Chen, B. Wei, A POSS based hydrogel with mechanical robustness, cohesiveness and a rapid self-healing ability by electrostatic interaction. *Soft matter* **13**, 5645-5648 (2017).
211. H. Wei *et al.*, Tunable, luminescent, and self-healing hybrid hydrogels of polyoxometalates and triblock copolymers based on electrostatic assembly. *Chemical Communications* **50**, 1447-1450 (2014).
212. W. Sun *et al.*, Polymer-Supramolecular Polymer Double-Network Hydrogel. *Advanced Functional Materials* **26**, 9044-9052 (2016).
213. L. Lin *et al.*, Bio-inspired hierarchical macromolecule–nanoclay hydrogels for robust underwater superoleophobicity. *Advanced materials* **22**, 4826-4830 (2010).
214. S. Chen, J. Duan, M. Jaroniec, S. Z. Qiao, Nitrogen and oxygen dual-doped carbon hydrogel film as a substrate-free electrode for highly efficient oxygen evolution reaction. *Advanced Materials* **26**, 2925-2930 (2014).
215. K. Shah, D. Vasileva, A. Karadaghy, S. Zustiak, Development and characterization of polyethylene glycol–carbon nanotube hydrogel composite. *Journal of Materials Chemistry B* **3**, 7950-7962 (2015).
216. A. Paul *et al.*, Injectable graphene oxide/hydrogel-based angiogenic gene delivery system for vasculogenesis and cardiac repair. *ACS nano* **8**, 8050-8062 (2014).
217. H. Bai, C. Li, X. Wang, G. Shi, A pH-sensitive graphene oxide composite hydrogel. *Chemical Communications* **46**, 2376-2378 (2010).
218. J. Liu, G. Song, C. He, H. Wang, Self-healing in tough graphene oxide composite hydrogels. *Macromolecular rapid communications* **34**, 1002-1007 (2013).
219. H. N. Tien *et al.*, Synthesis of a highly conductive and large surface area graphene oxide hydrogel and its use in a supercapacitor. *Journal of Materials Chemistry A* **1**, 208-211 (2013).
220. L. Zhang, G. Shi, Preparation of highly conductive graphene hydrogels for fabricating supercapacitors with high rate capability. *The Journal of Physical Chemistry C* **115**, 17206-17212 (2011).
221. R. Liu *et al.*, Tough and highly stretchable graphene oxide/polyacrylamide nanocomposite hydrogels. *Journal of Materials Chemistry* **22**, 14160-14167 (2012).
222. Q. Liu *et al.*, High-quality graphene ribbons prepared from graphene oxide hydrogels and their application for strain sensors. *ACS nano* **9**, 12320-12326 (2015).
223. S. R. Shin *et al.*, Cell-laden microengineered and mechanically tunable hybrid hydrogels of gelatin and graphene oxide. *Advanced materials* **25**, 6385-6391 (2013).
224. S. Wang, Z. Zhang, B. Chen, J. Shao, Z. Guo, Self-healing hydrogel of poly (vinyl alcohol)/graphite oxide with p H-sensitive and enhanced thermal properties. *Journal of Applied Polymer Science* **135**, 46143 (2018).
225. L. Sun *et al.*, Graphene Oxide hydrogel Particles from Microfluidics for Oil Decontamination. *Journal of colloid and interface science*, (2018).
226. K. Varaprasad, T. Jayaramudu, E. R. Sadiku, Removal of dye by carboxymethyl cellulose, acrylamide and graphene oxide via a free radical polymerization process. *Carbohydrate polymers* **164**, 186-194 (2017).
227. Z. Lei, Q. Wang, S. Sun, W. Zhu, P. Wu, A Bioinspired Mineral Hydrogel as a Self-Healable, Mechanically Adaptable Ionic Skin for Highly Sensitive Pressure Sensing. *Advanced Materials* **29**, 1700321 (2017).

228. C. Shao *et al.*, Mussel-Inspired Cellulose Nanocomposite Tough Hydrogels with Synergistic Self-Healing, Adhesive, and Strain-Sensitive Properties. *Chemistry of Materials* **30**, 3110-3121 (2018).
229. T. Cai, S. Huo, T. Wang, W. Sun, Z. Tong, Self-healable tough supramolecular hydrogels crosslinked by poly-cyclodextrin through host-guest interaction. *Carbohydrate polymers* **193**, 54-61 (2018).
230. T. Billiet, E. Gevaert, T. De Schryver, M. Cornelissen, P. Dubruel, The 3D printing of gelatin methacrylamide cell-laden tissue-engineered constructs with high cell viability. *Biomaterials* **35**, 49-62 (2014).
231. Z. Cheng *et al.*, 3D printing hydrogel with graphene oxide is functional in cartilage protection by influencing the signal pathway of Rank/Rankl/OPG. *Materials Science and Engineering: C* **82**, 244-252 (2018).
232. F. Gao *et al.*, Direct 3D Printing of High Strength Biohybrid Gradient Hydrogel Scaffolds for Efficient Repair of Osteochondral Defect. *Advanced Functional Materials* **28**, 1706644 (2018).

Appendix I

Biomimicry of oil infused layer on 3D printed poly(dimethylsiloxane): non-fouling, antibacterial and promoting infected wound healing

Abstract:

The nepenthes-inspired slippery liquid-infused surface has led to multiple potentials in biomedical devices' design. This study aims to develop a biomimetic, environmentally-friendly slippery layer of oil-infused 3D printed polydimethylsiloxane with anti-bacterial nanosilver (iPDMS/AgNPs) for wound dressing. The engineered 3D printed iPDMS can cater the different requirements of wounds with antifouling, anti-blood staining, and kill bacteria. iPDMS/AgNPs not only exhibits biocompatibility, against adherence and effective antibacterial activity but also effectively promotes neo-epithelial and granulation tissue formation to accelerate wound healing *in vivo*. Optimized rheologic parameters were obtained for the 3D printable iPDMS pre-polymerization condition. Scanning electronic micrograph (SEM) and Energy Dispersive Spectrometer (EDS) show a uniform mesh with AgNPs dotted on the printed dressing. No cytotoxicity of iPDMS/AgNPs has been found via cell Counting Kit-8(CCK-8) assay. Meanwhile, the membranes infused with silicon oil effectively prevented from the adherence of the standard drug-resistant bacteria, *Staphylococcus aureus* and *Escherichia coli* (PDMS vs. PDMS+oil, $p< 0.05$; PDMS+0.5%AgNPs vs. iPDMS+0.5%AgNPs, $p < 0.05$; PDMS+2.5%AgNPs vs. iPDMS+2.5%AgNPs, $p < 0.05$). By bacteria co-culture model iPDMS/AgNPs can kill about eighty percent of *Staphylococcus aureus* and *Escherichia coli*. When applied to a full-thickness wound defect model of murine, iPDMS/AgNPs was effective in anti-infection. It also promotes the epithelialization, the granulation tissue formation, and wound healing. These findings demonstrate that iPDMS/AgNPs may have therapeutic promise as an ideal wound dressing shortly.

Keywords: Biomimetics, 3D bioprinting; oil-infused polydimethylsiloxane; non-fouling; blood staining; antibacterial and anti-infection; wound healing

Introduction

Of the numerous threatens to skins, burn injury is a most dreadful healthy problem due to bacterial infection, which can damage both epidermis and dermis layers of human's skin, resulting in deeper wounds and even death (*232*). Therefore, preventing burn wound from invasive infection is of great significance to accelerate wound healing (*233*). Meanwhile, non-fouling is very important for wound dressing, because changing dressing may result in painful and harmful to neo-generated epidermis due to the adhesion of dressing to wound (*233*).

Wound dressing in burn wound is to keep wound clean and protect the wound from the external contamination (*233-235*). The traditional wound dressings such as cotton gauze and bandages can fulfill surfacing barrier to external agitation, but in fact, the efficiency of reducing bacterial infection is of below expectation. Plus, they are prone to adhere due to wound exudate soaking into dressing fibers, which leads to non-tolerable pain in dressing change(*236*). The natural and synthetic alternatives using chitosan (*237*), alginate (*238*), silicone (*239*), polyacrylamide (*240*) and polylactic acid (*241*) are soft, biocompatible and able to absorb wound exudate thus maintaining desirable humidity for wound healing. Wound dressing to efficiently battle bacterial infection, adhesion and clearing microorganisms remains a challenge. Usually, incorporated antimicrobial agents include such as Iodine (*242*), triclosan (*243*), quaternary ammonium (QA) salts (*244*), silver (*242*), and N-chloramines (*245*).

Polydimethylsiloxane (PDMS), a hydrophobic, non-toxic, biocompatible polymer with rubber-like elasticity, holds a competitive place in the fabrication of medical devices(*246, 247*). As biomimicry of insect shell in-out of liquid surface, PDMS was rendered a slippery surface by perfusing with a myriad quantity of a lubricating liquid (*248*). An anti-bacterial dressing cannot neglect bacterial attachment and biofilm formation. We thus employ non-fouling, lubricant-infused slippery

polymers as proof-of-concept medical materials that are based on oil-infused polydimethylsiloxane (iPDMS) for this purpose (*248*). 3D printing, an additive manufacturing technology, "draws" patterns on a substrate from bottom to up to patterned manipulated 3D shapes (*249*). Bioink and high-resolution mechanics render 3D printer to have more potential in bioengineering (*230*) such as biosensors (*250*) and tissue-engineering scaffolds (*251*) and customized wound dressing (*251*).

Herein, we proposed a multi-potential wound dressing by 3D printing PDMS including silver nanoparticles(AgNPs) and oil infusion (iPDMS) to ensure a better anti-adherence, anti-infection and pore-controllability (schematic illustration).This study verified firstly whether iPDMS/AgNPs possessed non-fouling and antibacterial capacity from *in vitro* and *in vivo*. *Staphylococcus aureus* and *Escherichia coli* were chosen as the model bacteria for the antibacterial and non-fouling properties investigation. We detected the biocompatibility of iPDMS/AgNPs to mammalian cells and organs. Finally, iPDMS/AgNPs was applied to the murine full-thickness skin defect infected wound model to estimate the antibacterial and biocompatible characteristics *in vivo*.

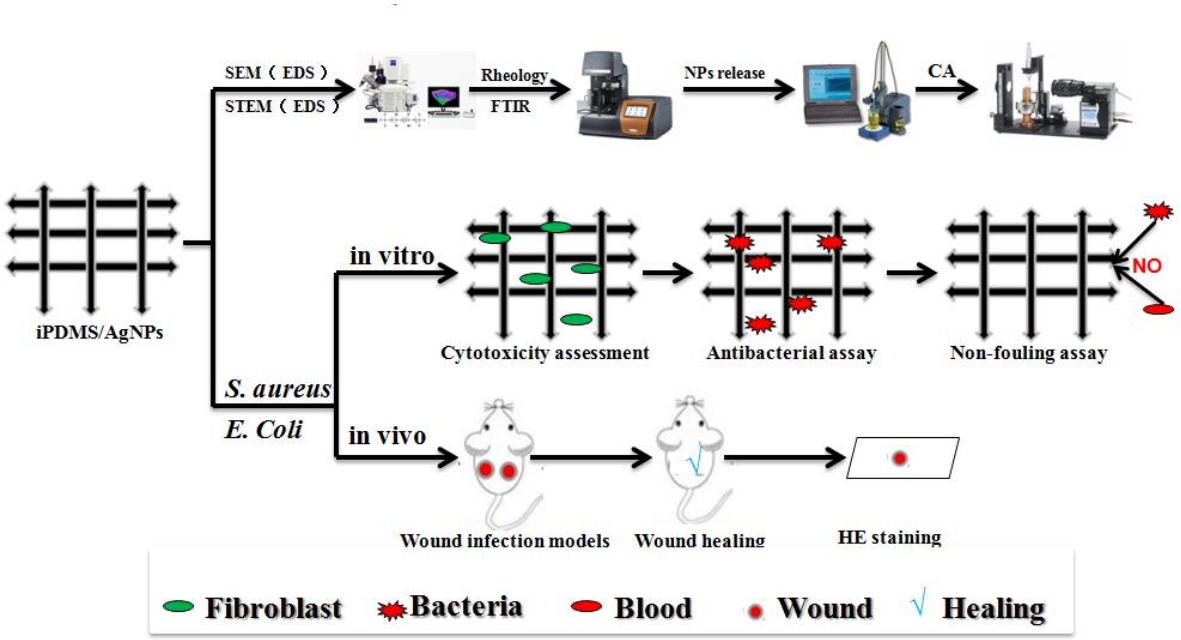

Schematic illustration: 3D printed biomimetic iPDMS/AgNP as a dressing with anti-fouling, anti-bacterial and promoting wound healing

Results and Discussions

Rheological Characterization of pre-curing PDMS for 3D printing

To investigate the printable ability of the ink, the dynamic oscillatory frequency sweep of pre-curing PDMS was performed for a constant frequency of 10 rad/s to study the storage moduli (G') and loss moduli (G''). As shown in Figure 1A, at experimental temperature of 50°C, within a 0~1600s range, G'' shows continuously greater than G', which indicates a liquid-like property, however, after 1600s, G' began to undergo a dramatic increase and exceeded G'', which illustrates more solid. Therefore, the best time for pre-curing should be beyond this time point of 1600s. In order to figure out a best printability of the prepolymer, it is also necessary to find out the best viscosity because appropriate concentration and their ratio should have shear-thinning to get through the extruder and help ink attach to substrate while printing, however, the ink shouldn't be too sticky since it would be hard to be squeezed out from syringe. Figure 1A shows the viscosity property under 50°C while pre-curing, we found that there is a surge of viscosity after 1500s, which concludes that the pre-curing time obtaining best viscosity for printing is about 1200s. A similar phenomenon was observed when increased the experimental temperature to 80°C, as shown in Figure 1B, it is advised that G'' curve was higher than G' curve at the beginning but G' went up rapidly and exceeded G'', which indicates the transformation from liquid to solid occurring very fast. Also, in the temperature of 80°C, viscosity surged since the very beginning and reached its plateau in 500s. Therefore, This is a good indication for ink deposition onto substrate and printing can be heated to 80°C to facilitate the ink cured and to maintain a stable shape.

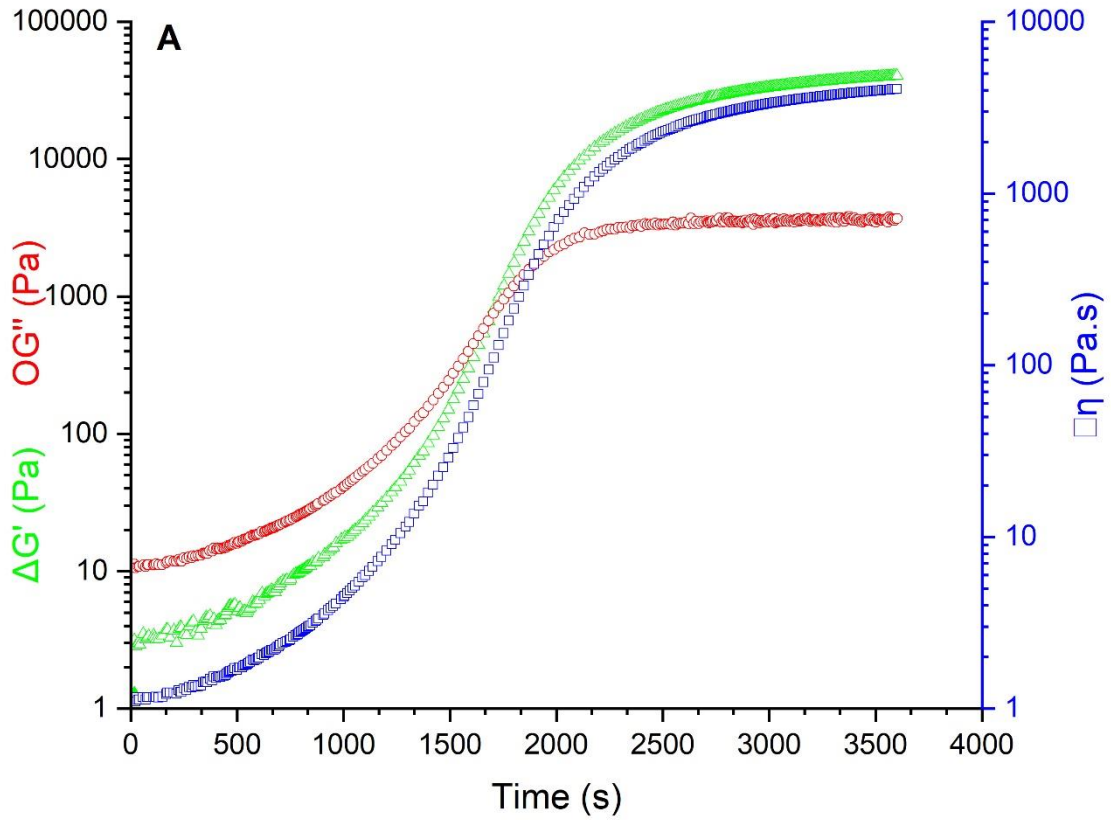
A
100000
10000
1000
100
10
1
ΔG' (Pa)
OG'' (Pa)
10000
1000
100
10
1
□η (Pa.s)
0
500
1000
1500
2000
2500
3000
3500
4000
Time (s)

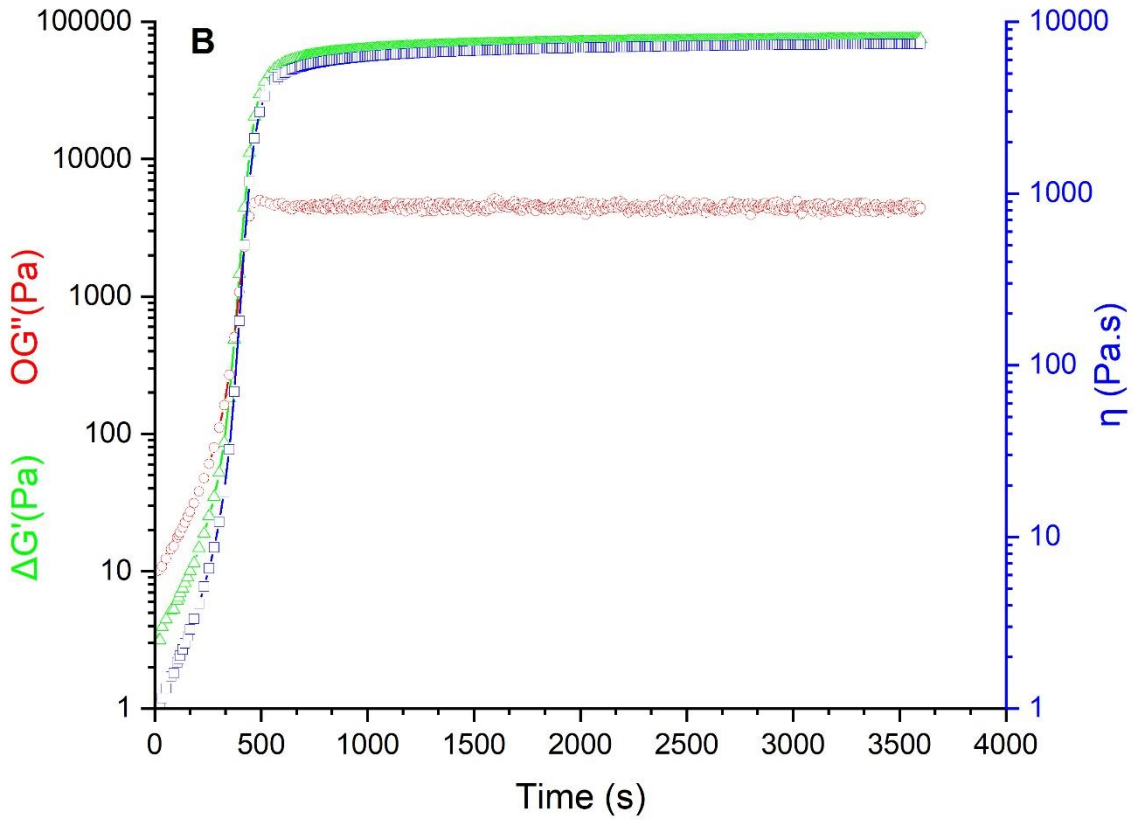

Figure 1. Rheological characterization during PDMS curing process at different temperature (A) at 50°C and (B) at 80°C.

Characterization of the iPDMS/AgNPs nanocomposite

Meanwhile, for the convenience of surface infusion, we considered using 5 Cst silicone oil for their similarity to PDMS in structure and polarity but better fluidity than PDMS. The 3D architecture of iPDMS/AgNPs wound dressing was obtained by using a versatile 3D bioprinter (3D HKable®) as shown in Figure 2A.

As shown in Figure 2B1-2B2, iPDMS/AgNP could be folded and stretched easily. It suggests that iPDMS/AgNP membrane have good flexibility. As shown in Figure 2C, PDMS membranes decorated with silicon oil showed a smooth surface without bumps. As shown in Figure 2D, AgNPs dotted the surface of oil-infused PDMS membranes with the average diameter 14.8 nm of the bump of the surface in keeping with the size of AgNPs (less than 100 nm) of the report (*252*). As shown

in Figure 2E, the dispersive energy analysis of iPDMS/AgNPs shows that 1.1% Ag was found using EDS.

The morphology and distribution of AgNPs were further investigated by scanning transmission electronic microscopy (STEM). As shown in Figure 2F, AgNPs were typically spherical and uniformly distributed on the PDMS surface, and the average diameter of AgNPs was 14.8 nm, as determined by an Image J analysis. Together with STEM, the energy-dispersive X-ray spectroscopy (EDS) analysis of the PDMS/AgNPs nanocomposite demonstrated the presence of Ag (Figure 2G). Moreover, FTIR-ATR characterization was run on PDMS, silver nanoparticles, and iPDMS/AgNPs 3D-printed composites. As shown in Figure 3, absorbance peaks in the PDMS/AgNPs spectrum contained all characteristic absorbance peaks in both PDMS polymer and AgNPs powder, suggesting the existence of silver nanoparticles in PDMS substrates.

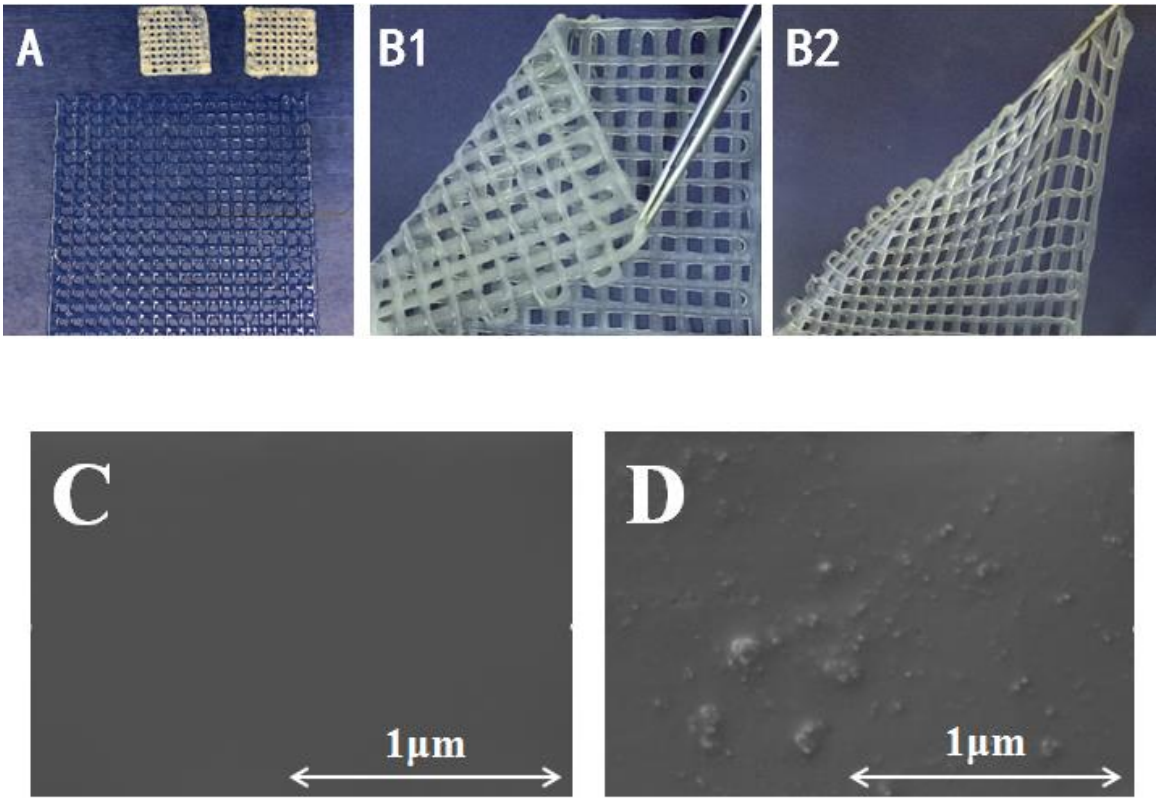

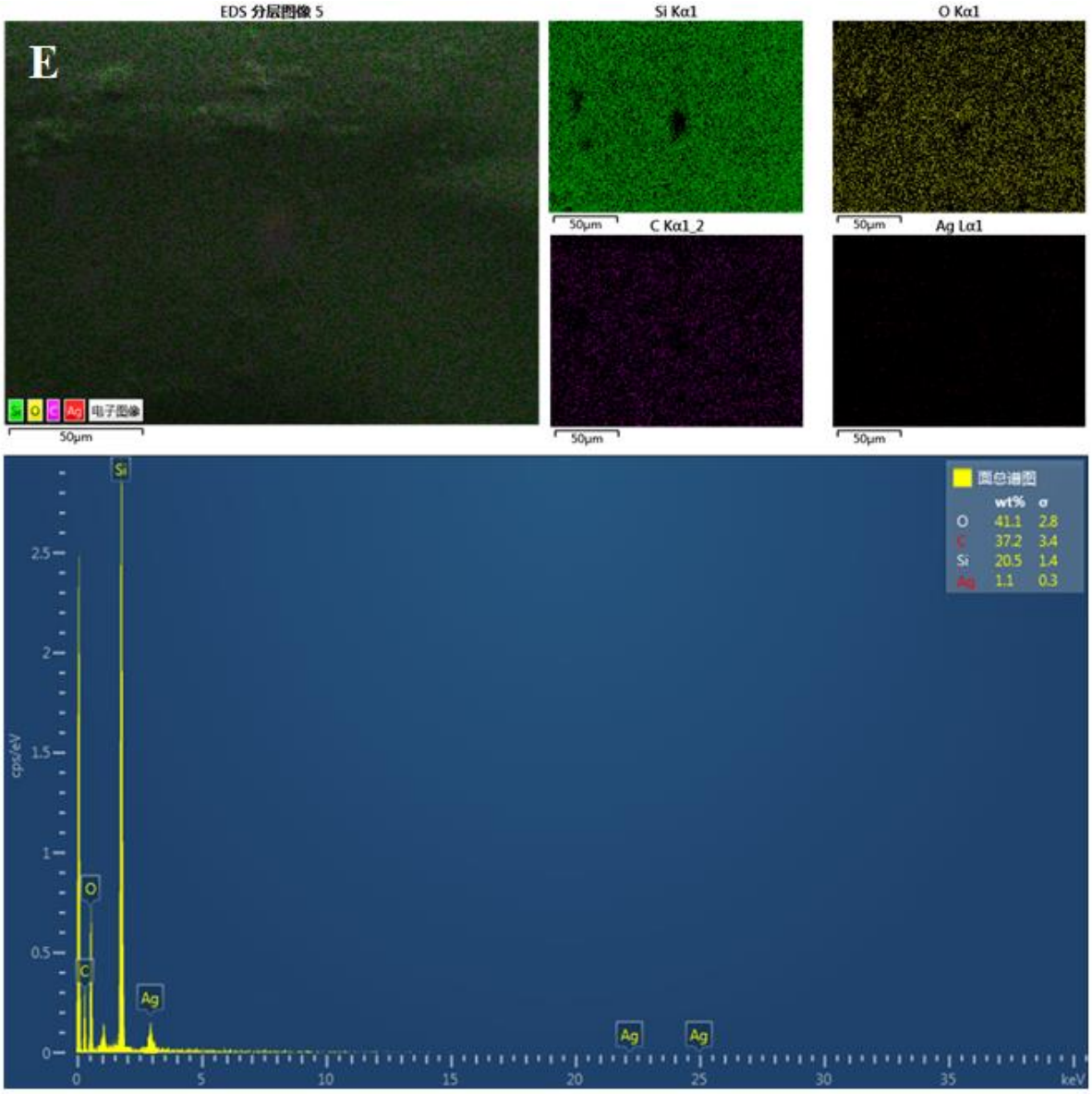
E
EDS 分层图像 5
Si Kα1
O Kα1
C Kα1_2
Ag Lα1
电子图像
50μm
元素谱图
wt% σ
O 41.1 2.8
C 37.2 3.4
Si 20.5 1.4
Ag 1.1 0.3
cps/eV
keV

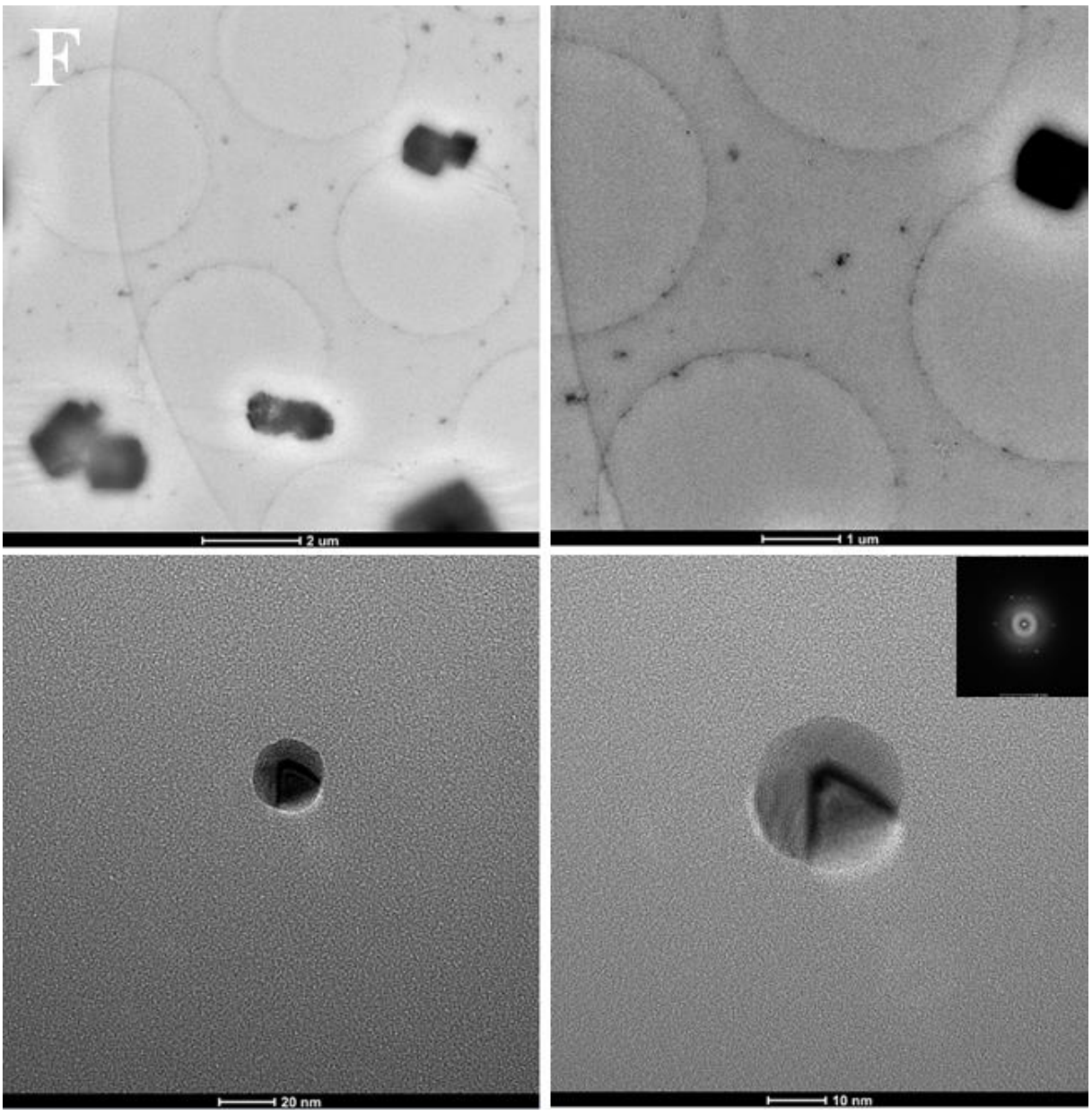
F
2 um
1 um
20 nm
10 nm

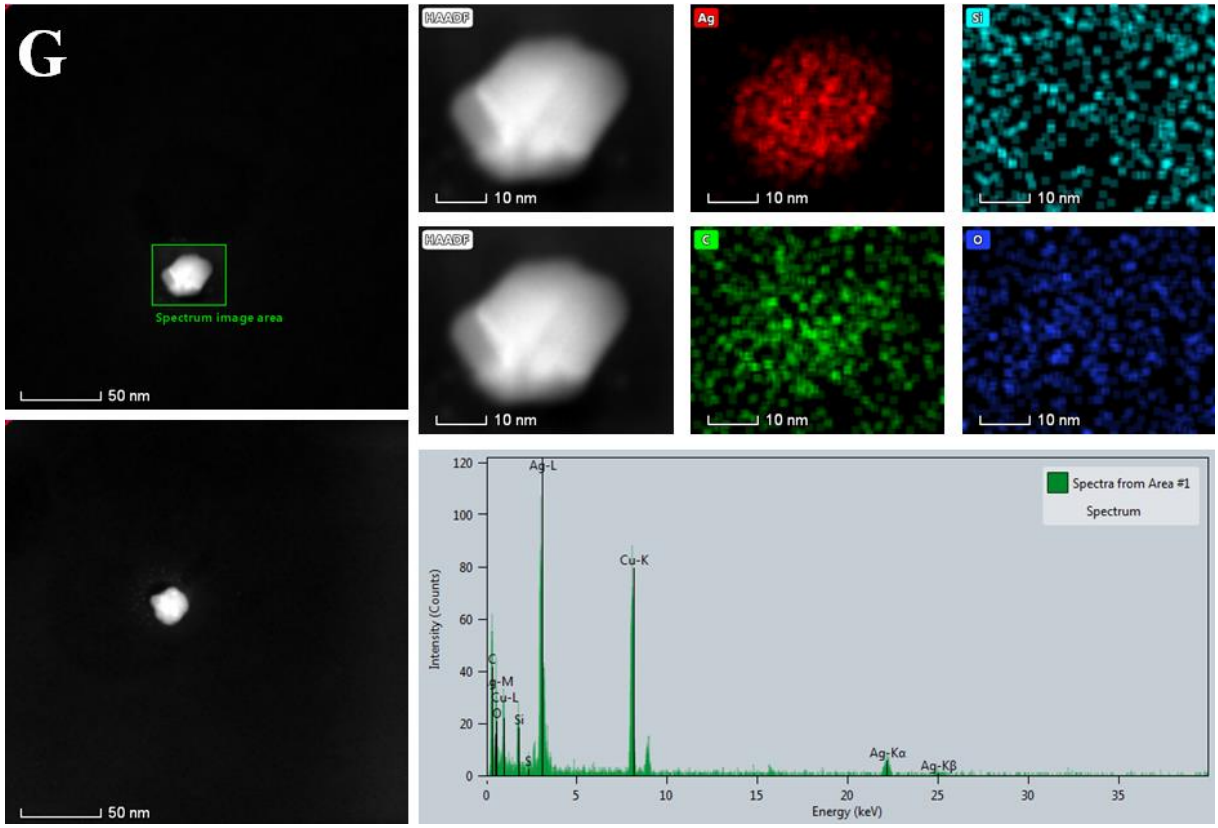

Figure 2. Micrographs of 3D-printed mesh and nanosilver dotting. A: iPDMS membrane with flexibility and different sizes; B1: folded iPDMS/AgNPs, B2: stretched iPDMS/AgNPs; C: the PDMS surface with silicon oil, D: the PDMS with silicon oil and silver nanoparticles; E: the dispersive energy analysis of iPDMS/AgNPs together with SEM. F: STEM images of iPDMS/AgNPs; G: the dispersive energy analysis of iPDMS/AgNPs together with STEM.

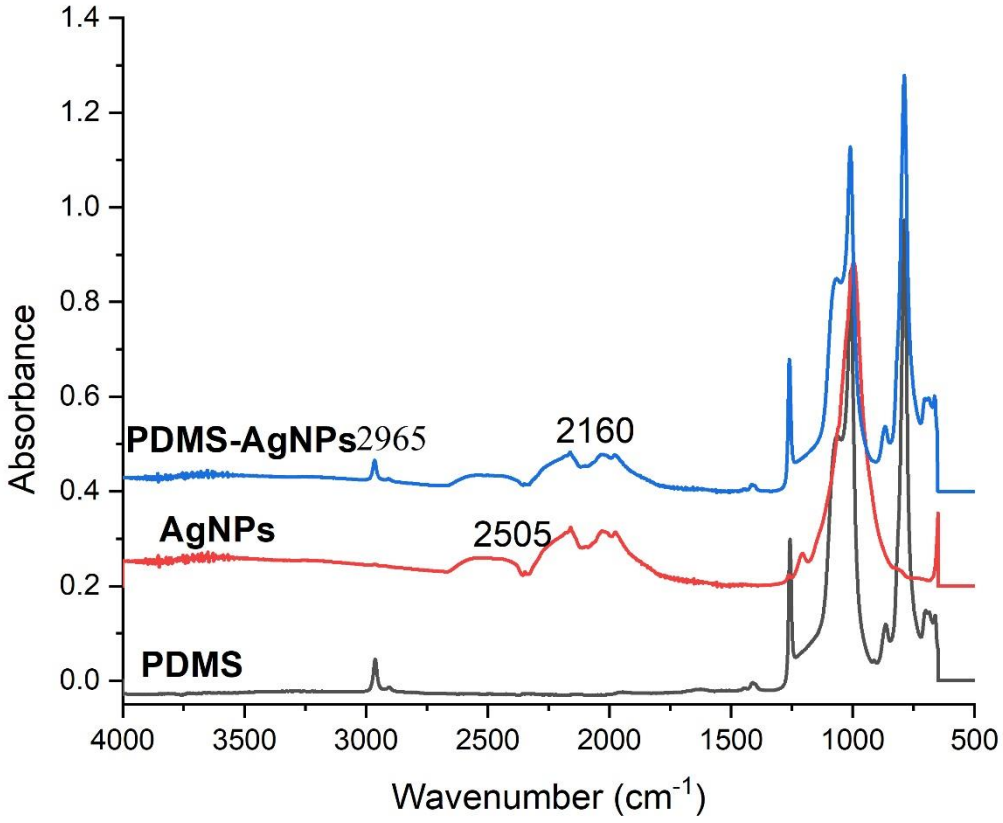

Figure 3. ATR-FTIR results for pristine PDMS film, AgNPs and PDMS-AgNPs film.

Silver ion release in PBS

Figure 4. illustrates the release of silver ions from PDMS/AgNPs examined at days 1, 3, 5 and 7 in PBS using ICP-AES. Silver ions were rapidly released from PDMS/AgNPs at day 1, which was subsequently followed by a relatively slow and sustained release. Briefly, the concentration of released silver ions was approximately 0.42 μg/mL at day 1. Furthermore, constant silver ion release could still be observed at day 7, suggesting that PDMS/AgNPs had a prolonged and steady antibacterial activity.

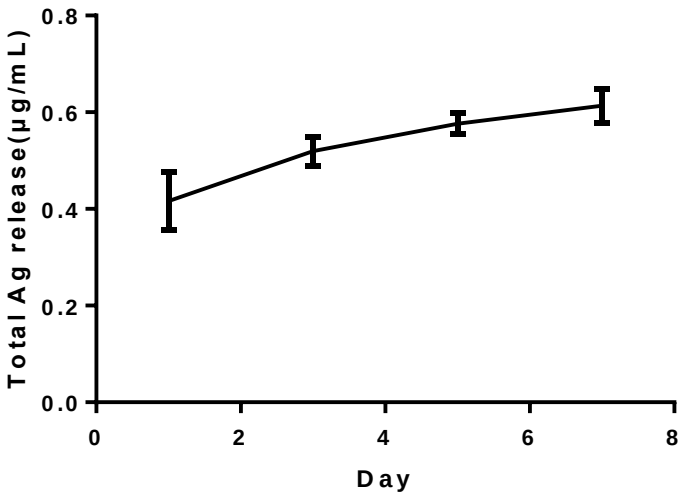

Figure 4.Silver ion release in PBS from PDMS/AgNPs at days 1, 3, 5 and 7. The values are shown as the mean ± SD (n = 3).

Contact angle (CA) characterization

Water static contact angle test was performed to characterize hydrophobicity, as demonstrated in Figure 5. pristine PDMS acted as a control group showed a contact angle of 101.02. After infusing the PDMS with 5 Cst silicone oil, the contact angle had an increase to 102.35. 2.5%AgNPs with PDMS shows the contact angle 109.23. It may be due to the reason that AgNPs could make the surface rougher and thus increased the contact angle. When infusing PDMS into silicone oil for an overnight after adding AgNPs, the contact angle increased dramatically to 117.03, which significantly increased hydrophobicity.

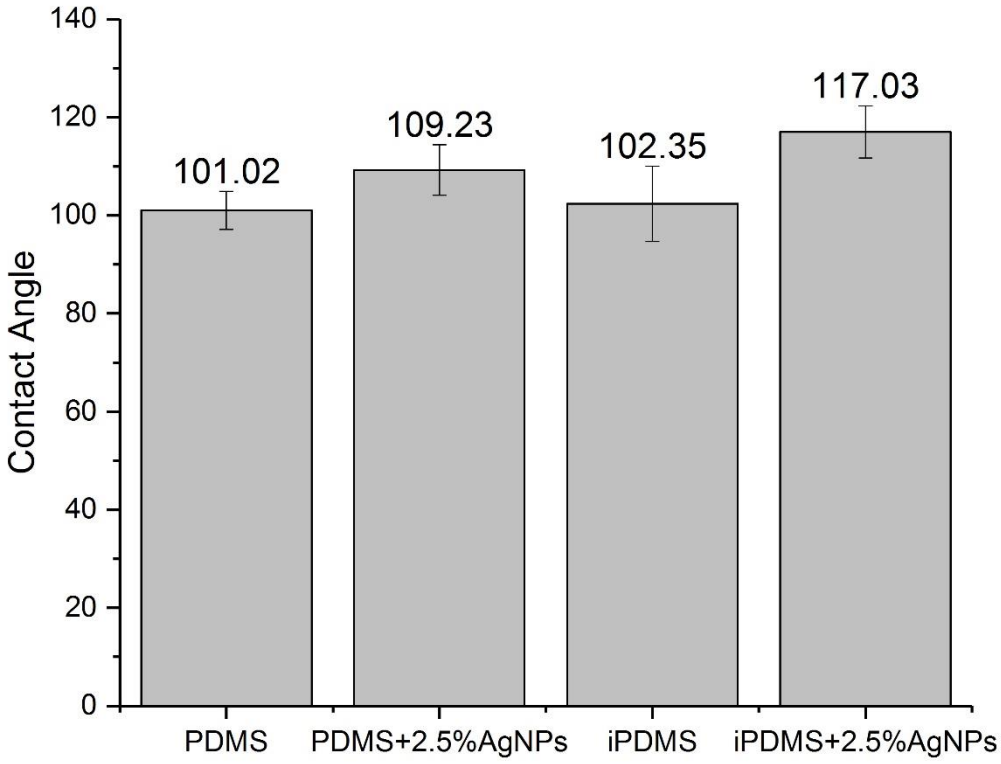

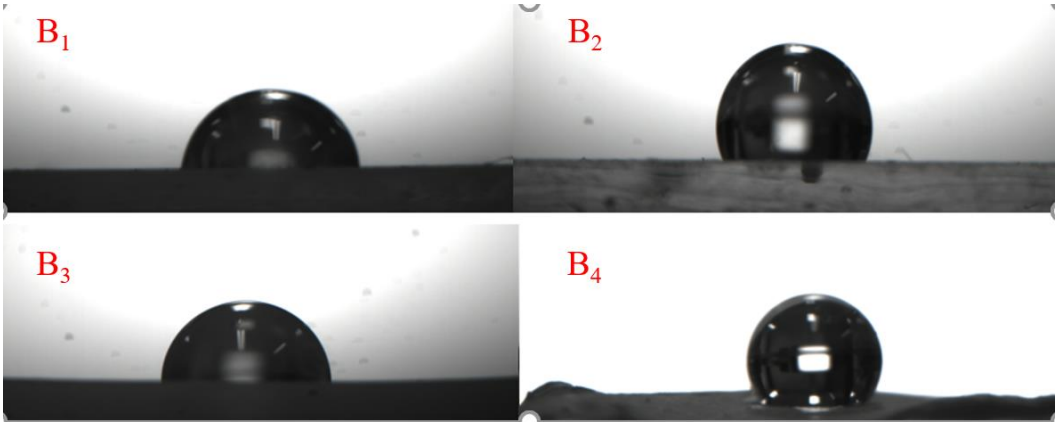

Figure 5. Contact analysis (A) water static contact angle (CA) characterization of PDMS, PDMS+2.5%AgNPs, iPDMS and iPDMS + 2.5% AgNPs; and (B_1) to (B_4) Optical contact angle images of PDMS, PDMS+2.5%AgNPs, iPDMS, and iPDMS + 2.5% AgNPs, respectively.

iPDMS/AgNPs on fibroblast viability and proliferation

The cytotoxicity of iPDMS/AgNPs on cultured fibroblasts is shown in Table 1 and Figue 6. iPDMS/AgNPs with different AgNPs concentrations shows little inhibitory effect on cell proliferation from day 1 to day 7 ($p > 0.05$).

We found that iPDMS/AgNPs had no obvious cytotoxic effect on fibroblasts by the CCK-8 assay (Figure 6). The results are a coincidence with the previous study that cytotoxicity of AgNPs was only found at high concentration (*253*).

Table 1 The effects of iPDMS/AgNPs mesh infused with silicon oil and different AgNPs concentration on mouse-derived fibroblasts

	OD values			
	Day 1	Day 3	Day 5	Day 7
PDMS	0.280±0.002	0.329±0.013	0.469±0.052	0.619±0.018
PDMS+oil	0.276±0.004	0.339±0.023	0.448±0.041	0.618±0.023
PDMS+0.5%AgNPs	0.276±0.005	0.343±0.002	0.452±0.053	0.594±0.011
PDMS+2.5%AgNPs	0.278±0.005	0.325±0.022	0.446±0.047	0.540±0.035
iPDMS+0.5%AgNPs	0.280±0.006	0.344±0.007	0.431±0.012	0.580±0.018
iPDMS+2.5%AgNPs	0.279±0.007	0.349±0.018	0.416±0.007	0.533±0.047

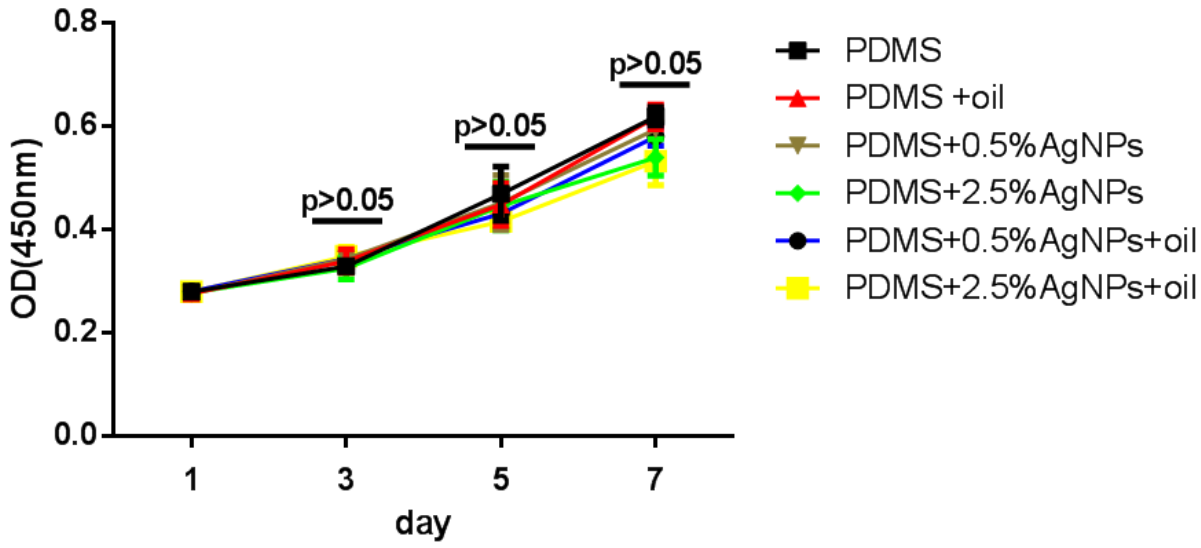

Figure 6. From day 1 to day 7, CCK-8 no obvious inhibitory effects found on fibroblasts in 6 groups ($p>0.05$).

iPDMS/AgNPs against the adherence of *S. aureus* and *E. coli*

An important indicator in anti-bacterial is the bacterial attachment and subsequent biofilm formation on medical devices. Two standard drug-resistant bacteria (*Staphylococcus aureus* and *Escherichia coli*) are commonly used in the clinical wound for in non-fouling assay.

The gross appearance of bacteria in six groups (co-cultured with *Staphylococcus Aureus or Escherichia Coli*) were presented in Figure 7.and Figure 8. The numbers of the bacterial colony (co-culture with *Staphylococcus Aureus*) were 10.333 ±2.517, 2.000 ±2.000, 50.667 ±3.512, 46.333 ±2.082, 9.667 ±3.055 and 0.333 ±0.577 Colony Forming Unit (CFU)/ tablet, respectively, in the PDMS, PDMS+oil, PDMS+0.5%AgNPs, PDMS+2.5%AgNPs, iPDMS+0.5%AgNPs and iPDMS+2.5%AgNPs. Co-culture with *Escherichia Coli*, the numbers were 9.333 ±2.517, 1.000 ±1.000, 43.667 ±3.512, 37.667 ±3.215, 10.333 ±1.528 and 0.667 ±1.155 CFU/ tablet, respectively. Obviously, the groups decorated with silicon oil had low bacteria colonies than the other groups (PDMS vs. PDMS+oil, $p< 0.05$; PDMS+0.5%AgNPs vs. iPDMS+0.5%AgNPs, $p < 0.05$; PDMS+2.5%AgNPs vs. iPDMS+2.5%AgNPs, $p < 0.05$). The values are shown as the mean ± SD ($n = 3$).

Notably, the groups infused with silicon oil had a better ability against adherence against *S. aureus* and *E. coli* than the corresponding group, which may efficiently improve wound healing microenvironment (*254*).

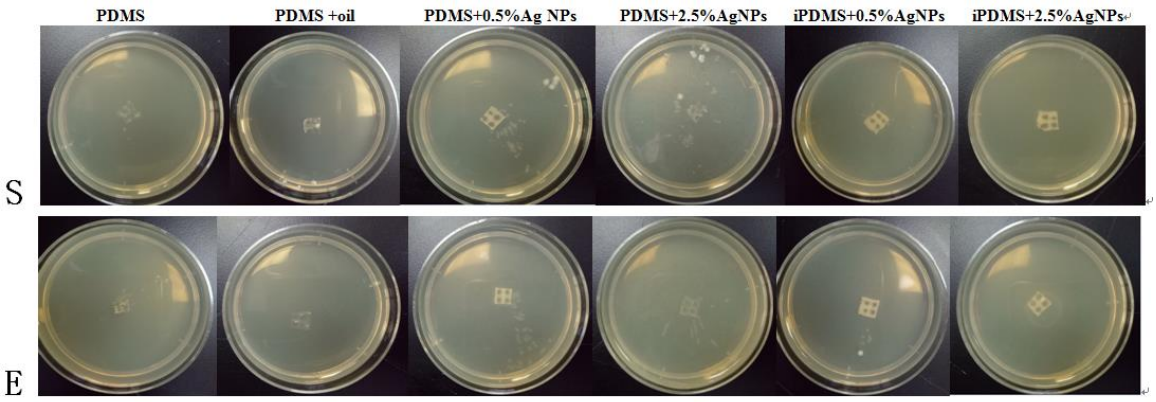

Figure 7. The gross appearance of bacteria of in six groups (co-cultured with *Staphylococcus Aureus or Escherichia Coli*) were presented.

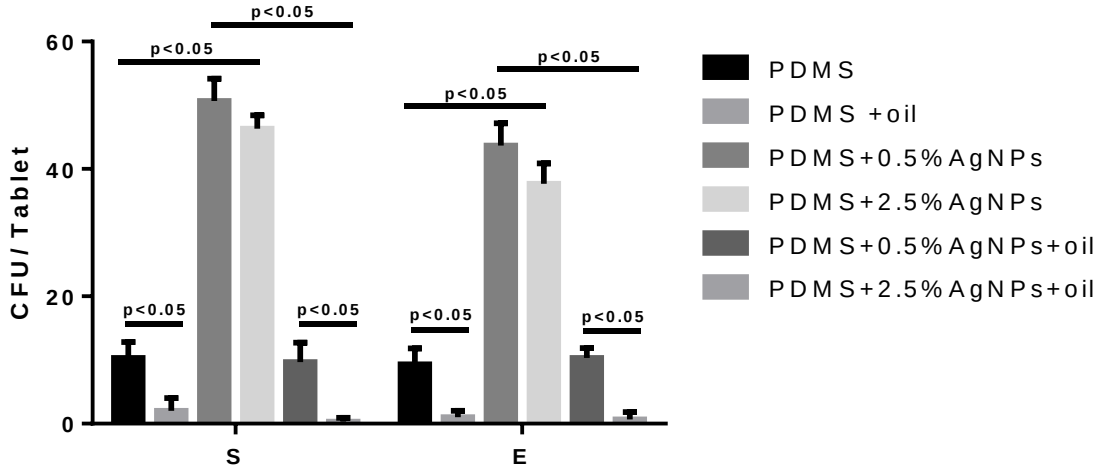

Figure 8. Bacteria colonies of each table. The groups infused with silicon oil had low bacteria colonies than the corresponding group ($p<0.05$).

iPDMS/AgNPs slippery surface repelled the blood without `staining

After confirming that iPDMS/AgNPs had an ability against adherence against *S. aureus* and *E. coli*, so we studied if iPDMS/AgNPs can repel the blood staining. As shown in Figure 9, a mice blood was dropped on the iPDMS/AgNPs slippery surface with the tilting was 30°at 0 second. Then the

blood of mice was mobile respectively at 1 s and 10 s with no stain. Our research results were confirmed that iPDMS/AgNPs had an ability against adherence against the blood with no stain.

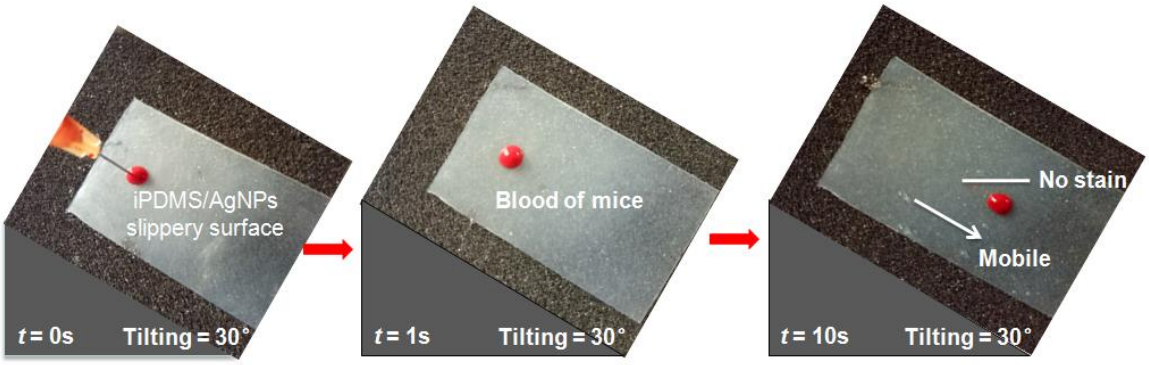

Figure 9. Time-sequence images reflected mobility of the blood on the iPDMS/AgNPs slippery surface. The blood was repelled on the surface.

iPDMS/AgNPs had an antibacterial activity against *S. aureus* and *E. Coli* in vitro

As shown in Figure 10, co-cultured with *Staphylococcus Aureus*, the OD value was 1.215, 1.103, 0.928, 0.707, 0.698 and 0.599, respectively in the PDMS, PDMS+oil, PDMS+0.5%AgNPs, PDMS+2.5%AgNPs, iPDMS+0.5%AgNPs and iPDMS+2.5%AgNPs. Co-cultured with *Escherichia Coli*, the OD value was 0.604, 0.572, 0.521, 0.397, 0.385 and 0.292, respectively. The groups with 2.5%AgNPs had lower OD value than other groups, indicating a stronger capacity against *Staphylococcus Aureus* or *Escherichia Coli* respectively (PDMS vs. PDMS+2.5%AgNPs, $p < 0.05$; PDMS vs. iPDMS+2.5%AgNPs, $p < 0.05$; PDMS+0.5%AgNPs vs. PDMS+2.5%AgNPs, $p < 0.05$; iPDMS+0.5%AgNPs vs. iPDMS+2.5%AgNPs, $p < 0.05$).

Our research results showed that iPDMS/AgNPs *in vitro* could protect effectively infected wounds, which may efficiently promote wound healing as previous studies that the better antibacterial activity against *S. aureus* than *E. Coli* of mesh may attribute to the different cellular wall structures between *S. aureus* and *E. Coli*(*255*).

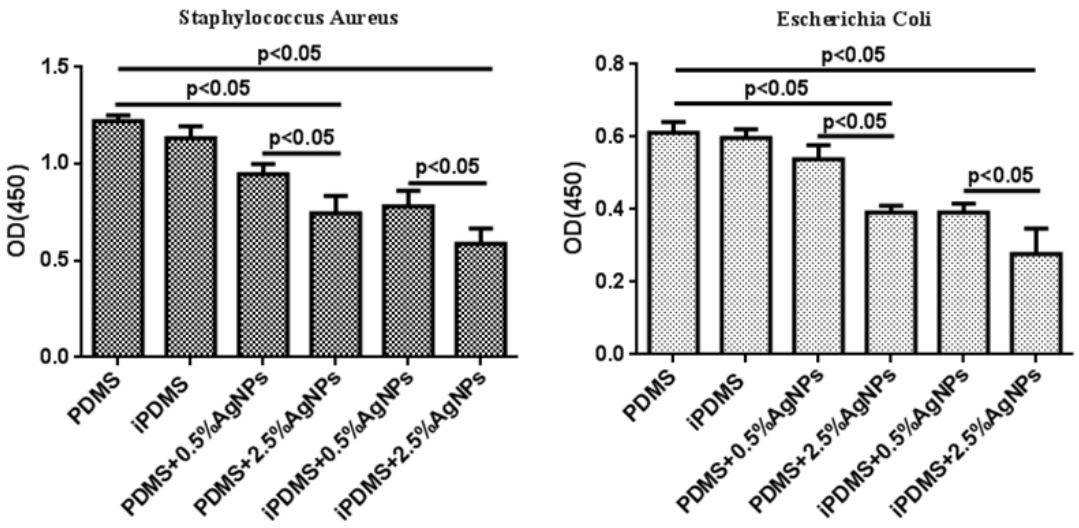

Figure 10. OD values of six groups co-cultured with *Staphylococcus Aureus or Escherichia Coli*.

iPDMS/AgNPs on neo-epithelial and granulation tissue formation in wound infection models

To further test iPDMS/AgNPs'effect on the wound healing, the number of the bacterial colony, **wound infection**, the new epithelial length and the granulation tissue thickness were investigated in a murine full-thickness skin defect wound model.

The gross appearances of eight groups of wound healing from day 1 to day 7 were presented in Figure 11. As shown in Figure 12, the wound healing rates of **infected wound** on day 3 are 19.2%, 5.5%, 10.5%, 12.4%, 23.3%, 29.4%, 30.2% and 32.1% , respectively, in the A, B, C, D, E, F, G and H group. On day 7, the wound healing rates are 58.8%, 19.7%, 27.5%, 39.8%, 61.4%, 69.1%, 72.6% and 80.2%, respectively. On day 3 and seven post-wounding, the wound healing rate of E, F, G and H groups were higher than that of group B ($p < 0.05$). On day 7 post-wounding, the wound healing rate of group H is higher than that of group A ($p < 0.05$), which revealed iPDMS/AgNPs could significantly promote wound healing compared with other groups, consistent with previous study (*256*).

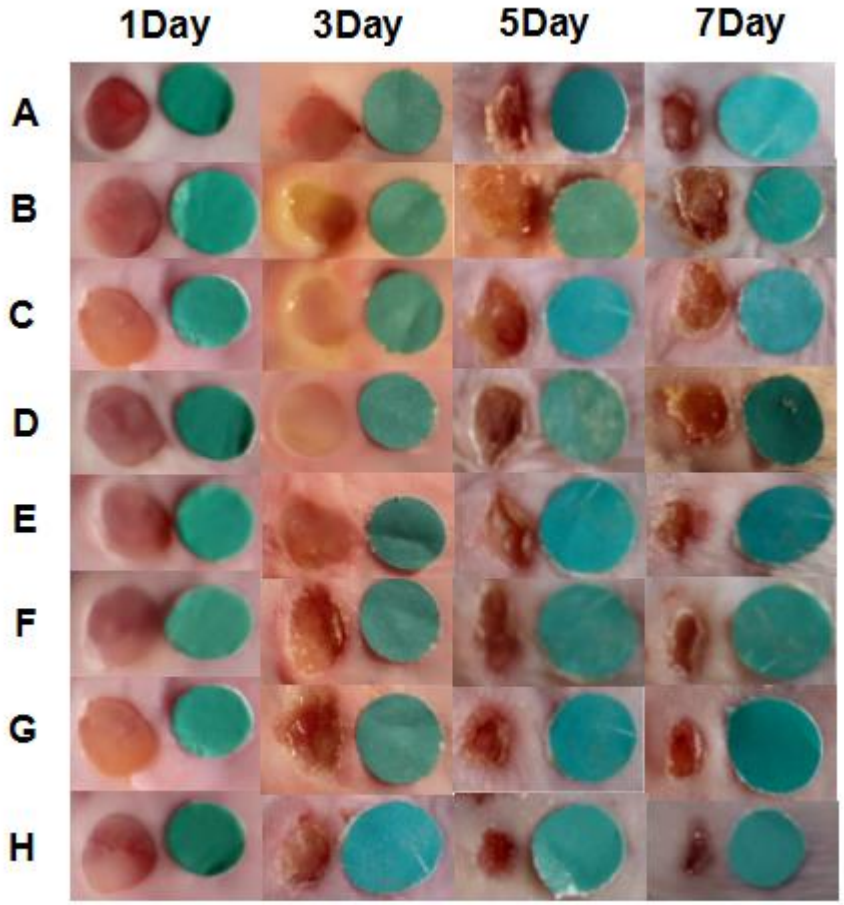

Figure 11. The wound profiles of the infected wound from 1 day to 7 days**.**

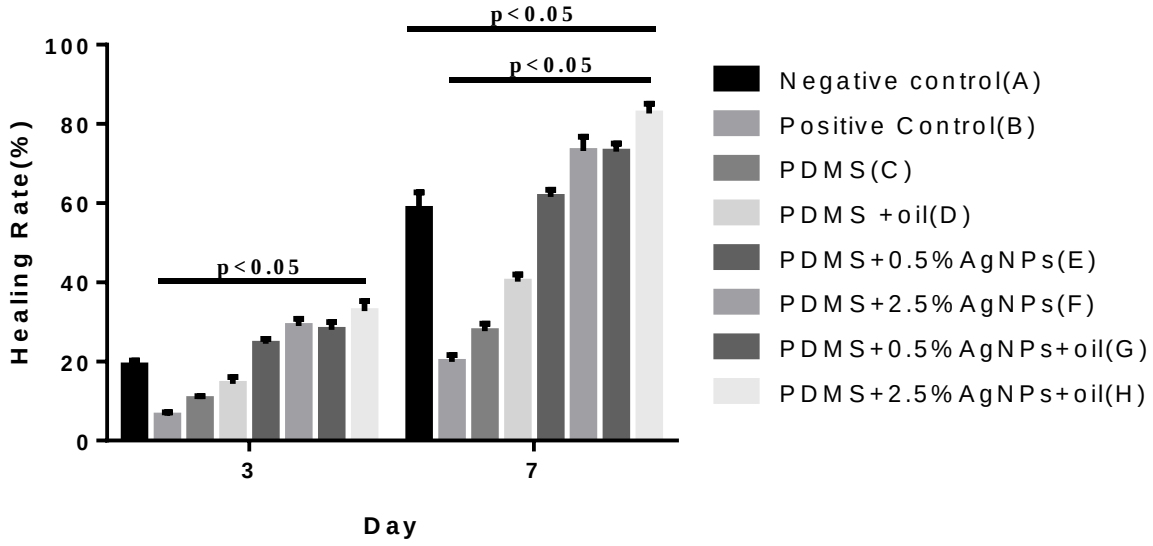

Figure 12. On day 3 and 7 post-wounding, the wound healing rate.

The gross appearance of eight groups of bacteria count on day 3 and day 7 post-wounding are presented in Figure 13. As shown in Figure 14, the numbers of the bacterial colony on day 3 were 0,

239, 198, 101, 71, 59, 48 and 16 CFU/ tablet, respectively, in the A, B, C, D, E, F, G and H groups. On day 7, the numbers of the bacterial colony were 1, 178, 95, 42, 27, 15, 12 and 2 CFU/ tablet, respectively. At day 3 and 7 post-wounding, the number of the bacterial colony of group B was higher than that of A, E, F, G, and H group ($p < 0.05$), which shows iPDMS/AgNPs have effective antibacterial activity *in vivo*.

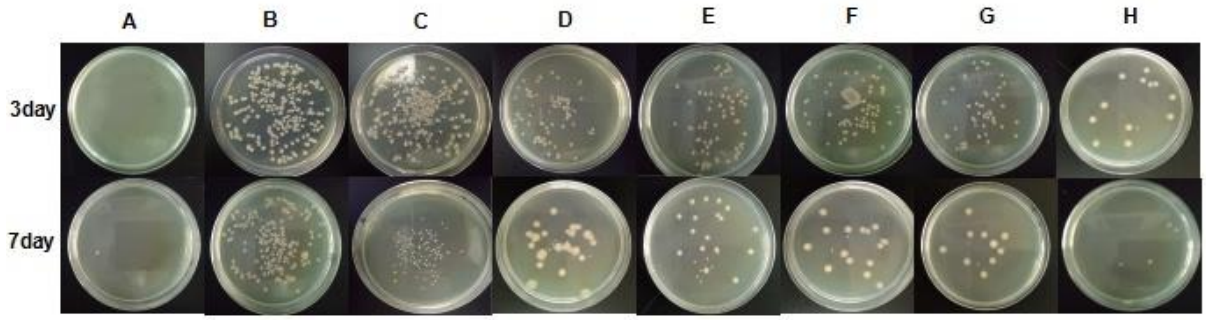

Figure 13. The gross appearance of eight groups of bacteria count on day 3 and day 7 post-wounding.

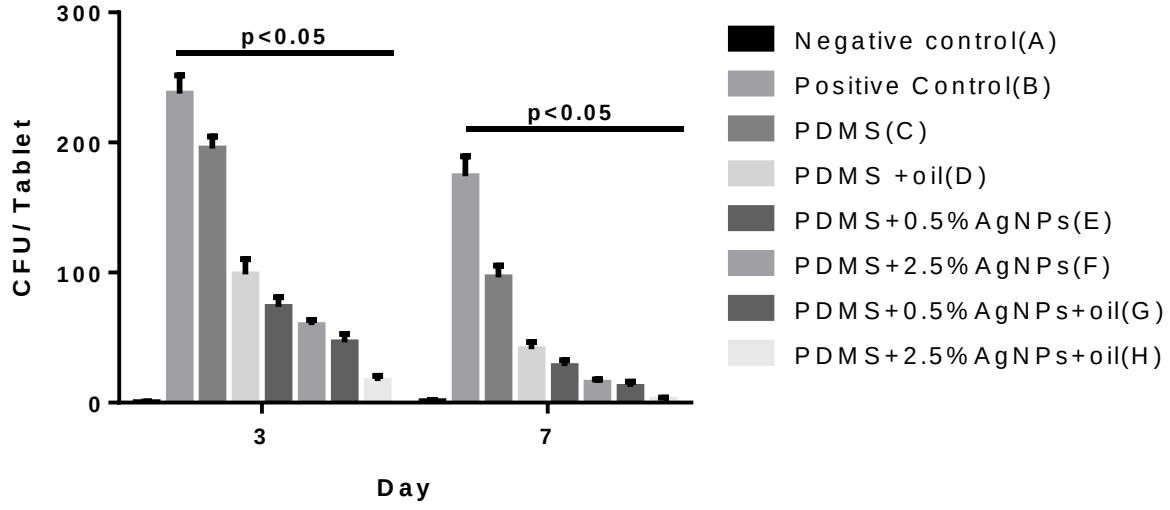

Figure 14. Counted the bacteria of wound secretion after diluted 100 times. At day 3 and day 7 post-wounding, the number of the bacterial colony in group B was higher than that in groups E, F, G and H ($p < 0.05$).

The newly formed epithelium was represented by the length of epithelium on the granulation tissue on day 3 and 7 post-wounding (Figure 15. And Figure 16). At day 3 post-wounding,

there was no obvious difference among the groups (p> 0.05). At day 7 post-wounding, the neo-epithelial length was 712.9 μm, 413.2 μm, 443.2μm, 607.1 μm, 760.8μm, 814.8 μm, 987.7 μm and 1189.9 μm in A, B, C, D, E, F, G and H groups, respectively. At day 7 post-wounding, neo-epithelial length in groups E, F, G and H was longer than that in group B and C (p <0.05).

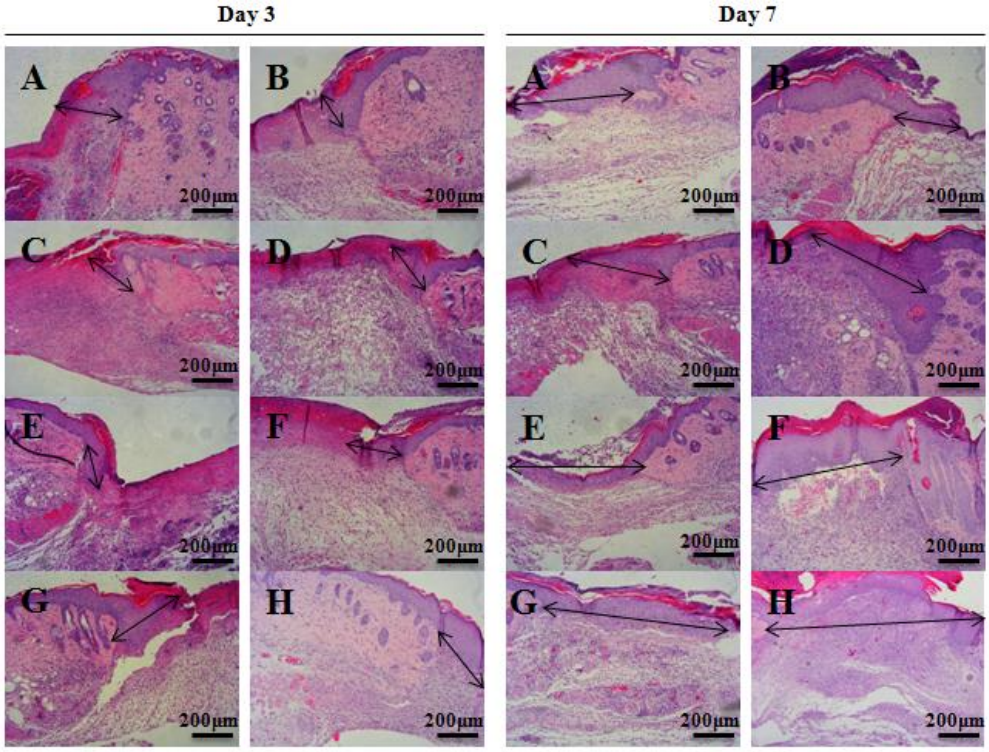

Figure 15. H&E staining of wound tissue sections obtained at day 3 and 7 post-wounding. The neo-epithelial length was indicated by the arrow.

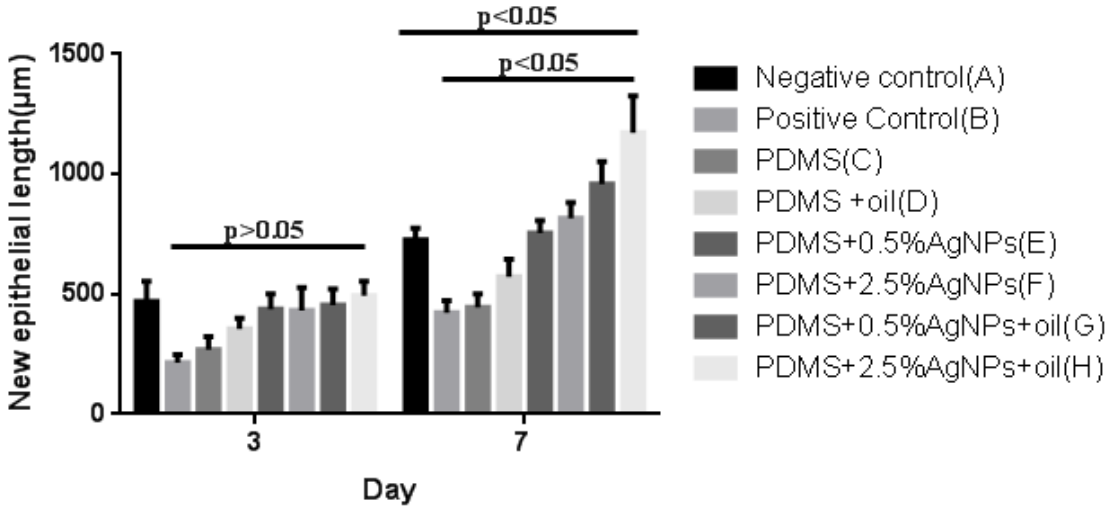

Figure 16. At day 7 post-wounding, neo-epithelial length in groups E, F, G, and H was longer than that in groups B and C (p <0.05).

As shown in Figure 17, the thickness of the granulation tissue on day 7 was 521.2, 212.4, 304.2, 503.7, 636.6, 766.9, 812.6 and 952.4μm in A, B, C, D, E, F, G and H groups, respectively. The average thickness of group A, E, F, G and H was much greater than that in group B ($p < 0.05$). At the same time, the average thickness of group G and group H were greater than that of group A ($p < 0.05$).

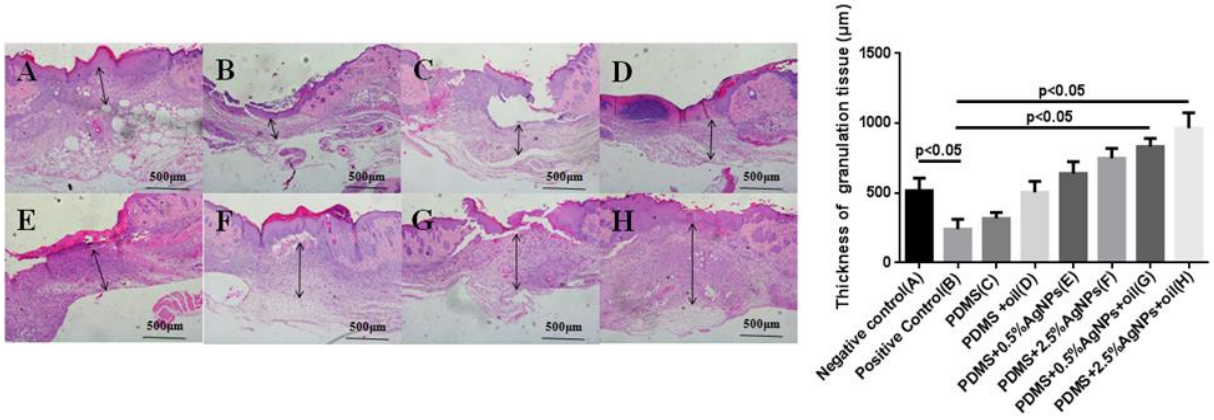

Figure 17. The thickness of the granulation tissue (H&E staining) on day 7 of post-wounding. The average thickness of group A, E, F, G, and H was much greater than that of group B ($p < 0.05$).

The wound healing was decided by the re-epithelialization for the compact-skin species(*257, 258*). The histological analysis shows that the neo-epithelial length and the granulation tissue thickness were obviously increased in the presence of for iPDMS/AgNPs (Figure 15, 16 and 17).

In short, iPDMS/AgNPs can promote neo-epithelial and granulation tissue formation to promote accelerated wound healing, which due to excellent biocompatibility, a better ability against adherence, and effective antibacterial activity of the iPDMS/AgNPs, with the same with previous studies (*259, 260*).

Conclusions

We developed a novel wound dressing iPDMS/AgNPs using 3D printing method and biometics of the oil-infused layer to cater for different requirements from patients in burn injuries. The eco-friendly iPDMS/AgNPs novel wound dressing not only exhibited excellent biocompatibility, longer service longevity, a better ability against adherence, and effective antibacterial activity but also could effectively promote the wound healing. In a nutshell, iPDMS/AgNPs can potentially be served as an ideal wound dressing in the near future.

Materials and methods

Materials

Polydimethylsiloxane (PDMS) and curing agent were purchased from Tianying Technology Industry Co.,Ltd, China. 5 Cst silicone oil was bought from Beijing HagebesTechnology Co., Ltd. Silver nanoparticles are bought from Dongge Nano Technology Co., Ltd . 3D Bioprinter was from HKable Biotechnology Co.

Ink formulation

The printable ink was prepared by mixing the prepolymer agent with the curing agent in a mass ratio of 1:1, after thorough stirring, 0.5%, 2.5% (silver/total weight) of silver nanoparticles was added and then the mixture was sonicated in an ice bath for 1 hour. The mixture was kept in a hot-water bath at 50° C for 20 minutes for pre-curing to obtain the ink.

3D printing

All wound dressing were architectured using a 3D bioprinter (HKable 3D). The ink was carefully loaded into a 5 ml of extrusion syringe, which was fixed on the conveyor for extrusion through a 20G flat tip needle. During printing, different desired 3D shapes were encased in a glass slide according to gcode generated on Computer Aid Design (CAD). After printing, the samples were kept on a hotbed (80 ^{0}C) for 2 hours for a complete curing.

Preparation of iPDMS

After curing, the 3D printed PDMS membranes were washed double distilled water for 3 times and rinsed with ethanol and dried. They were then transferred to a glass container full of 5 Cst silicon oil for 18 hours.

Rheology Characterization

To study the printable ability of the ink, the dynamic oscillatory frequency sweep of pre-curing PDMS was performed for a constant frequency of 10 rad/s to study the storage moduli (G') and loss moduli (G'') using a TA Discovery Hybrid Rheometer. Two different temperature were 50ºC and 80ºC; the dynamic viscosity was also observed in this experiment.

Scanning electron microscopy (SEM) observation and Energy Dispersive Spectrometer (EDS)

The morphological characteristics of the iPDMS/AgNPs samples mesh were characterized by scanning electron microscopy (SEM) and Energy Dispersive Spectrometer (EDS) (Hitachi, S-3400N, Japan). Briefly, the specimens were firstly washed carefully with deionized water, dried and sputter-coated with Au for 3 minutes, then observed under vacuum condition by SEM and EDS.

Scanning transmission electron microscopy (STEM) observation

A scanning transmission electron microscope (Zeiss LIBRA 200 FEG, 200 kV) was used to detect the detailed morphology and size distribution of the AgNPs, and energy-dispersive X-ray spectroscopy (EDS) was used for a compositional analysis. Briefly, after the PDMS/AgNPs films were ultrasonicated in DDH_2O, a drop of the prepared solution was deposited on a carbon-coated copper grid and dried at room temperature prior to the STEM analysis.

Ag+ release test

To investigate the release of silver ions from the PDMS/AgNPs films, specimens ($n = 3$) were each cut into (10×10 mm) pieces and immersed in 6 mL of phosphate-buffered solution (PBS) at 37 °C in darkness. The total supernatant of each group was harvested at each determined point, i.e. day 1, 3, 5 and 7 after PDMS/AgNPs membrane immersed in PBS and analyzed using inductively coupled plasma-atomic emission spectrometry (ICP-AES, Leeman, USA).

Contact Angle Characterization

An optical contact angle meter (JY-PHA, Shengding Co, LTD.) was used to measure water static contact angles on flat substrates. The excess lubricant was removed from all iPDMS samples before

testing. For every sample,15μl deionized water droplet was added on the substrate surfaces and the contact angle was obtained using JY-PHA software.

Animals

The BALB/c mice (male, 18-25 g) and transgenic neonatal mice of green fluorescent protein (GFP) were obtained from the Experimental Animal Department (EAD) of the Third Military Medical University (TMMU). All animal experiments had been approved by the Institutional Animal Use and Care Committee of TMMU. All the animals were raised in plastic cages individually for 7 days before the experiments. All the animals were fed with free access to both autoclaved standard rodent chow and water. Living conditions of all the animals were under standardized conditions (relative humidity: 50%; circadian rhythm: 12 h; and room temperature: 25 °C). All the animal experiments were performed according to the guidelines of TMMU.

Cytotoxicity test

Cell culture

Fibroblasts were extracted from green fluorescent protein (GFP) transgenic neonatal mice as described by Cheng et al (*261*). Briefly, skin tissue was obtained from transgenic neonatal mice, then washed three times with PBS, afterwards adding dispase II 0.5 mg/mL (Sigma, USA) and keeping at 4 °C overnight to separate the dermis and epidermis. After removing the epidermis, the dermis samples were minced and digested in 1 mL of trypsin 0.25 mg/mL (Boster, China) for 10 minutes. Then, Dulbecco's Modified Eagle's Medium 3 mL (DMEM, Gibco, USA) containing fetal bovine serum 10% (Gibco, USA) was added to interdict the digestion. Then the mixture solution was centrifuged at a speed of 1000 rpm for 6 minutes. Finally, the cells were incubated and collected in Dulbecco's modified Eagle medium including fetal bovine serum10%, streptomycin (100 μg/mL) and penicillin (100 U/mL) at 37 °C in a 5% CO_2 incubator.

CCK-8 assay

The third-generation fibroblasts were seeded on 96-well plates in 3×10^3/100 μl/well. Afterward, the culture medium was replaced by the leach liquor extracting from CTPM and HTPM. The untreated medium was used as the blank control group. The biocompatibility of the materials was estimated by CCK-8 (Dojindo, Kyushu, Japan) proliferation assays respectively on day 1, 3, 5 and 7 after seeded. Briefly, at each time point, replaced the medium with Dulbecco's modified Eagle medium, and CCK-8 solution10 μl was added in each well, then incubated for 2h at 37 °C. The mean value of optical density (OD) was at 450 nm reading by the assay reader of enzyme-linked immunosorbent (Thermo Varioskan Flash, USA) (*262*).

Non-fouling assay

The normal *Staphylococcus Aureus* and *Escherichia Coli* were used for the non-fouling assay. To start with, the bacterial concentration was amplified (shake overnight) to 1×10^9 CFU/ml, then adjusted to 1×10^4 CFU/ml. The mesh were punched to 6mm diameter discs. After sterilized by 75% alcohol at room temperature for 20 min, the mesh was washed with PBS for three times. For bacterial adhesion and developing, 200 ul dilution bacteria liquid was joined into the hole of containing the material and was incubated at 37°C for 1.5 h. Then the membrane was washed with PBS for one time and sticked to the bottom of the dish flatly. The preheated cooling to 45°C of LB AGAR was poured into the hole of containing the material. After solidification, the dish was developed for the night at 37°C. Last, the dishes' images were taken photos and counted.

The test of antibacterial activity in vitro

The normal *Staphylococcus Aureus* and *Escherichia Coli* were used for the test of antibacterial activity in vitro respectively. First, bacterial stock 200 μL was mixed with Luria-Bertani (LB) medium five mL, then shaked at 37°C at 200 rpm overnight. LB bacterial suspension was diluted to the predetermined initial concentration (OD=0.07; optical density at 600 nm), then 500 μL bacterial solution was added to each well of 24-well plate. Six groups membranes were punched into 10 × 10 mm in size discs, then sterilized by 75% alcohol for 30 minutes, followed by PBS washing for three

times. Finally, the six groups membranes were immersed into the bacterial solution, incubated in the shaker incubator at 50 rpm at 37°C for 24 h. 100 μL of bacterial solution was transferred into the 96-well plate, and the OD_{600} value were measured (*263*).

Wound infection models

To test the potential roles in wound healing, wound bacterial counting, epithelialisation and granulation tissue were measured in a defect wound model of murine full-thickness skin (*264*). First, the BALB/c mice were anesthetized with 1% pentobarbital by intraperitoneal injection, then the dorsal surface of the mice was shaved by a razor and cleaned with 75% alcohol. Full-thickness wound at a size of 0.6cm in diameter at both sides of the mice back were created by a punch. We then prepared the microbial concentration of 10^8CFU/mL of a mixture of standard *Staphylococcus aureus* and *Escherichia coli*. 15 to 20 ul bacterial suspension was added to the wound hole. Finally, a standard 0.6 cm diameter meshwas placed close to the hole to represent the day 0 wound area. A digital camera was used to monitor the wound contour by taking pictures. Eight groups were prepared: negative control (not bacteria covered by the negative pressure membrane)(A), positive Control (adding bacteria covered by the negative pressure membrane) (B), PDMS (C), PDMS+oil(D), PDMS+0.5%AgNPs(E) , PDMS+2.5%AgNPs(F), PDMS+0.5%AgNPs+oil(G), and PDMS+2.5%AgNPs+oil(H), respectively.

Then we glued the adhesive biological membrane (Negative Pressure Wound Therapy Kit (NPWT-1), China) on the surface of each wound as fixed membrane.

The wound healing evaluation

The wounds were taken pictures on day 1, 3, 5 and 7 post- wounding, and measured by IPP 6.0 software. The wound healing rate was calculated by the formula:

The wound healing rate = $(O - R) / O \times 100\%$.

O represents original wound area, and R represents residual wound area on the determined point.

The bacterial wound count

The exudate (1 ul) of wound infection models was taken at day 3 and 7 post-wounding. After diluted 10^4 times, the exudate was cultivated overnight. Then the wound bacterial colony was taked photos and counted.

Hematoxylin-eosin (H&E) staining

After 3 and 7 post-wounding, the wound tissues were harvested and fixed in paraformaldehyde 4%, embedded in paraffin, sliced, and stained by Hematoxylin-eosin (H&E). The new epithelial length and the granulation tissue thickness were measured by Image J. As most of the infected wounds had little granulation tissue on day 3 post-wounding, thickness had histologically measured just on day 7 post-wounding.

Statistical analysis

All data are expressed as the mean ± SD(n=5) and analyzed by one-way ANOVA.

Reference

1. Z. Fan *et al.*, A novel wound dressing based on Ag/graphene polymer hydrogel: effectively kill bacteria and accelerate wound healing. *Advanced Functional Materials* **24**, 3933-3943 (2014).
2. H. J. Jung, M. Abou-Jaoude, B. E. Carbia, C. Plummer, A. Chauhan, Glaucoma therapy by extended release of timolol from nanoparticle loaded silicone-hydrogel contact lenses. *Journal of controlled release* **165**, 82-89 (2013).
3. Y. Jiang, J. Chen, C. Deng, E. J. Suuronen, Z. Zhong, Click hydrogels, microgels and nanogels: emerging platforms for drug delivery and tissue engineering. *Biomaterials* **35**, 4969-4985 (2014).
4. C. S. Boland *et al.*, Sensitive, high-strain, high-rate bodily motion sensors based on graphene–rubber composites. *ACS nano* **8**, 8819-8830 (2014).
5. C. Mattmann, F. Clemens, G. Tröster, Sensor for measuring strain in textile. *Sensors* **8**, 3719-3732 (2008).
6. T. Yamada *et al.*, A stretchable carbon nanotube strain sensor for human-motion detection. *Nature nanotechnology* **6**, 296-301 (2011).
7. D. Zhai *et al.*, Highly sensitive glucose sensor based on Pt nanoparticle/polyaniline hydrogel heterostructures. *ACS nano* **7**, 3540-3546 (2013).
8. Y. Wang, X. Yang, L. Qiu, D. Li, Revisiting the capacitance of polyaniline by using graphene hydrogel films as a substrate: the importance of nano-architecturing. *Energy & Environmental Science* **6**, 477-481 (2013).
9. H. Bai, K. Sheng, P. Zhang, C. Li, G. Shi, Graphene oxide/conducting polymer composite hydrogels. *Journal of Materials Chemistry* **21**, 18653-18658 (2011).
10. C. Fan, L. Liao, C. Zhang, L. Liu, A tough double network hydrogel for cartilage tissue engineering. *Journal of Materials Chemistry B* **1**, 4251-4258 (2013).
11. Q. Chen *et al.*, A Novel Design Strategy for Fully Physically Linked Double Network Hydrogels with Tough, Fatigue Resistant, and Self-Healing Properties. *Advanced Functional Materials* **25**, 1598-1607 (2015).
12. A. K. Gaharwar, N. A. Peppas, A. Khademhosseini, Nanocomposite hydrogels for biomedical applications. *Biotechnology and bioengineering* **111**, 441-453 (2014).
13. K. Nishi, K. Fujii, Y. Katsumoto, T. Sakai, M. Shibayama, Kinetic aspect on gelation mechanism of tetra-PEG hydrogel. *Macromolecules* **47**, 3274-3281 (2014).
14. S. Zeng *et al.*, Electrochemical fabrication of carbon nanotube/polyaniline hydrogel film for all-solid-state flexible supercapacitor with high areal capacitance. *Journal of Materials Chemistry A* **3**, 23864-23870 (2015).
15. Y. Xu *et al.*, Flexible solid-state supercapacitors based on three-dimensional graphene hydrogel films. *ACS nano* **7**, 4042-4049 (2013).
16. J. L. Erkal *et al.*, 3D printed microfluidic devices with integrated versatile and reusable electrodes. *Lab on a Chip* **14**, 2023-2032 (2014).
17. S. A. Gowers *et al.*, 3D printed microfluidic device with integrated biosensors for online analysis of subcutaneous human microdialysate. *Analytical chemistry* **87**, 7763-7770 (2015).
18. P. Thibon, X. Le Coutour, R. Leroyer, J. Fabry, Randomized multi-centre trial of the effects of a catheter coated with hydrogel and silver salts on the incidence of hospital-acquired urinary tract infections. *Journal of Hospital Infection* **45**, 117-124 (2000).
19. E. M. Ahmed, Hydrogel: Preparation, characterization, and applications: A review. *Journal of advanced research* **6**, 105-121 (2015).
20. J. H. Holtz, S. A. Asher, Polymerized colloidal crystal hydrogel films as intelligent chemical sensing materials. *Nature* **389**, 829 (1997).
21. Q. Wang *et al.*, High-water-content mouldable hydrogels by mixing clay and a dendritic molecular binder. *Nature* **463**, 339 (2010).
22. H.-Y. Hsieh *et al.*, Gradient Strain Chip for Stimulating Cellular Behaviors in Cell-laden Hydrogel. *Journal of visualized experiments: JoVE*, (2017).

23. S. B. Sonnenberg *et al.*, Delivery of an engineered HGF fragment in an extracellular matrix-derived hydrogel prevents negative LV remodeling post-myocardial infarction. *Biomaterials* **45**, 56-63 (2015).
24. E. A. Kamoun, X. Chen, M. S. M. Eldin, E.-R. S. Kenawy, Crosslinked poly (vinyl alcohol) hydrogels for wound dressing applications: A review of remarkably blended polymers. *Arabian Journal of chemistry* **8**, 1-14 (2015).
25. X. Zhao *et al.*, Antibacterial anti-oxidant electroactive injectable hydrogel as self-healing wound dressing with hemostasis and adhesiveness for cutaneous wound healing. *Biomaterials* **122**, 34-47 (2017).
26. F. A. Maulvi *et al.*, In vitro and in vivo evaluation of novel implantation technology in hydrogel contact lenses for controlled drug delivery. *Journal of Controlled Release* **226**, 47-56 (2016).
27. C. Coles-Brennan, T. Wilson, R. Butterfield, M. Guillon, Visual performance and subjective response to digital device use with daily wear, reusable, silicone hydrogel contact lenses in a controlled environme. *Contact Lens and Anterior Eye* **41**, S3 (2018).
28. K.-H. Hsu *et al.*, Release of betaine and dexpanthenol from vitamin E modified silicone-hydrogel contact lenses. *Current eye research* **40**, 267-273 (2015).
29. W. L. Murphy *et al.* (Google Patents, 2017).
30. M. K. Lima-Tenório *et al.*, Water transport properties through starch-based hydrogel nanocomposites responding to both pH and a remote magnetic field. *Chemical Engineering Journal* **259**, 620-629 (2015).
31. J. Witono, I. Noordergraaf, H. Heeres, L. Janssen, Water absorption, retention and the swelling characteristics of cassava starch grafted with polyacrylic acid. *Carbohydrate polymers* **103**, 325-332 (2014).
32. V. K. Thakur, M. K. Thakur, Recent advances in green hydrogels from lignin: a review. *International Journal of Biological Macromolecules* **72**, 834-847 (2015).
33. Y. Hashimoto, S.-a. Mukai, S.-i. Sawada, Y. Sasaki, K. Akiyoshi, Nanogel tectonic porous gel loading biologics, nanocarriers, and cells for advanced scaffold. *Biomaterials* **37**, 107-115 (2015).
34. H. S. Song, O. S. Kwon, J.-H. Kim, J. Conde, N. Artzi, 3D hydrogel scaffold doped with 2D graphene materials for biosensors and bioelectronics. *Biosensors and Bioelectronics* **89**, 187-200 (2017).
35. S. Deepthi, K. Jeevitha, M. N. Sundaram, K. Chennazhi, R. Jayakumar, Chitosan–hyaluronic acid hydrogel coated poly (caprolactone) multiscale bilayer scaffold for ligament regeneration. *Chemical Engineering Journal* **260**, 478-485 (2015).
36. Y. Liu, C. Jiang, S. Li, Q. Hu, Composite vascular scaffold combining electrospun fibers and physically-crosslinked hydrogel with copper wire-induced grooves structure. *journal of the mechanical behavior of biomedical materials* **61**, 12-25 (2016).
37. S. Merino, C. Martín, K. Kostarelos, M. Prato, E. Vázquez, Nanocomposite hydrogels: 3D polymer–nanoparticle synergies for on-demand drug delivery. *Acs Nano* **9**, 4686-4697 (2015).
38. E. L. Schneider, J. Henise, R. Reid, G. W. Ashley, D. V. Santi, Hydrogel drug delivery system using self-cleaving covalent linkers for once-a-week administration of exenatide. *Bioconjugate chemistry* **27**, 1210-1215 (2016).
39. L. Li *et al.*, A nanostructured conductive hydrogels-based biosensor platform for human metabolite detection. *Nano letters* **15**, 1146-1151 (2015).
40. L. Li *et al.*, All Inkjet-Printed Amperometric Multiplexed Biosensors Based on Nanostructured Conductive Hydrogel Electrodes. *Nano letters*, (2018).
41. L. Liu *et al.*, One-pot synthesis of 3-dimensional reduced graphene oxide-based hydrogel as support for microbe immobilization and BOD biosensor preparation. *Biosensors and Bioelectronics* **63**, 483-489 (2015).

42. W. Cai, S. Xie, J. Zhang, D. Tang, Y. Tang, An electrochemical impedance biosensor for Hg2+ detection based on DNA hydrogel by coupling with DNAzyme-assisted target recycling and hybridization chain reaction. *Biosensors and Bioelectronics* **98**, 466-472 (2017).
43. B. Tan, H. Zhao, L. Du, X. Gan, X. Quan, A versatile fluorescent biosensor based on target-responsive graphene oxide hydrogel for antibiotic detection. *Biosensors and Bioelectronics* **83**, 267-273 (2016).
44. M. A. Darabi, A. Khosrozadeh, Q. Wang, M. Xing, Gum sensor: a stretchable, wearable, and foldable sensor based on carbon nanotube/chewing gum membrane. *ACS applied materials & interfaces* **7**, 26195-26205 (2015).
45. I. Y. Jung, J. S. Kim, B. R. Choi, K. Lee, H. Lee, Hydrogel based biosensors for in vitro diagnostics of biochemicals, proteins, and genes. *Advanced healthcare materials* **6**, 1601475 (2017).
46. N. S. Kehr, S. Atay, B. Ergün, Self-assembled Monolayers and Nanocomposite Hydrogels of Functional Nanomaterials for Tissue Engineering Applications. *Macromolecular bioscience* **15**, 445-463 (2015).
47. Y. Chen *et al.*, Injectable self-crosslinking HA-SH/Col I blend hydrogels for in vitro construction of engineered cartilage. *Carbohydrate polymers* **190**, 57-66 (2018).
48. X. Zhao *et al.*, Photocrosslinkable gelatin hydrogel for epidermal tissue engineering. *Advanced healthcare materials* **5**, 108-118 (2016).
49. S. Das *et al.*, Bioprintable, cell-laden silk fibroin–gelatin hydrogel supporting multilineage differentiation of stem cells for fabrication of three-dimensional tissue constructs. *Acta biomaterialia* **11**, 233-246 (2015).
50. N.-C. Cheng, W.-J. Lin, T.-Y. Ling, T.-H. Young, Sustained release of adipose-derived stem cells by thermosensitive chitosan/gelatin hydrogel for therapeutic angiogenesis. *Acta biomaterialia* **51**, 258-267 (2017).
51. H. Chen *et al.*, Covalently antibacterial alginate-chitosan hydrogel dressing integrated gelatin microspheres containing tetracycline hydrochloride for wound healing. *Materials Science and Engineering: C* **70**, 287-295 (2017).
52. N. Helfricht *et al.*, Probing the adhesion properties of alginate hydrogels: a new approach towards the preparation of soft colloidal probes for direct force measurements. *Soft matter* **13**, 578-589 (2017).
53. C. Bertagnolli, A. Grishin, T. Vincent, E. Guibal, Boron removal by a composite sorbent: Polyethylenimine/tannic acid derivative immobilized in alginate hydrogel beads. *Journal of Environmental Science and Health, Part A* **52**, 359-367 (2017).
54. Y. Yang, S. Song, Z. Zhao, Graphene oxide (GO)/polyacrylamide (PAM) composite hydrogels as efficient cationic dye adsorbents. *Colloids and Surfaces A: Physicochemical and Engineering Aspects* **513**, 315-324 (2017).
55. L. Han *et al.*, A Mussel-Inspired Conductive, Self-Adhesive, and Self-Healable Tough Hydrogel as Cell Stimulators and Implantable Bioelectronics. *Small* **13**, 1601916 (2017).
56. J. Chen, X. Shi, L. Ren, Y. Wang, Graphene oxide/PVA inorganic/organic interpenetrating hydrogels with excellent mechanical properties and biocompatibility. *Carbon* **111**, 18-27 (2017).
57. A. Marrella *et al.*, 3D Porous Gelatin/PVA Hydrogel as Meniscus Substitute Using Alginate Micro-Particles as Porogens. *Polymers* **10**, 380 (2018).
58. A. Vedadghavami *et al.*, Manufacturing of hydrogel biomaterials with controlled mechanical properties for tissue engineering applications. *Acta biomaterialia* **62**, 42-63 (2017).
59. S. E. Bakarich, R. Gorkin III, R. Gately, S. Naficy, G. M. Spinks, 3D printing of tough hydrogel composites with spatially varying materials properties. *Additive Manufacturing* **14**, 24-30 (2017).

60. A. Zheng *et al.*, Biocompatible silk/calcium silicate/sodium alginate composite scaffolds for bone tissue engineering. *Carbohydrate Polymers* **199**, 244-255 (2018).
61. A. Mohandas, S. Deepthi, R. Biswas, R. Jayakumar, Chitosan based metallic nanocomposite scaffolds as antimicrobial wound dressings. *Bioactive materials*, (2017).
62. P. Tirino *et al.*, Synthesis of chitosan–PEO hydrogels via mesylation and regioselective Cu (I)-catalyzed cycloaddition. *Carbohydrate polymers* **112**, 736-745 (2014).
63. L. Fan, H. Yang, J. Yang, M. Peng, J. Hu, Preparation and characterization of chitosan/gelatin/PVA hydrogel for wound dressings. *Carbohydrate polymers* **146**, 427-434 (2016).
64. X.-l. Xu *et al.*, Solution blowing of chitosan/PLA/PEG hydrogel nanofibers for wound dressing. *Fibers and Polymers* **17**, 205-211 (2016).
65. K. Wang *et al.*, Chemically crosslinked hydrogel film leads to integrated flexible supercapacitors with superior performance. *Advanced Materials* **27**, 7451-7457 (2015).
66. K. J. De France, K. J. Chan, E. D. Cranston, T. Hoare, Enhanced mechanical properties in cellulose nanocrystal–poly (oligoethylene glycol methacrylate) injectable nanocomposite hydrogels through control of physical and chemical cross-linking. *Biomacromolecules* **17**, 649-660 (2016).
67. D. Zhao *et al.*, High-Strength and High-Toughness Double-Cross-Linked Cellulose Hydrogels: A New Strategy Using Sequential Chemical and Physical Cross-Linking. *Advanced Functional Materials* **26**, 6279-6287 (2016).
68. X. Dai *et al.*, A Mechanically Strong, Highly Stable, Thermoplastic, and self-healable supramolecular polymer hydrogel. *Advanced Materials* **27**, 3566-3571 (2015).
69. F.-K. Shi, X.-P. Wang, R.-H. Guo, M. Zhong, X.-M. Xie, Highly stretchable and super tough nanocomposite physical hydrogels facilitated by the coupling of intermolecular hydrogen bonds and analogous chemical crosslinking of nanoparticles. *Journal of Materials Chemistry B* **3**, 1187-1192 (2015).
70. R. Du *et al.*, Hierarchical Hydrogen Bonds Directed Multi-Functional Carbon Nanotube-Based Supramolecular Hydrogels. *Small* **10**, 1387-1393 (2014).
71. M. Zhong, Y.-T. Liu, X.-M. Xie, Self-healable, super tough graphene oxide–poly (acrylic acid) nanocomposite hydrogels facilitated by dual cross-linking effects through dynamic ionic interactions. *Journal of Materials Chemistry B* **3**, 4001-4008 (2015).
72. M. Zhong *et al.*, Self-healable, tough and highly stretchable ionic nanocomposite physical hydrogels. *Soft Matter* **11**, 4235-4241 (2015).
73. Y. Guo *et al.*, A self-healable and easily recyclable supramolecular hydrogel electrolyte for flexible supercapacitors. *Journal of Materials Chemistry A* **4**, 8769-8776 (2016).
74. P. W. Frederix *et al.*, Exploring the sequence space for (tri-) peptide self-assembly to design and discover new hydrogels. *Nature chemistry* **7**, 30 (2015).
75. L. Li, B. Yan, J. Yang, L. Chen, H. Zeng, Novel Mussel-Inspired Injectable Self-Healing Hydrogel with Anti-Biofouling Property. *Advanced Materials* **27**, 1294-1299 (2015).
76. M. C. Koetting, J. F. Guido, M. Gupta, A. Zhang, N. A. Peppas, pH-responsive and enzymatically-responsive hydrogel microparticles for the oral delivery of therapeutic proteins: effects of protein size, crosslinking density, and hydrogel degradation on protein delivery. *Journal of Controlled Release* **221**, 18-25 (2016).
77. S. Lee, X. Tong, F. Yang, The effects of varying poly (ethylene glycol) hydrogel crosslinking density and the crosslinking mechanism on protein accumulation in three-dimensional hydrogels. *Acta biomaterialia* **10**, 4167-4174 (2014).
78. P. Lin, S. Ma, X. Wang, F. Zhou, Molecularly Engineered Dual-Crosslinked Hydrogel with Ultrahigh Mechanical Strength, Toughness, and Good Self-Recovery. *Advanced Materials* **27**, 2054-2059 (2015).
79. R. M. Desai, S. T. Koshy, S. A. Hilderbrand, D. J. Mooney, N. S. Joshi, Versatile click alginate hydrogels crosslinked via tetrazine–norbornene chemistry. *Biomaterials* **50**, 30-37 (2015).

80. X. Hu, M. Vatankhah-Varnoosfaderani, J. Zhou, Q. Li, S. S. Sheiko, Weak hydrogen bonding enables hard, strong, tough, and elastic hydrogels. *Advanced Materials* **27**, 6899-6905 (2015).
81. M. Guo *et al.*, Tough stimuli-responsive supramolecular hydrogels with hydrogen-bonding network junctions. *Journal of the American Chemical Society* **136**, 6969-6977 (2014).
82. Y. Choi *et al.*, Low-Voltage Complementary Electronics from Ion-Gel-Gated Vertical Van der Waals Heterostructures. *Advanced Materials* **28**, 3742-3748 (2016).
83. J. Visser *et al.*, Reinforcement of hydrogels using three-dimensionally printed microfibres. *Nature communications* **6**, 6933 (2015).
84. Y. Lu, Y. Wu, J. Liang, M. R. Libera, S. A. Sukhishvili, Self-defensive antibacterial layer-by-layer hydrogel coatings with pH-triggered hydrophobicity. *Biomaterials* **45**, 64-71 (2015).
85. Y. Geng *et al.*, Hydrophobic association mediated physical hydrogels with high strength and healing ability. *Polymer* **100**, 60-68 (2016).
86. H. He *et al.*, Multifunctional photo-crosslinked polymeric ionic hydrogel films. *Polymer Chemistry* **5**, 2824-2835 (2014).
87. X. Pu *et al.*, Ultrastretchable, transparent triboelectric nanogenerator as electronic skin for biomechanical energy harvesting and tactile sensing. *Science advances* **3**, e1700015 (2017).
88. S. Tosatti *et al.*, Coefficient of friction comparison of worn daily disposable silicone hydrogel contact lenses to human corneal tissue. *Contact Lens and Anterior Eye* **41**, S4-S5 (2018).
89. K. Zhang *et al.*, Strategy for constructing vascularized adipose units in poly (l-glutamic acid) hydrogel porous scaffold through inducing in-situ formation of ASCs spheroids. *Acta biomaterialia* **51**, 246-257 (2017).
90. S. Anjum, A. Arora, M. Alam, B. Gupta, Development of antimicrobial and scar preventive chitosan hydrogel wound dressings. *International journal of pharmaceutics* **508**, 92-101 (2016).
91. N. A. Peppas, D. S. Van Blarcom, Hydrogel-based biosensors and sensing devices for drug delivery. *Journal of Controlled Release* **240**, 142-150 (2016).
92. L. Sun *et al.*, A hydrogel biosensor for high selective and sensitive detection of amyloid-beta oligomers. *International journal of nanomedicine* **13**, 843 (2018).
93. S. Gu, L. Duan, X. Ren, G. H. Gao, Robust, tough and anti-fatigue cationic latex composite hydrogels based on dual physically cross-linked networks. *Journal of colloid and interface science* **492**, 119-126 (2017).
94. W. J. Zheng, N. An, J. H. Yang, J. Zhou, Y. M. Chen, Tough Al-alginate/poly (N-isopropylacrylamide) hydrogel with tunable LCST for soft robotics. *ACS applied materials & interfaces* **7**, 1758-1764 (2015).
95. Z. Li *et al.*, A novel biocompatible double network hydrogel consisting of konjac glucomannan with high mechanical strength and ability to be freely shaped. *Journal of Materials Chemistry B* **3**, 1769-1778 (2015).
96. S. Liu, W. Su, Y. Li, L. Zhang, X. Ding, Manufacturing of an electrochemical biosensing platform based on hybrid DNA hydrogel: Taking lung cancer-specific miR-21 as an example. *Biosensors and Bioelectronics* **103**, 1-5 (2018).
97. T. Kajisa, T. Sakata, Glucose-responsive hydrogel electrode for biocompatible glucose transistor. *Science and Technology of advanced MaTerialS* **18**, 26-33 (2017).
98. J. Deng, W. Liang, J. Fang, Liquid crystal droplet-embedded biopolymer hydrogel sheets for biosensor applications. *ACS applied materials & interfaces* **8**, 3928-3932 (2016).
99. Y.-N. Chou *et al.*, Ultra-low fouling and high antibody loading zwitterionic hydrogel coatings for sensing and detection in complex media. *Acta biomaterialia* **40**, 31-37 (2016).
100. S. Burrs *et al.*, A comparative study of graphene–hydrogel hybrid bionanocomposites for biosensing. *Analyst* **140**, 1466-1476 (2015).

101. K. Goh, H. Li, K. Y. Lam, Development of a multiphysics model to characterize the responsive behavior of urea-sensitive hydrogel as biosensor. *Biosensors and Bioelectronics* **91**, 673-679 (2017).
102. P. Pinyou *et al.*, Design of an Os Complex-Modified Hydrogel with Optimized Redox Potential for Biosensors and Biofuel Cells. *Chemistry–A European Journal* **22**, 5319-5326 (2016).
103. H. Xiong *et al.*, A convenient purification method for silver nanoclusters and its applications in fluorescent pH sensors for bacterial monitoring. *Biosensors and Bioelectronics* **86**, 164-168 (2016).
104. K. Goh, H. Li, K. Lam, Characterization of dual urea-and pH-induced behaviors of smart hydrogel at human physiological conditions. *Procedia Engineering* **214**, 86-92 (2017).
105. D. Puchberger, M. J. Vellekoop, Hydrogels for Imaging, Sensing and Diagnostics. *Hydrogels: Design, Synthesis and Application in Drug Delivery and Regenerative Medicine*, 140 (2018).
106. H. Yuk, T. Zhang, S. Lin, G. A. Parada, X. Zhao, Tough bonding of hydrogels to diverse non-porous surfaces. *Nature materials* **15**, 190 (2016).
107. V. X. Truong, M. P. Ablett, S. M. Richardson, J. A. Hoyland, A. P. Dove, Simultaneous orthogonal dual-click approach to tough, in-situ-forming hydrogels for cell encapsulation. *Journal of the American Chemical Society* **137**, 1618-1622 (2015).
108. L. Qiu *et al.*, Mechanically Robust, Electrically Conductive and Stimuli-Responsive Binary Network Hydrogels Enabled by Superelastic Graphene Aerogels. *Advanced Materials* **26**, 3333-3337 (2014).
109. X. Xu *et al.*, Naturally dried graphene aerogels with superelasticity and tunable Poisson's ratio. *Advanced materials* **28**, 9223-9230 (2016).
110. B. Yao *et al.*, Ultrahigh-Conductivity Polymer Hydrogels with Arbitrary Structures. *Advanced Materials* **29**, 1700974 (2017).
111. W. Zhao, L. Glavas, K. Odelius, U. Edlund, A.-C. Albertsson, Facile and green approach towards electrically conductive hemicellulose hydrogels with tunable conductivity and swelling behavior. *Chemistry of Materials* **26**, 4265-4273 (2014).
112. C. B. Highley, C. B. Rodell, J. A. Burdick, Direct 3D printing of shear-thinning hydrogels into self-healing hydrogels. *Advanced Materials* **27**, 5075-5079 (2015).
113. Q. Feng *et al.*, Mechanically resilient, injectable, and bioadhesive supramolecular gelatin hydrogels crosslinked by weak host-guest interactions assist cell infiltration and in situ tissue regeneration. *Biomaterials* **101**, 217-228 (2016).
114. L. Cai, R. E. Dewi, S. C. Heilshorn, Injectable hydrogels with in situ double network formation enhance retention of transplanted stem cells. *Advanced functional materials* **25**, 1344-1351 (2015).
115. S. Gao *et al.*, A robust polyionized hydrogel with an unprecedented underwater anti-crude-oil-adhesion property. *Advanced Materials* **28**, 5307-5314 (2016).
116. F. Yu, X. Cao, J. Du, G. Wang, X. Chen, Multifunctional hydrogel with good structure integrity, self-healing, and tissue-adhesive property formed by combining Diels–Alder click reaction and acylhydrazone bond. *ACS applied materials & interfaces* **7**, 24023-24031 (2015).
117. C. Li *et al.*, Responsive double network hydrogels of interpenetrating DNA and CB [8] host–guest supramolecular systems. *Advanced Materials* **27**, 3298-3304 (2015).
118. Z. Gong *et al.*, High-strength, tough, fatigue resistant, and self-healing hydrogel based on dual physically cross-linked network. *ACS applied materials & interfaces* **8**, 24030-24037 (2016).
119. T. Nonoyama *et al.*, Double-network hydrogels strongly bondable to bones by spontaneous osteogenesis penetration. *Advanced Materials* **28**, 6740-6745 (2016).
120. C. García-Astrain *et al.*, Biocompatible hydrogel nanocomposite with covalently embedded silver nanoparticles. *Biomacromolecules* **16**, 1301-1310 (2015).

121. A. Pourjavadi, M. Nazari, S. H. Hosseini, Synthesis of magnetic graphene oxide-containing nanocomposite hydrogels for adsorption of crystal violet from aqueous solution. *RSC Advances* **5**, 32263-32271 (2015).
122. J. Li, J. Xie, L. Gao, C. M. Li, Au nanoparticles–3D graphene hydrogel nanocomposite to boost synergistically in situ detection sensitivity toward cell-released nitric oxide. *ACS applied materials & interfaces* **7**, 2726-2734 (2015).
123. H. Chen *et al.*, A comparative study of the mechanical properties of hybrid double-network hydrogels in swollen and as-prepared states. *Journal of Materials Chemistry B* **4**, 5814-5824 (2016).
124. M. A. Darabi *et al.*, Skin-Inspired Multifunctional Autonomic-Intrinsic Conductive Self-Healing Hydrogels with Pressure Sensitivity, Stretchability, and 3D Printability. *Advanced Materials* **29**, (2017).
125. R. Xu *et al.*, New double network hydrogel adsorbent: highly efficient removal of Cd (II) and Mn (II) ions in aqueous solution. *Chemical Engineering Journal* **275**, 179-188 (2015).
126. E. S. Dragan, Design and applications of interpenetrating polymer network hydrogels. A review. *Chemical Engineering Journal* **243**, 572-590 (2014).
127. W. Xiao *et al.*, Synthesis and characterization of photocrosslinkable gelatin and silk fibroin interpenetrating polymer network hydrogels. *Acta biomaterialia* **7**, 2384-2393 (2011).
128. R. E. Webber, C. Creton, H. R. Brown, J. P. Gong, Large strain hysteresis and mullins effect of tough double-network hydrogels. *Macromolecules* **40**, 2919-2927 (2007).
129. S. Hong *et al.*, 3D printing of highly stretchable and tough hydrogels into complex, cellularized structures. *Advanced materials* **27**, 4035-4040 (2015).
130. L. Li, W. Smitthipong, H. Zeng, Mussel-inspired hydrogels for biomedical and environmental applications. *Polymer Chemistry* **6**, 353-358 (2015).
131. J. Liu *et al.*, Synthesis of graphene peroxide and its application in fabricating super extensible and highly resilient nanocomposite hydrogels. *Acs Nano* **6**, 8194-8202 (2012).
132. H.-P. Cong, P. Wang, S.-H. Yu, Stretchable and self-healing graphene oxide–polymer composite hydrogels: a dual-network design. *Chemistry of Materials* **25**, 3357-3362 (2013).
133. X. Feng, W. Chen, L. Yan, Reduced graphene oxide hydrogel film with a continuous ion transport network for supercapacitors. *Nanoscale* **7**, 3712-3718 (2015).
134. K. Yue *et al.*, Synthesis, properties, and biomedical applications of gelatin methacryloyl (GelMA) hydrogels. *Biomaterials* **73**, 254-271 (2015).
135. S. Ahadian *et al.*, Hybrid hydrogels containing vertically aligned carbon nanotubes with anisotropic electrical conductivity for muscle myofiber fabrication. *Scientific reports* **4**, 4271 (2014).
136. M. Bora, A. G. P. Kottapalli, J. Miao, M. S. Triantafyllou, Biomimetic hydrogel-CNT network induced enhancement of fluid-structure interactions for ultrasensitive nanosensors. *NPG Asia Materials* **9**, e440 (2017).
137. B. Mathieu, C. Anthony, A. Arnaud, F. Lionel, CNT aggregation mechanisms probed by electrical and dielectric measurements. *Journal of Materials Chemistry C* **3**, 5769-5774 (2015).
138. F. Inam, A. Heaton, P. Brown, T. Peijs, M. J. Reece, Effects of dispersion surfactants on the properties of ceramic–carbon nanotube (CNT) nanocomposites. *Ceramics International* **40**, 511-516 (2014).
139. Y. S. Song, J. R. Youn, Influence of dispersion states of carbon nanotubes on physical properties of epoxy nanocomposites. *Carbon* **43**, 1378-1385 (2005).
140. J. Sun *et al.*, Ultra-high dielectric constant of poly (vinylidene fluoride) composites filled with hydroxyl modified graphite powders. *Polymer Composites* **37**, 327-333 (2016).
141. L. Ma *et al.*, Enhanced Li–S batteries using amine-functionalized carbon nanotubes in the cathode. *ACS nano* **10**, 1050-1059 (2015).

142. X. Gao, A. Omosebi, J. Landon, K. Liu, Enhanced salt removal in an inverted capacitive deionization cell using amine modified microporous carbon cathodes. *Environmental science & technology* **49**, 10920-10926 (2015).
143. Z. Guan, X.-Y. Tang, T. Nishimura, Y.-M. Huang, B. J. Reid, Adsorption of linear alkylbenzene sulfonates on carboxyl modified multi-walled carbon nanotubes. *Journal of hazardous materials* **322**, 205-214 (2017).
144. T. W. Odom, J.-L. Huang, P. Kim, C. M. Lieber, Atomic structure and electronic properties of single-walled carbon nanotubes. *Nature* **391**, 62 (1998).
145. J. Kong *et al.*, Nanotube molecular wires as chemical sensors. *science* **287**, 622-625 (2000).
146. A. Vashist *et al.*, Nanocomposite Hydrogels: Advances in Nanofillers Used for Nanomedicine. *Gels* **4**, 75 (2018).
147. K. D. Behler *et al.*, Nanodiamond-polymer composite fibers and coatings. *ACS nano* **3**, 363-369 (2009).
148. Y. Zhu *et al.*, The biocompatibility of nanodiamonds and their application in drug delivery systems. *Theranostics* **2**, 302 (2012).
149. V. N. Mochalin, O. Shenderova, D. Ho, Y. Gogotsi, The properties and applications of nanodiamonds. *Nature nanotechnology* **7**, 11 (2012).
150. K. H. Nakayama, L. Hou, N. F. Huang, Role of extracellular matrix signaling cues in modulating cell fate commitment for cardiovascular tissue engineering. *Advanced healthcare materials* **3**, 628-641 (2014).
151. S. Bauer *et al.*, 25th anniversary article: a soft future: from robots and sensor skin to energy harvesters. *Advanced Materials* **26**, 149-162 (2014).
152. Y. Liu *et al.*, Highly flexible and resilient elastin hybrid cryogels with shape memory, injectability, conductivity, and magnetic responsive properties. *Advanced Materials* **28**, 7758-7767 (2016).
153. N. Annabi *et al.*, Highly Elastic and Conductive Human-Based Protein Hybrid Hydrogels. *Adv Mater* **28**, 40-49 (2016).
154. S. Liu *et al.*, Antibacterial activity of graphite, graphite oxide, graphene oxide, and reduced graphene oxide: membrane and oxidative stress. *ACS nano* **5**, 6971-6980 (2011).
155. S. Stankovich *et al.*, Synthesis of graphene-based nanosheets via chemical reduction of exfoliated graphite oxide. *carbon* **45**, 1558-1565 (2007).
156. S. Sowmya *et al.*, Tri-Layered Nanocomposite Hydrogel Scaffold for the Concurrent Regeneration of Cementum, Periodontal Ligament, and Alveolar Bone. *Advanced Healthcare Materials*, (2017).
157. M. Y. Kim *et al.*, Augmentation of tendon healing with an injectable tendon hydrogel in a rat Achilles tendon model. *Plastic and reconstructive surgery* **133**, 645e-653e (2014).
158. J. Cui, A. del Campo, Multivalent H-bonds for self-healing hydrogels. *Chemical Communications* **48**, 9302-9304 (2012).
159. H. Zhang, H. Xia, Y. Zhao, Poly (vinyl alcohol) hydrogel can autonomously self-heal. *Acs Macro Letters* **1**, 1233-1236 (2012).
160. B. Liu *et al.*, Hydrogen bonds autonomously powered gelatin methacrylate hydrogels with super-elasticity, self-heal and underwater self-adhesion for sutureless skin and stomach surgery and E-skin. *Biomaterials* **171**, 83-96 (2018).
161. Z. Wei *et al.*, Autonomous self-healing of poly (acrylic acid) hydrogels induced by the migration of ferric ions. *Polymer Chemistry* **4**, 4601-4605 (2013).
162. D. C. Tuncaboylu, M. Sari, W. Oppermann, O. Okay, Tough and self-healing hydrogels formed via hydrophobic interactions. *Macromolecules* **44**, 4997-5005 (2011).
163. A. B. Ihsan *et al.*, Self-healing behaviors of tough polyampholyte hydrogels. *Macromolecules* **49**, 4245-4252 (2016).
164. J. Chen *et al.*, High-toughness polyacrylamide gel containing hydrophobic crosslinking and its double network gel. *Polymer* **87**, 73-80 (2016).

165. F. Rengier *et al.*, 3D printing based on imaging data: review of medical applications. *International journal of computer assisted radiology and surgery* **5**, 335-341 (2010).
166. S. Bose, S. Vahabzadeh, A. Bandyopadhyay, Bone tissue engineering using 3D printing. *Materials today* **16**, 496-504 (2013).
167. G. Matzeu, L. Florea, D. Diamond, Advances in wearable chemical sensor design for monitoring biological fluids. *Sensors and Actuators B: Chemical* **211**, 403-418 (2015).
168. D. Diamond, S. Coyle, S. Scarmagnani, J. Hayes, Wireless sensor networks and chemo-/biosensing. *Chemical reviews* **108**, 652-679 (2008).
169. J. R. Windmiller, J. Wang, Wearable electrochemical sensors and biosensors: a review. *Electroanalysis* **25**, 29-46 (2013).
170. M. A. Darabi *et al.*, Skin-Inspired Multifunctional Autonomic-Intrinsic Conductive Self-Healing Hydrogels with Pressure Sensitivity, Stretchability, and 3D Printability. *Advanced Materials* **29**, 1700533 (2017).
171. J. T. Muth *et al.*, Embedded 3D printing of strain sensors within highly stretchable elastomers. *Advanced Materials* **26**, 6307-6312 (2014).
172. K. Li *et al.*, 3D printed stretchable capacitive sensors for highly sensitive tactile and electrochemical sensing. *Nanotechnology* **29**, 185501 (2018).
173. A. P. Periasamy, Y.-J. Chang, S.-M. Chen, Amperometric glucose sensor based on glucose oxidase immobilized on gelatin-multiwalled carbon nanotube modified glassy carbon electrode. *Bioelectrochemistry* **80**, 114-120 (2011).
174. A. Roda *et al.*, A 3D-printed device for a smartphone-based chemiluminescence biosensor for lactate in oral fluid and sweat. *Analyst* **139**, 6494-6501 (2014).
175. P. T. Charles *et al.*, Fabrication and characterization of 3D hydrogel microarrays to measure antigenicity and antibody functionality for biosensor applications. *Biosensors and Bioelectronics* **20**, 753-764 (2004).
176. S. Pei, J. Zhao, J. Du, W. Ren, H.-M. Cheng, Direct reduction of graphene oxide films into highly conductive and flexible graphene films by hydrohalic acids. *Carbon* **48**, 4466-4474 (2010).
177. H. P. Cong, P. Wang, S. H. Yu, Highly elastic and superstretchable graphene oxide/polyacrylamide hydrogels. *Small* **10**, 448-453 (2014).
178. J. Wang, C. Liu, Y. Shuai, X. Cui, L. Nie, Controlled release of anticancer drug using graphene oxide as a drug-binding effector in konjac glucomannan/sodium alginate hydrogels. *Colloids and Surfaces B: Biointerfaces* **113**, 223-229 (2014).
179. M. Mabrouk *et al.*, Design of a novel crosslinked HEC-PAA porous hydrogel composite for dissolution rate and solubility enhancement of efavirenz. *International journal of pharmaceutics* **490**, 429-437 (2015).
180. K. Qiao *et al.*, Effects of graphene on the structure, properties, electro-response behaviors of GO/PAA composite hydrogels and influence of electro-mechanical coupling on BMSC differentiation. *Materials Science and Engineering: C* **93**, 853-863 (2018).
181. S. J. Kim, S. J. Park, S. I. Kim, Swelling behavior of interpenetrating polymer network hydrogels composed of poly (vinyl alcohol) and chitosan. *Reactive and Functional Polymers* **55**, 53-59 (2003).
182. T. Miyata, N. Asami, T. Uragami, A reversibly antigen-responsive hydrogel. *Nature* **399**, 766 (1999).
183. E. Jabbari, S. Nozari, Swelling behavior of acrylic acid hydrogels prepared by γ-radiation crosslinking of polyacrylic acid in aqueous solution. *European Polymer Journal* **36**, 2685-2692 (2000).
184. J. E. Elliott, M. Macdonald, J. Nie, C. N. Bowman, Structure and swelling of poly (acrylic acid) hydrogels: effect of pH, ionic strength, and dilution on the crosslinked polymer structure. *Polymer* **45**, 1503-1510 (2004).
185. B. Timmer, W. Olthuis, A. Van Den Berg, Ammonia sensors and their applications—a review. *Sensors and Actuators B: Chemical* **107**, 666-677 (2005).

186. S. Bhadra, D. J. Thomson, G. E. Bridges, Monitoring acidic and basic volatile concentration using a pH-electrode based wireless passive sensor. *Sensors and Actuators B: Chemical* **209**, 803-810 (2015).
187. Z. Wei *et al.*, Novel biocompatible polysaccharide-based self-healing hydrogel. *Advanced Functional Materials* **25**, 1352-1359 (2015).
188. C. Ghobril, M. Grinstaff, The chemistry and engineering of polymeric hydrogel adhesives for wound closure: a tutorial. *Chemical Society Reviews* **44**, 1820-1835 (2015).
189. J. Duan, X. Liang, Y. Cao, S. Wang, L. Zhang, High strength chitosan hydrogels with biocompatibility via new avenue based on constructing nanofibrous architecture. *Macromolecules* **48**, 2706-2714 (2015).
190. D. J. Miller, D. R. Dreyer, C. W. Bielawski, D. R. Paul, B. D. Freeman, Surface modification of water purification membranes. *Angewandte Chemie International Edition* **56**, 4662-4711 (2017).
191. S. Lin *et al.*, Stretchable hydrogel electronics and devices. *Advanced Materials* **28**, 4497-4505 (2016).
192. J. Zhang, H. Xiao, N. Li, Q. Ping, Y. Zhang, Synthesis and characterization of super-absorbent hydrogels based on hemicellulose. *Journal of Applied Polymer Science* **132**, (2015).
193. E. A. Kamoun, E.-R. S. Kenawy, X. Chen, A review on polymeric hydrogel membranes for wound dressing applications: PVA-based hydrogel dressings. *Journal of advanced research* **8**, 217-233 (2017).
194. J. P. Gong, Y. Katsuyama, T. Kurokawa, Y. Osada, Double-network hydrogels with extremely high mechanical strength. *Advanced materials* **15**, 1155-1158 (2003).
195. J. P. Gong, Why are double network hydrogels so tough? *Soft Matter* **6**, 2583-2590 (2010).
196. X. Zhang *et al.*, Double-network hydrogel with high mechanical strength prepared from two biocompatible polymers. *Journal of applied polymer science* **112**, 3063-3070 (2009).
197. C. B. Rodell, N. N. Dusaj, C. B. Highley, J. A. Burdick, Injectable and cytocompatible tough double-network hydrogels through tandem supramolecular and covalent crosslinking. *Advanced materials* **28**, 8419-8424 (2016).
198. J.-Y. Sun *et al.*, Highly stretchable and tough hydrogels. *Nature* **489**, 133 (2012).
199. M. D. Hager, P. Greil, C. Leyens, S. van der Zwaag, U. S. Schubert, Self-healing materials. *Advanced Materials* **22**, 5424-5430 (2010).
200. V. K. Thakur, M. R. Kessler, Self-healing polymer nanocomposite materials: A review. *Polymer* **69**, 369-383 (2015).
201. N. Roy, B. Bruchmann, J.-M. Lehn, DYNAMERS: dynamic polymers as self-healing materials. *Chemical Society Reviews* **44**, 3786-3807 (2015).
202. K. Imato *et al.*, Self-healing of chemical gels cross-linked by diarylbibenzofuranone-based trigger-free dynamic covalent bonds at room temperature. *Angewandte Chemie* **124**, 1164-1168 (2012).
203. G. Deng, C. Tang, F. Li, H. Jiang, Y. Chen, Covalent cross-linked polymer gels with reversible sol− gel transition and self-healing properties. *Macromolecules* **43**, 1191-1194 (2010).
204. B. K. Ahn, D. W. Lee, J. N. Israelachvili, J. H. Waite, Surface-initiated self-healing of polymers in aqueous media. *Nature materials* **13**, 867 (2014).
205. C.-H. Li *et al.*, A highly stretchable autonomous self-healing elastomer. *Nature chemistry* **8**, 618 (2016).
206. P. Michael, D. Doehler, W. H. Binder, Improving autonomous self healing via combined chemical/physical principles. *Polymer* **69**, 216-227 (2015).
207. P. Wei, X. Yan, F. Huang, Supramolecular polymers constructed by orthogonal self-assembly based on host–guest and metal–ligand interactions. *Chemical Society Reviews* **44**, 815-832 (2015).

208. I. Jeon, J. Cui, W. R. Illeperuma, J. Aizenberg, J. J. Vlassak, Extremely Stretchable and Fast Self-Healing Hydrogels. *Advanced Materials* **28**, 4678-4683 (2016).
209. S. Owusu-Nkwantabisah, J. R. Gillmor, S. C. Switalski, G. L. Slater, An autonomous self-healing hydrogel based on surfactant-free hydrophobic association. *Journal of Applied Polymer Science* **134**, (2017).
210. W. Pu, F. Jiang, P. Chen, B. Wei, A POSS based hydrogel with mechanical robustness, cohesiveness and a rapid self-healing ability by electrostatic interaction. *Soft matter* **13**, 5645-5648 (2017).
211. H. Wei *et al.*, Tunable, luminescent, and self-healing hybrid hydrogels of polyoxometalates and triblock copolymers based on electrostatic assembly. *Chemical Communications* **50**, 1447-1450 (2014).
212. W. Sun *et al.*, Polymer-Supramolecular Polymer Double-Network Hydrogel. *Advanced Functional Materials* **26**, 9044-9052 (2016).
213. L. Lin *et al.*, Bio-inspired hierarchical macromolecule–nanoclay hydrogels for robust underwater superoleophobicity. *Advanced materials* **22**, 4826-4830 (2010).
214. S. Chen, J. Duan, M. Jaroniec, S. Z. Qiao, Nitrogen and oxygen dual-doped carbon hydrogel film as a substrate-free electrode for highly efficient oxygen evolution reaction. *Advanced Materials* **26**, 2925-2930 (2014).
215. K. Shah, D. Vasileva, A. Karadaghy, S. Zustiak, Development and characterization of polyethylene glycol–carbon nanotube hydrogel composite. *Journal of Materials Chemistry B* **3**, 7950-7962 (2015).
216. A. Paul *et al.*, Injectable graphene oxide/hydrogel-based angiogenic gene delivery system for vasculogenesis and cardiac repair. *ACS nano* **8**, 8050-8062 (2014).
217. H. Bai, C. Li, X. Wang, G. Shi, A pH-sensitive graphene oxide composite hydrogel. *Chemical Communications* **46**, 2376-2378 (2010).
218. J. Liu, G. Song, C. He, H. Wang, Self-healing in tough graphene oxide composite hydrogels. *Macromolecular rapid communications* **34**, 1002-1007 (2013).
219. H. N. Tien *et al.*, Synthesis of a highly conductive and large surface area graphene oxide hydrogel and its use in a supercapacitor. *Journal of Materials Chemistry A* **1**, 208-211 (2013).
220. L. Zhang, G. Shi, Preparation of highly conductive graphene hydrogels for fabricating supercapacitors with high rate capability. *The Journal of Physical Chemistry C* **115**, 17206-17212 (2011).
221. R. Liu *et al.*, Tough and highly stretchable graphene oxide/polyacrylamide nanocomposite hydrogels. *Journal of Materials Chemistry* **22**, 14160-14167 (2012).
222. Q. Liu *et al.*, High-quality graphene ribbons prepared from graphene oxide hydrogels and their application for strain sensors. *ACS nano* **9**, 12320-12326 (2015).
223. S. R. Shin *et al.*, Cell-laden microengineered and mechanically tunable hybrid hydrogels of gelatin and graphene oxide. *Advanced materials* **25**, 6385-6391 (2013).
224. S. Wang, Z. Zhang, B. Chen, J. Shao, Z. Guo, Self-healing hydrogel of poly (vinyl alcohol)/graphite oxide with p H-sensitive and enhanced thermal properties. *Journal of Applied Polymer Science* **135**, 46143 (2018).
225. L. Sun *et al.*, Graphene Oxide hydrogel Particles from Microfluidics for Oil Decontamination. *Journal of colloid and interface science*, (2018).
226. K. Varaprasad, T. Jayaramudu, E. R. Sadiku, Removal of dye by carboxymethyl cellulose, acrylamide and graphene oxide via a free radical polymerization process. *Carbohydrate polymers* **164**, 186-194 (2017).
227. Z. Lei, Q. Wang, S. Sun, W. Zhu, P. Wu, A Bioinspired Mineral Hydrogel as a Self-Healable, Mechanically Adaptable Ionic Skin for Highly Sensitive Pressure Sensing. *Advanced Materials* **29**, 1700321 (2017).

228. C. Shao *et al.*, Mussel-Inspired Cellulose Nanocomposite Tough Hydrogels with Synergistic Self-Healing, Adhesive, and Strain-Sensitive Properties. *Chemistry of Materials* **30**, 3110-3121 (2018).
229. T. Cai, S. Huo, T. Wang, W. Sun, Z. Tong, Self-healable tough supramolecular hydrogels crosslinked by poly-cyclodextrin through host-guest interaction. *Carbohydrate polymers* **193**, 54-61 (2018).
230. T. Billiet, E. Gevaert, T. De Schryver, M. Cornelissen, P. Dubruel, The 3D printing of gelatin methacrylamide cell-laden tissue-engineered constructs with high cell viability. *Biomaterials* **35**, 49-62 (2014).
231. Z. Cheng *et al.*, 3D printing hydrogel with graphene oxide is functional in cartilage protection by influencing the signal pathway of Rank/Rankl/OPG. *Materials Science and Engineering: C* **82**, 244-252 (2018).
232. D. Church, S. Elsayed, O. Reid, B. Winston, R. Lindsay, Burn wound infections. *Clinical microbiology reviews* **19**, 403-434 (2006).
233. A. Mehbod *et al.*, Postoperative deep wound infections in adults after spinal fusion: management with vacuum-assisted wound closure. *Clinical Spine Surgery* **18**, 14-17 (2005).
234. X. Meng *et al.*, Chitosan and alginate polyelectrolyte complex membranes and their properties for wound dressing application. *Journal of Materials Science: Materials in Medicine* **21**, 1751-1759 (2010).
235. R. Jayakumar, M. Prabaharan, P. S. Kumar, S. Nair, H. Tamura, Biomaterials based on chitin and chitosan in wound dressing applications. *Biotechnology advances* **29**, 322-337 (2011).
236. J. S. Boateng, K. H. Matthews, H. N. Stevens, G. M. Eccleston, Wound healing dressings and drug delivery systems: a review. *Journal of pharmaceutical sciences* **97**, 2892-2923 (2008).
237. F. L. Mi *et al.*, Control of wound infections using a bilayer chitosan wound dressing with sustainable antibiotic delivery. *Journal of biomedical materials research* **59**, 438-449 (2002).
238. B. Balakrishnan, M. Mohanty, P. Umashankar, A. Jayakrishnan, Evaluation of an in situ forming hydrogel wound dressing based on oxidized alginate and gelatin. *Biomaterials* **26**, 6335-6342 (2005).
239. M. L. Patton, D. Smith, R. Korentager, An open, prospective, randomized pilot investigation evaluating pain with the use of a soft silicone wound contact layer vs bridal veil and staples on split thickness skin grafts as a primary dressing. *Journal of Burn Care & Research* **34**, 674-681 (2013).
240. M. Walker, P. G. Bowler, C. A. Cochrane, In vitro studies to show sequestration of matrix metalloproteinases by silver-containing wound care products. *Ostomy/wound management* **53**, 18-25 (2007).
241. S. G. Kumbar, S. P. Nukavarapu, R. James, L. S. Nair, C. T. Laurencin, Electrospun poly (lactic acid-co-glycolic acid) scaffolds for skin tissue engineering. *Biomaterials* **29**, 4100-4107 (2008).
242. H. C. Guthrie *et al.*, A pre-clinical evaluation of silver, iodine and Manuka honey based dressings in a model of traumatic extremity wounds contaminated with Staphylococcus aureus. *Injury* **45**, 1171-1178 (2014).
243. T. Nakamura *et al.*, Triclosan-coated sutures reduce the incidence of wound infections and the costs after colorectal surgery: a randomized controlled trial. *Surgery* **153**, 576-583 (2013).
244. J. Wen, M. Weinhart, B. Lai, J. Kizhakkedathu, D. E. Brooks, Reversible hemostatic properties of sulfabetaine/quaternary ammonium modified hyperbranched polyglycerol. *Biomaterials* **86**, 42-55 (2016).
245. W. Gottardi, D. Debabov, M. Nagl, N-chloramines, a promising class of well-tolerated topical anti-infectives. *Antimicrobial agents and chemotherapy* **57**, 1107-1114 (2013).

246. P. Atanasov *et al.*, Fs-laser processing of medical grade polydimethylsiloxane (PDMS). *Applied Surface Science* **374**, 229-234 (2016).
247. N. Stankova *et al.*, Optical properties of polydimethylsiloxane (PDMS) during nanosecond laser processing. *Applied Surface Science* **374**, 96-103 (2016).
248. A. Eifert, D. Paulssen, S. N. Varanakkottu, T. Baier, S. Hardt, Simple fabrication of robust water-repellent surfaces with low contact-angle hysteresis based on impregnation. *Advanced Materials Interfaces* **1**, (2014).
249. Food, D. Administration, Guidance for Industry and FDA Staff. Surgical Masks-Premarket Notification [510 (k)] Submissions: Guidance for Industry and FDA. *Washington, DC: US Department of Health and Human Services, Food and Drug Administration, Center for Devices and Radiological Health. Available at http://www. fda. gov/cdrh/ode/guidance/094. html (accessed March 15, 2013)*, (2003).
250. S. Z. Guo, K. Qiu, F. Meng, S. H. Park, M. C. McAlpine, 3D Printed Stretchable Tactile Sensors. *Advanced Materials*, (2017).
251. Z. Muwaffak *et al.*, Patient-specific 3D scanned and 3D printed antimicrobial polycaprolactone wound dressings. *International Journal of Pharmaceutics* **527**, 161-170 (2017).
252. X. Chen, H. Schluesener, Nanosilver: a nanoproduct in medical application. *Toxicology letters* **176**, 1-12 (2008).
253. L. Pauksch *et al.*, Biocompatibility of silver nanoparticles and silver ions in primary human mesenchymal stem cells and osteoblasts. *Acta biomaterialia* **10**, 439-449 (2014).
254. N. MacCallum *et al.*, Liquid-infused silicone as a biofouling-free medical material. *ACS Biomaterials Science & Engineering* **1**, 43-51 (2014).
255. C. Wu *et al.*, Bioinspired synthesis of polydopamine/Ag nanocomposite particles with antibacterial activities. *Materials Science and Engineering: C* **55**, 155-165 (2015).
256. A. GhavamiNejad *et al.*, Mussel-inspired electrospun nanofibers functionalized with size-controlled silver nanoparticles for wound dressing application. *ACS applied materials & interfaces* **7**, 12176-12183 (2015).
257. N. Jangpromma *et al.*, In Vitro and in Vivo Wound Healing Properties of Plasma and Serum from Crocodylus siamensis Blood. *Journal of microbiology and biotechnology* **26**, 1140-1147 (2016).
258. D. Liang, Z. Lu, H. Yang, J. Gao, R. Chen, Novel asymmetric wettable AgNPs/chitosan wound dressing: in vitro and in vivo evaluation. *ACS applied materials & interfaces* **8**, 3958-3968 (2016).
259. R. H. Demling, M. L. DeSanti, The rate of re-epithelialization across meshed skin grafts is increased with exposure to silver. *Burns* **28**, 264-266 (2002).
260. Z. Jia *et al.*, Bioinspired anchoring AgNPs onto micro-nanoporous TiO 2 orthopedic coatings: trap-killing of bacteria, surface-regulated osteoblast functions and host responses. *Biomaterials* **75**, 203-222 (2016).
261. B. Cheng, H. W. Liu, X. B. Fu, Z. Y. Sheng, J. F. Li, Coexistence and upregulation of three types of opioid receptors, mu, delta and kappa, in human hypertrophic scars. *British Journal of Dermatology* **158**, 713-720 (2008).
262. Y. Dong *et al.*, The improvement of fibroblast growth on hydrophobic biopolyesters by coating with polyhydroxyalkanoate granule binding protein PhaP fused with cell adhesion motif RGD. *Biomaterials* **31**, 8921-8930 (2010).
263. M. R. Reithofer, A. Lakshmanan, A. T. Ping, J. M. Chin, C. A. Hauser, In situ synthesis of size-controlled, stable silver nanoparticles within ultrashort peptide hydrogels and their anti-bacterial properties. *Biomaterials* **35**, 7535-7542 (2014).
264. Y. Wang *et al.*, Biomimetic fibroblast-loaded artificial dermis with "sandwich" structure and designed gradient pore sizes promotes wound healing by favoring granulation tissue formation and wound re-epithelialization. *Acta biomaterialia* **30**, 246-257 (2016).